Nonlinear vibration control: A frequency domain approach

Carmen Ho

Department of Automatic Control and Systems Engineering

University of Sheffield

A thesis submitted for the degree of

Doctor of Philosophy

December 2013

Abstract

A vibration isolator, sometimes called an isolating mount, is the device situating between the vibration source and the sensitive system preventing the transmission of undesired disturbances. The performance is measured by the force or the displacement transmissibility, both functions of frequency. A good vibration isolation system has three main properties - a low resonant peak, a large isolation range and low transmissibility at non-resonant regions. Unfortunately, these characteristics cannot be achieved simultaneously by a simple linear vibration isolation system. The thesis addresses this problem for single-degree-of-freedom (sdof) vibration isolation systems by introducing nonlinear damping and stiffness devices into the system. First, theoretical studies were carried out to rigorously reveal the benefits of the proposed nonlinear vibration isolation systems over linear ones. Next, the performance of these nonlinear systems were analysed by simulations. Then, experimental studies were conducted to verify the theoretical and simulations results. Finally, a systematic approach was developed to design the parameters of the nonlinear damping and stiffness devices in order to satisfy specific vibration isolation requirements.

Many vibration isolators can be modelled as a single-degree-of-freedom mass-spring-damper system. Many researchers have attempted to enhance the vibration isolation performance by designing springs with nonlinear stiffness. Others have focused on different types of damping nonlinearities. The new vibration isolation system proposed in the thesis combines both spring and damping nonlinearities in one system to exploit the advantages of both components while avoiding their undesirable effects. The theoretical properties of this proposed nonlinear vibration isolation system were analysed rigorously using the output

frequency response function (OFRF) approach, a novel and unique method recently proposed at Sheffield.

The stiffness nonlinearity is already a well researched area and can readily be realised in practice. Therefore, the implementation of the proposed nonlinear vibration suppression system focused on the realisation of the nonlinear damping component using commercially available magnetorheological (MR) dampers which provide a damping force that is dependent on a control current. With feedback control, the force-velocity relationship of an MR damper can be shaped into a designed function. This implementation has been incorporated first in a vibration isolation system by simulation, then in a physical experimental rig which has a moving mass. The simulation and experimental data not only showed the successful realisation of a damping device with a particular nonlinear damping characteristic, but also confirmed the theoretical findings on the beneficial effects of nonlinear damping on a vibration isolation application.

The final part of the thesis is devoted to the practical design of the proposed vibration isolation system. Given specific transmissibility requirements at certain critical frequencies, the values of the linear parameters are first designed, then the OFRF approach is applied to determine the nonlinear parameters. This pragmatic method simplifies the design of a complicated nonlinear system, which was traditionally difficult to work with, into a step-by-step guide and, therefore, has significant potential of industrial applications.

The thesis has exploited the special effects of two nonlinear components on the performance of a passive sdof vibration isolation system. With the support of theoretical, simulation and experimental studies, the newly proposed configuration has shown substantial benefits to many vibration isolation problems. The simple yet effective design and implementation has significant implications for a wide range of engineering applications such as car suspension designs and building protection against earthquakes.

Acknowledgements

First and foremost, I would like to express my gratitude to my supervisors Prof Zi-Qiang Lang and Prof Stephen A. Billings. Prof Lang has provided tremendous support and guidance during my degree. His insights into the subject and his meticulous approach to research have been a great inspiration to me. Prof Billings has always been incredibly supportive and I have benefited greatly from his advice and encouragement.

Second, I would like to thank Dr Hatim Laalej for his assistance at the initial phrase of the experimental work. The ongoing support from Mr Ian Hammond and Mr Craig Bacon has also been very important.

Third, I would like to give special thanks to the research group at the AGH University of Science and Technology led by Prof Bogdan Sapinski. Their support and their provision of test facilities have contributed to an essential part of the thesis. Mr Marcin Wegrzynowski and Dr Martynowicz Pawel have provided constant support during the experiments. I hope we will have the opportunity to collaborate again in the future.

And finally, I would like to acknowledge the financial support from the Engineering and Physical Science Research Council UK, and the European Research Council.

Contents

List of Figures

Nomenclature

Roman Symbols

A_D	Input displacement amplitude [m]
A_F	Input force amplitude [N]
C	Linear damping constant [Nsm^{-1}]
C_3	Cubic damping constant [$Ns^3\ m^{-3}$]
z	Nonlinear damping constant [$Ns^p m^{-1}$]
f	Input (temporal) frequency [Hz]
F_c	Nonlinear damping force [N]
F_{in}	Input force [N]
F_{out}	Output force [N]
K	Linear spring constant [Nm^{-1}]
K_3	Cubic spring constant [Nm^{-3}]
M	Mass [kg]
ω_0	Resonant frequency [$rads^{-1}$]
$\bar{\omega}$	Input (angular) frequency [$rads^{-1}$]
p	Nonlinear damping exponent

t time [s]

$T_D(\cdot)$ Displacement transmissibility

$T_F(\cdot)$ Force transmissibility

x_{in} Input displacement [m]

x_{out} Output displacement [m]

z Relative displacement [m]

Greek Symbols

Ω Normalised frequency

τ Normalised time

ξ_1 Linear damping coefficient

γ_3 Cubic spring coefficient

ξ_3 Cubic damping coefficient

ξ_p Nonlinear damping coefficient

Chapter 1

Introduction

1.1 Backgrounds of studies

1.1.1 Vibration and vibration control

Galileo was said to be the first to study the characteristics of a simple pendulum toward the end of the sixteenth century. The swinging motion of a pendulum under the restoring force due to gravity is described as oscillatory because of the alternating increases and decreases of displacement. Vibration can be simply described as a back and forth motion, which may occur in free or unforced form as in the pendulum case where no external force is applied after the initial input or in a forced vibration resulting from external excitation, such as the swaying of skyscrapers due to strong wind.

Vibration is certainly a desirable phenomenon in some situations. The generation of sound relies on acoustic vibration, so is the transmission or reproduction of sound in loudspeakers. Without vibration, speech and music cannot be produced. However, in other situations, vibration is seen as a problem that engineers have to contend with. The first chapter of Bishop's book [1979], titled *Vibration: friend or foe*, gives examples of areas where vibration plays an important role but also draws readers' attention to the problematic mechanical vibration that has caused the dramatic collapse of the Tacoma Narrows Bridge in Washington state in 1940. It is therefore of paramount importance to find solutions to eliminate unwanted vibration.

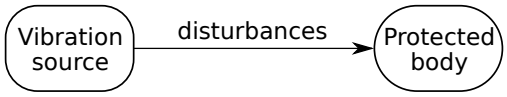

Figure 1.1: Vibration transmission path

Vibration control is becoming more significant in engineering designs due to the rising demand for accuracy, safety and reliability. It is relevant, if not crucial, in many different areas of applications. To protect motor vehicles and their passengers from rapid accelerations and strong pitching and rolling caused by bumpy roads, car suspensions are required to filter out these undesirable inputs. Seismic protection is another obvious area where vibration control is essential to reduce the devastating effects of earthquakes. Vibration due to human activities also requires attention in many structural designs. The London Millennium Footbridge was closed immediately after its opening in 2000 because of the unexpected lateral movements exacerbated by a large number of pedestrians walking with an unconscious tendency to synchronise their steps [Dallard *et al.*, 2001]. Although there may not be any real safety concerns, floor vibration in buildings caused by the occupants has a serviceability issue as human's sensitivity to vibration could be as low as 0.001 mm [Allen, 1990; Bachmann, 1995].

In applications where high precision is required, vibration control becomes a fundamental part of the design. Developed for a range of scientific disciplines, such as high resolution imaging, the high velocity electron beam at the Diamond Synchrotron Light in Oxfordshire is required to be within 0.6 μm RMS in the vertical plane [Napier *et al.*, 2011]. Modern technologies, led by miniaturisation trend in electronic industry, strengthens the need of vibration control. In other applications, the overlook of the potential problems of vibration may bring excessive wear and damage to the equipments and affect their reliability and durability.

The source of vibration exists in many different forms. Fig. 1.1 represents the transmission of vibration from the source to the protected body. Mechanical vibration inputs, usually displacement, acceleration, force or torque, may be a single-tone sinusoidal signal or may contain many frequency components. They may could also be random. The aim of vibration control is to minimise the effects of these signals on the protected body and this is usually achieved by one of

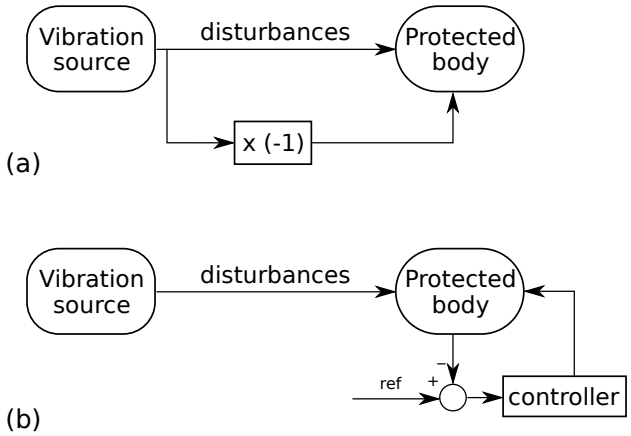

Figure 1.2: Active vibration control (a) noise cancellation (b) feedback control

the following methods - (a) active control (b) passive control and (c) semi-active control.

The concept of active vibration control, first proposed by Lueg [1936], involves attenuating the disturbance by a cancelling signal. This method, depicted by Fig. 1.2(a), depends on the accurate measurement of the disturbance signal so that an anti-signal can be applied to counteract the effects of the original disturbance. Normally achieved by analogue circuits or digital signal processing, the active noise cancellation technique is popular in reducing low frequency audio noise. Another active method is feedback control as shown in Fig. 1.2(b). In a mechanical system, based on the error between the desire reference signal, usually displacement, and the actual measurement, the controller applied a controlled signal to the plant via actuators. To produce a satisfactory result, the controller design is dependent on the modelling of the plant, the sensors and the actuators whereas poor designs may cause instability. Active vibration control offers a flexible solution as the characteristics of the applied signal can be adjusted accordingly when the operating condition changes but its performance may be hindered by the accessibility of the disturbance and the quality of the actuators.

In contrast to active control, the passive method does not draw any external power so does not affect the system stability. Because of the relatively low cost of implementation and its inherent stability, passive vibration control methods are preferable to active control in some applications, particularly when the

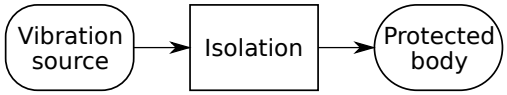

Figure 1.3: Passive vibration control.

noise contains mainly high frequencies [Rivin, 2003]. Active methods therefore are rarely employed if the passive design produces satisfactory results. The diagram in Fig. 1.3 shows the concept of vibration isolation, which is a type of passive control. It can be viewed as a device installed in the vibration transmission path between the source and the plant. Rubber engine mounts is a type of vibration isolation.

1.1.2 Vibration isolation and transmissibility

In the simplest case, a vibration isolator can be modelled as a mass-spring-damper model where the stiffness and the damping forces are linear functions of displacement and velocity respectively, as illustrated by Fig. 1.4. Such single-degree-of-freedom (sdof) system with mass M, stiffness K and damper C could also represent the dynamics of a simple pendulum for small oscillation amplitude. Well studied by a large number of authors , this basic linear system is a natural starting point for vibration isolation analysis [Crede, 1951; Mead, 1999; Rivin, 2003; Snowdon, 1968, 1979; Thureau *et al.*, 1981; Vernon, 1967]. Fig. 1.4 represents a displacement vibration isolator when it is excited by an input displacement $x_{in}(t)$ aiming to minimise the output $x_{out}(t)$. It can also be the model of a force vibration isolator when driven by an input force $F_{in}(t)$ trying to reduce the output $F_{out}(t)$.

In order to compare the quality of vibration isolation, a common performance metric is called the displacement or force transmissibility. For an isolator under a single-tone sinusoidal input, its transmissibility T, a function of the excitation frequency, is defined as the ratio of the output amplitude to the input amplitude. i.e. $|x_{out}(t)|/|x_{in}(t)|$ or $|F_{out}(t)|/|F_{in}(t)|$. An ideal vibration isolation system would give $T = 0$ meaning that all vibration inputs are totally blocked, but, in reality, T indicates the proportion of the input vibration transmitted across the vibration isolator, so a smaller T is always preferable.

Fig. 1.5 shows the relationship between the excitation frequency and T of a sdof System (i), a typical linear vibration isolator. Some notable features of the trans-

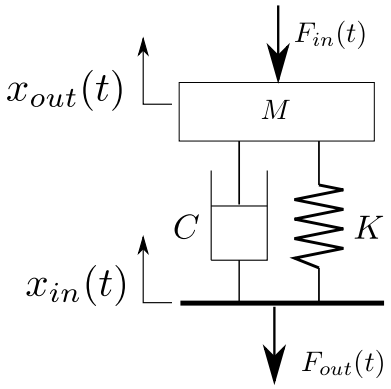

Figure 1.4: A mass-spring-damping system representing a vibration isolation

missibility curve of a sdof system are the low frequency transmissibility starting at 0 dB, the resonance at which maximum transmissibility occurs and the cut-off frequency where isolation begins. The transmissibility over frequencies higher than the resonant frequency is important too. System (ii) with its transmissibility also shown in Fig. 1.5 is a hypothetical vibration isolator that has a lower transmissibility than System (i) for all excitation frequencies and is therefore a superior system. In addition to a lower resonant peak, System (ii) has a lower cut-off frequency that provides a larger frequency range of isolation.

Unfortunately, it is not possible to improve the performance of System (i) to match that of System (ii) by varying one or all of the three linear systems parameters, M, K and C. M and K can only determine the resonant frequency. The size of the resonance can be reduced by increasing C but this has a side effect of raising the transmissibility over the high frequencies. These are the well-known properties of linear damping [Crede, 1951]. To create a high performance vibration isolation system that behaves like System (ii), one option is to use nonlinear vibration systems.

To overcome the limitations of linear vibration isolation systems, many engineers have successfully modified the transmissibility properties by introducing stiffness nonlinearities as described in a review paper by Ibrahim [2008]. Stiffness nonlinearity influences the shape of the transmissibility curve and the resonant frequency. It is known that springs with a softening nonlinearity reduce the resonant frequency resulting in a larger isolation range while hardening springs have the

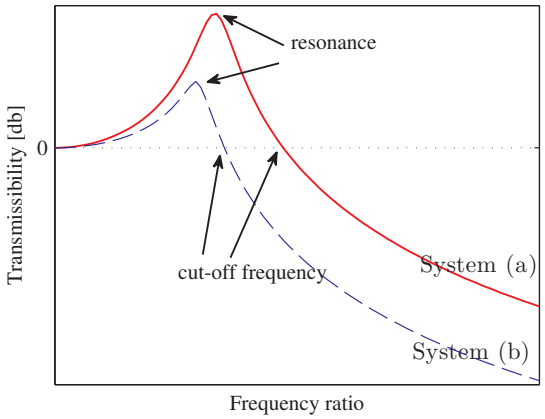

Figure 1.5: Transmissibility curves. Solid: a typical linear vibration isolator; Dashed: a hypothetical vibration isolatior.

opposite effects [Kolovsky *et al.*, 1999; Ravindra & Mallik, 1994a]. Although the results of the introduction of stiffness nonlinearity is welcoming in many situations, especially where low frequency vibration is of concern, nonlinear system are more difficult to analyse and design as the output frequency content is much richer than the input in the nonlinear case. When excited by a single-tone sinusoid, the output of a linear system is also a single-tone sinusoid that has a different amplitude and phase. Whereas the output of a nonlinear system may contain subharmonics and superharmonics of the excitation frequency and chaotic motion may occur under certain conditions. The jump phenomena may also appear which is described as a discontinuity in the frequency response where a large change in the output amplitude can be produced by only a small change in the input frequency.

Besides the benefits of including nonlinear stiffness, Ravindra & Mallik [1994a] have suggested nonlinear viscous damping as an alternative way to improve the performance of a vibration isolation system. It was found that a damping force that is proportional to the power of the relative velocity has a significant effect on the resonance. When the power of the nonlinearity is suitably chosen, it is possible to suppress the resonance with negligible effects on other frequency regions. This provides a good solution to the dilemma regarding the detrimental effects of linear damping over the high frequency region. Another interesting property of

nonlinear damping is its influence on the jump phenomena introduced by a nonlinear stiffness. Like linear damping, the jumps can be completely eliminated by a sufficient level of nonlinear damping. Except the addition of harmonics to the system outputs, nonlinear damping preserves the advantages of linear damping while overcomes its weaknesses.

1.1.3 Analysis of nonlinear vibration isolators

There are a number of analysis approaches for nonlinear systems. Most methods start with an assumption of the solution of a particular form with parameters to be found. For example, the perturbation method assumes the solution to be a polynomial sum of a small parameter with coefficients that are functions of time [Nayfeh & Corporation, 1973]. The more mainstream technique is the method of harmonic balance which lets the solution be a truncated Fourier series, the coefficients of which can be found by a set of simultaneous equations obtained by equating the amplitude of the each harmonic in the equation of motion. As the number of simultaneous equations increases with the terms of the Fourier series, it is common to simplify the calculation by assuming the solution to be just a single-tone sinusoid. The harmonic balance method is particularly useful when the input is a pure sinusoid.

For nonlinear vibration isolation systems, the transmissibility is the amplitude of the steady-state fundamental output harmonic divided by that of the input. The simultaneous equations found by the harmonic balance method may be reduced to one high degree equation that is an implicit expression relating the transmissibility, the excitation frequency and all system parameters. From this implicit equation, it is difficult, if not impossible, to obtain an expression for the transmissibility as a function of frequency, or as a function of the system parameters. Without a direct relationship between the transmissibility and the system parameters, the effects of a particular parameters on the transmissibility function is unclear.

Recently, a new frequency domain method based on a Volterra series model developed by Lang *et al.* [2007] provides a good alternative to the harmonic balance method. The output frequency response function (OFRF) defines an explicit relationship between the output spectrum and the parameters which define the

nonlinearity of Volterra systems for a given input and fixed values for the linear terms. When applied to a nonlinear vibration isolation system, the OFRF is a polynomial expression of the transmissibility in terms of the nonlinear stiffness and/or damping parameters. The polynomial coefficients depend on the excitation frequency. This concept facilitates the understanding of how the nonlinear parameters affects the vibration isolation performance so is very useful for the design of nonlinear systems. Lang *et al.* [2009] later applied the OFRF concept to the analysis of cubic viscous damping and provided a rigorous theoretical proof for the results of Ravindra & Mallik [1994a] obtained by the harmonic balance method.

Given the advantages of nonlinearities in vibration isolation systems, the instinctive question which arises is how those theoretical nonlinear forces can be realised and implemented for practical applications. Stiffness nonlinearity naturally exists in some structures but a number of measures may be used to deliberately introduce spring nonlinearity into a system. Ibrahim [2008] have reviewed a range of nonlinear passive vibration isolators, including the use of magnetic force and special geometrical arrangement of cantilever beams.

The realisation of nonlinear viscous damping is less straightforward but is enabled by the continual development of semi-active devices such as controllable-fluid dampers, namely electrorheological (ER) dampers and magnetorheological (MR) dampers. The viscosity of the fluid inside these dampers can be changed by a supply current. The work of Sims *et al.* [1999, 2000] on ER dampers has demonstrated that the force-velocity relationship can be reshaped by a feedback control loop implemented on the ER dampers. The proposed proportional-integral controller adjusts the output force of the damper by controlling the current supplied to the damper such that a particular nonlinear viscous damping characteristic can be created. These results have paved the way for the realisation of a vibration isolation system with a nonlinear damping force.

Given the importance of vibration isolation and all the existing techniques and solutions mentioned above, this thesis aims to further develop some of the nonlinear concepts to provide a deeper understanding of their properties and improve the performance and design of vibration isolation systems.

1.2 Aims and objectives

The general idea of vibration control focusing on passive vibration isolation has been introduced in the previous section. By exploring different types of nonlinearities, the recent developments have achieved great progress in improving the vibration isolation performance of a basic linear vibration isolator. Despite these accomplishments, there are still a number of important issues of vibration isolation that needs addressing.

The performance of vibration isolation systems with stiffness and damping nonlinearities have been studied. Nonlinear systems are known for producing outputs with a rich frequency content. One problem of current analysis methods that are based on an output approximation is oversimplification. To find an accurate solution that can capture these much richer output frequency characteristics, it is necessary to approximate the output with a more complicated function. This however leads to inefficient computation and sometimes solutions cannot be found. As a result, there is a tradeoff between accuracy and computational efficiency.

Most analysis methods based on an output approximation only provide an implicit relationship between the nonlinear parameters and the vibration isolation performance measured by the force or displacement transmissibility. A direct relationship between the nonlinear parameters and the transmissibility cannot be deduced. To see the effects of the nonlinear terms on the transmissibility, it is often resorted to graphical examination of the numerical solutions of the implicit relationship. This provides an indication of the characteristics of the nonlinear vibration systems but lacks a solid theoretical support.

The nonlinear stiffness can be implemented by various means to confirm the theoretical findings but there are few publications on the practical verification of the theoretical effects of nonlinear damping on vibration isolation. The results of Sims *et al.* [1999, 2000] focused on the damper force control without incorporating it into a vibration isolation system. Experimental confirmation of the performance of vibration isolators with nonlinear viscous damping is needed before such concept can be widely adopted.

The final element missing from a comprehensive nonlinear vibration isolation study is a systematic design method. Currently, various methods can be used to

find the transmissibility curve for given values of systems parameters. Without a direct formulation of the transmissibility in terms of the system parameters, the system parameters design for specific transmissibility requirements becomes a trial and error process, which may be speed up by a more systematic iterative search algorithms.

Motivated by the above mentioned issues, the work in this thesis aims to address these shortfalls in order to achieve the following objectives.

- To obtain an analytical expression of the force and displacement transmissibility of a nonlinear single-degree-of-freedom vibration isolation system in terms of the nonlinear stiffness and damping parameters.

- To conduct a rigorous theoretical analysis on the effects of nonlinear stiffness and damping forces on the performance of a nonlinear vibration isolation system.

- To find the damping characteristic that would improve the transmissibility of a vibration isolator over a wide frequency range.

- To conduct simulation and experimental studies on the implementation of nonlinear damping using a magnetorheological damper under a feedback damping force control.

- To verify the theoretical properties of nonlinear damping by experiments.

- To provide a systematic design method for the system parameters of a nonlinear vibration isolator according to specified requirements in the frequency domain.

These aims and objectives will be achieved through a number of stages, starting from analytical studies of the force and displacement transmissibilities of a nonlinear vibration isolation system, then validation by simulation and experiments and finally a systematic design method of a high-performance nonlinear vibration isolation system.

1.3 Thesis outline

Following the introduction, a review of relevant literatures is provided in Chapter 2. The original contributions are presented in Chapters 3 to 6 and conclusions are given in Chapter 7. A brief summary of each chapter is provided below.

Chapter 2 covers a literature review on vibration control. It begins with a description of a basic linear vibration isolator and its weaknesses, followed by discussions on the effects of nonlinear stiffness and nonlinear viscous damping. The common analysis methods for nonlinear systems are reviewed with special focus on the application of the OFRF based approach for vibration control system analysis. Additionally, semi-active vibration control devices and their control are discussed.

Chapter 3 is a theoretical study on a force vibration isolation system that has both stiffness and damping nonlinearities. Using the OFRF approach, an analytical expression of the force transmissibilities of a nonlinearly damped Duffing system is obtained for the theoretical analysis of the effects of the nonlinear parameters. The theoretical results, supported by simulation, show that a cubic nonlinear damping characteristic is beneficial to a Duffing-type system as it has the ability to suppress the resonance without causing detrimental effects in other frequency regions.

The structure of Chapter 4 is very similar to that of Chapter 3. While Chapter 3 is concerned with the force transmissibility, Chapter 4 studies how damping nonlinearity affects the displacement transmissibility. A general expression of the displacement transmissibility of a vibration isolation with the nonlinear damping force as a power function of the relative velocity is deduced using the OFRF approach. Then, the comparison of the performance of systems that have different nonlinear damping exponent over two frequency regions is performed to reveal that a small nonlinear damping exponent is beneficial.

Simulation and experimental studies of nonlinear vibration isolation systems are presented in Chapter 5. Semi-active magnetorheological dampers under a closed-loop control is developed to provide an appropriate nonlinear viscous damping characteristic. The practical realisation of the ideal nonlinear damping characteristic is incorporated into a force and a displacement vibration isolation system

respectively to verify the theoretical results in Chapters 3 and 4.

Chapter 6 presents a novel systematic method of designing nonlinear vibration isolation system according to given transmissibility requirements. Under the stringent requirements of a low resonant peak, a low cut-off frequency and a low high-frequency transmissibility, the parameters of a force vibration isolation system with nonlinear viscous damping and nonlinear stiffness are designed with the aid of the OFRF estimation technique. The outcome of the design procedure is a high performing nonlinear vibration isolation system that produces better a vibration isolation than a basic linear system for the whole frequency range. The systematic design approach is not only applicable to vibration isolator design but also to a wider range of nonlinear systems.

Finally, conclusions are given in Chapter 7. The significance of the results in the thesis are highlighted as well as some suggestions for future developments.

1.4 Publications by the author

Some of the research results in this thesis have been presented at conferences and published in journals, while some have been submitted to a journal for review. The complete list is given below.

Conferences

- Ho, C., Lang, Z. Q., & Billings, S. A. (2012, September). The benefits of nonlinear cubic viscous damping on the force transmissibility of a Duffing-type vibration isolator. In *Control (CONTROL), 2012 UKACC International Conference on* (pp. 479-484). IEEE.

- Ho, C., Lang, Z. Q., Billings, S. A., & Sapinski, B. (2013, May). Simulation study of a vibration isolation system with nonlinear damping implemented by an MR damper. In *Carpathian Control Conference (ICCC), 2013 14th International* (pp. 117-122). IEEE.

Journals

- Ho, C., Lang, Z. Q., Sapinski, B., & Billings, S. A. (2013). Vibration isolation using nonlinear damping implemented by a feedback-controlled MR damper. *Smart Materials and Structures*, **22**, 105010.

- Ho, C., Lang, Z. Q., & Billings, S. A., A frequency domain analysis of the effects of nonlinear damping on the Duffing equation. *Mechanical systems and signal processing*, accepted for publication (available online).

- Ho, C., Lang, Z. Q., & Billings, S. A., Design of vibration isolators by exploiting the beneficial effects of stiffness and damping nonlinearities. *Journal of Sound and Vibration*, submitted for review.

Chapter 2

Linear and nonlinear vibration control systems

2.1 Introduction

A vast amount of literature has been attributed to active vibration control. Some books focusing on this topic includes [Fuller *et al.*, 1996; Preumont, 1999; Soong, 1990; Tokhi & Veres, 2002]. Active control cancels or reduces the unwanted disturbances by adding signals, using a wide variety of actuators, to produce the opposite affects. These strategies require external power and depend on the observability and controllability of the plant. Therefore, Housner *et al.* [1997] has suggested that passive control is more suitable in situations where the external power source is not reliable in a review of many active and passive structural control methods. As passive control includes devices such as springs and dampers to alter the dynamic response of a plant instead of using a feedback control loop, it may be viewed as a plant redesign. The difference between active and passive control in structural protection has been also studied by Soong & Costantinou [1994] and more recent active and passive control designs have been reviewed by Soong & Spencer Jr [2002]. Other works on passive vibration control include [Mead, 1999; Takewaki, 2011]. Passive control solutions are inherently stable and more robust as they do not rely on the real time measurements.

Another type of vibration control approach is known as semi-active control.

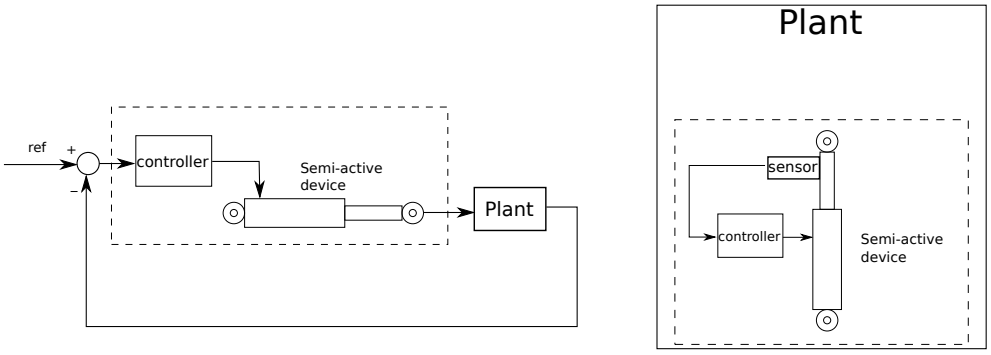

(a) Active control (b) Passive control

Figure 2.1: Semi-active device in (a) active control (b) passive control

Like active control, it requires external energy input but does not add mechanical energy to the plant. The stability of passive control has been preserved yet some flexibility offered by active control method can still be exploited. Many passive devices with variable settings are viewed as semi-active control devices. They can form part of the feedback control loop like an actuator in the active control case as depicted in Fig. 2.1(a) or can become part of the plant as in the passive control case in Fig. 2.1(b).

This chapter will first provide an overview of passive vibration isolation systems, starting with a basic linear single-degree-of-freedom system. Then, the effects of nonlinear stiffness and nonlinear viscous damping on the vibration isolation performance, together with their analysis methods, will be discussed. One very important technique for analysing nonlinear systems, called the output frequency response function, will then be presented. Finally, different uses of magnetorheological(MR) dampers in practical semi-active vibration control will be introduced before the summary.

2.2 Linear vibration isolation system

A basic vibration isolation system is a single-degree-of-freedom (sdof) mass-spring-damper system. In the simplest case, the stiffness and the damping constants are linear functions of displacement and velocity respectively. Fig. 2.2(a) shows a force vibration isolation system and Fig. 2.2(b) shows a displacement vibration isolation

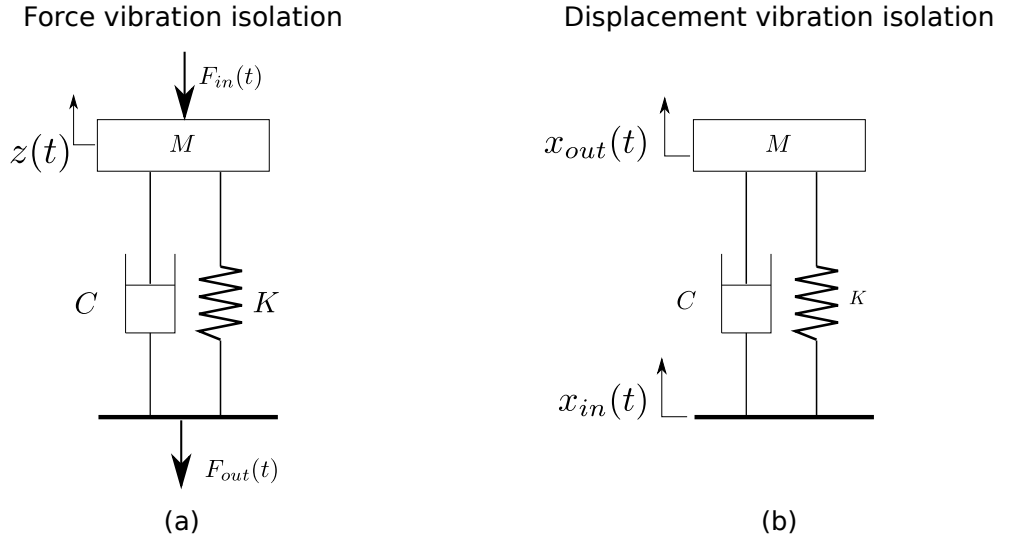

Figure 2.2: (a) A linear force vibration isolation system (a) a linear displacement vibration isolation system

system. These two types of basic linear systems, well studied by a large amount of authors [Crede, 1951; Mead, 1999; Rivin, 2003; Snowdon, 1968, 1979; Thureau *et al.*, 1981; Vernon, 1967] is a natural starting point for the study of passive vibration isolation.

Under a single-tone sinusoidal force input $F_{in}(t)$ with amplitude A_F and frequency $\bar{\omega}$, the dynamics of the force isolation system in Fig. 2.2(a) can be expressed as

$$\begin{cases} M\ddot{z}(t) + C\dot{z}(t) + Kz(t) = F_{in}(t) = A_F \sin(\bar{\omega}t) \\ F_{out}(t) = C\dot{z}(t) + Kz(t) \end{cases} \tag{2.1}$$

where M is the mass, K is the linear spring constant, C the linear viscous damping constant, $z(t)$, $\dot{z}(t)$ and $\ddot{z}(t)$ are the displacement, velocity and acceleration of the moving mass respectively. The vibration isolation performance of System (2.1) is measured by the ratio of the output force amplitude to the input force amplitude known as the force transmissibility. In terms of the normalised frequency $\Omega = \frac{\bar{\omega}}{\omega_0}$, where

$$\omega_0 = \sqrt{\frac{K}{M}} \tag{2.2}$$

the force transmissibility denoted by $T_F(\Omega)$ is represented by

$$T_F(\Omega) = \sqrt{\frac{1 + (\xi_1 \Omega)^2}{(1 - \Omega^2)^2 + (\xi_1 \Omega)^2}} \tag{2.3}$$

where

$$\xi_1 = \frac{C}{\sqrt{KM}}. \tag{2.4}$$

Eq. (2.3) clearly shows that the force transmissibility function is only affected by the linear damping ratio ξ_1, which creates a major limitation on the design of a force vibration isolation system. In Fig. 2.3, the force transmissibility function given by Eq. (2.3) is plotted for different ξ_1. Each curve has three features that are most important for the vibration isolator design - the height of the resonant peak at $\Omega \approx 1$, the high frequency transmissibility where Ω is much larger than 1, and the cut-off frequency where the vibration isolation starts. A large damping ratio is necessary for the reduction of the resonant peak, but this leads to an undesirable rise in the high frequency transmissibility as indicated by the arrows in the figure. At $\Omega = \sqrt{2}$, all curves intersect at $T_F(\Omega) = 1$ indicating this is the cut-off frequency and the frequency cannot be altered by changing ξ_1.

For a displacement vibration isolator represented by a sdof system in Fig. 2.2(b), the equation of motion is given by

$$M\ddot{z}(t) + Kz(t) + C\dot{z}(t) = -M\ddot{x}_{in}(t) \tag{2.5}$$

where M is the mass, K is the spring stiffness, C is the linear damping constant, $z(t) = x_{out}(t) - x_{in}(t)$ is the output displacement relative to the input and $x_{in}(t)$ is a sinusoid with amplitude A_D and frequency $\bar{\omega}$. To measure the quality of the vibration isolation of System (2.5), the absolute displacement transmissibility $T_D(\Omega)$ is defined as the ratio of the output displacement amplitude to the input displacement amplitude. Although the equation of motion of a force vibration isolation system in Eq. (2.1) is different from that of a displacement vibration isolation system in Eq. (2.5), it can be shown that the displacement transmissibility of System (2.5), the amplitude ratio of $x_{out}(t)$ to $x_{in}(t)$, is identical to the force

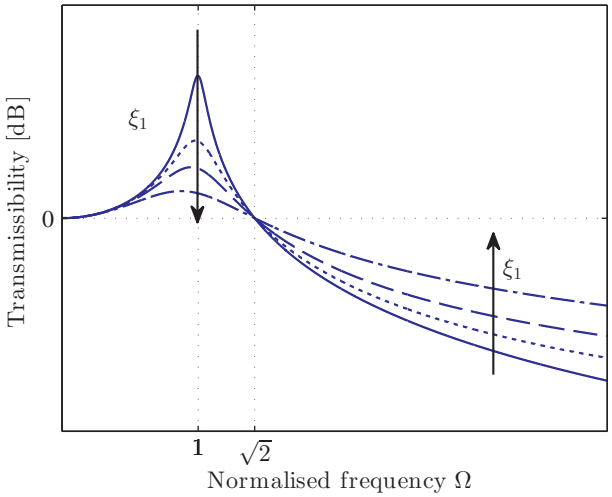

Figure 2.3: Transmissibility of a linear vibration isolation where $\xi_1 = 0.1$ (solid), 0.3 (solid), 0.5 (dashed), 0.9 (dot-dashed).

transmissibility of System (2.1) given that they have the same damping ratio, that is

$$T_D(\Omega) = T_F(\Omega) = \sqrt{\frac{1 + (\xi_1\Omega)^2}{(1-\Omega^2)^2 + (\xi_1\Omega)^2}}. \tag{2.6}$$

Therefore, the transmissibility curves in Fig. 2.3 also represent the displacement transmissibility of System (2.5).

Linear vibration isolation systems, either for force reduction or for displacement reduction, are straightforward to design and to implement. Their vibration isolation performance solely relies on the choice of the damping ratio which has opposite effects on the transmissibility curve over two different regions. The height of the resonant peak falls with an increase of the damping ratio, but this leads to the rise of transmissibility over higher frequencies. Another special property of linear vibration isolation systems is that the cut-off frequency is fixed at $\Omega = \sqrt{2}$ for all ξ_1.

An ideal vibration isolation system should have low transmissibility across the whole frequency range. This general goal can be broken down into three specific

requirements - a low resonant peak, low high-frequency transmissibility and a low cut-off frequency. Because of the limitations of linear force or displacement vibration isolation systems mentioned above, these requirements cannot be achieved simultaneously by simply changing the linear damping ratio. Consequently, spring and damping nonlinearities are introduced to improve the vibration isolation performance.

2.3 Nonlinear vibration isolation systems

2.3.1 Nonlinear stiffness

The nonlinear strategies can be broadly divided into two categories, the first of which is the introduction of stiffness nonlinearities. Ibrahim [2008] has provided an extensive review on recent developments of nonlinear vibration isolation systems ranging from base isolation of structures to isolator material design. Most of the studies have focused on the reduction of the isolator's natural frequency by using various types of springs such as the cantilever spring [Ju & Blair, 1994] and the highly deformed continuous elastic beam spring [Virgin *et al.*, 2008]. Another simpler yet effective method involving nonlinear stiffness, proposed by Alabuzhev *et al.* [1989], is the installation of auxiliary springs to achieve a quasi-zero stiffness. An illustration is provided in Fig. 2.4. Carrella *et al.* [2009] later showed that this type of nonlinear system lowers the natural frequency and increases the isolation range as a result.

Most of the above mentioned systems can be modelled by the Duffing equation, the most general form of which is given by

$$\ddot{y}(t) + \alpha_1 \xi_1 \dot{y}(t) + \alpha_2 y(t) + \alpha_3 [y(t)]^3 = \beta \sin(\bar{\omega} t) \tag{2.7}$$

where α_1,α_2,α_3 and β are constants, and $\alpha_3[y(t)]^3$ is the nonlinear restoring force. When $\alpha_3 > 0$, Eq. (2.7) is known as the hardening Duffing system as the resonant peak is bent towards the high frequency. Duffing himself gave a few examples relating to the motion of a pendulum and an electrical circuit [Duffing, 1918]. More examples including beams with nonlinear stiffness and nonlinear cable vibrations

are explained in Kovacic & Brennan's book [2011]. To understand the chaotic dynamics caused by the nonlinear stiffness term in the Duffing equation, researchers are challenged to consider a range of nonlinear system analytical and numerical methods. The common approach is to use an analytical method, such as perturbation methods [Bush, 1992; Nayfeh & Corporation, 1973; Senator & Bapat, 1993; Yu & Leung, 2003] or harmonic balance methods [Genesio & Tesi, 1992; Hu & Tang, 2006; Liu *et al.*, 2006; Mickens, 1984, 1986; Schmidt & Tondl, 1986], which approximates the system output by a particular form of function.

For example, the harmonic balance method assumes the output to be a truncated Fourier series, such as

$$y(t) = \sum_{q=1}^{Q} a_q \cos(q\bar{\omega}t) + \sum_{q=1}^{Q} b_q \sin(q\bar{\omega}t). \tag{2.8}$$

After substituting Eq. (2.8) into Eq.(2.7) and expanding all the terms, a set of $2Q$ simultaneous equations can be found by equating the coefficients of the sine and cosine terms, assuming that the output does not have a DC component. These simultaneous equations are implicit functions that relate a_q, b_q, $\bar{\omega}$, β and the system parameters α_1,α_2 and α_3. To simplify the calculation, Q, the order of Fourier series approximation, is usually rather small so that higher harmonics are ignored. In the common case where only the fundamental harmonic is considered, $Q = 1$ and the result is reached by using the approximations such as

$$\sin^3(\bar{\omega}t) = \frac{1}{4}\left[3\sin(\bar{\omega}t) - \sin(3\bar{\omega}t)\right] \approx \frac{3}{4}\sin(\bar{\omega}t). \tag{2.9}$$

For systems with strong nonlinearities, higher harmonics terms, e.g. $\sin(3\bar{\omega}t)$ and $\sin(5\bar{\omega}t)$ must be included in order to obtain a more accurate results.

The harmonic balance method is the most popular and also a very powerful tool in analysing certain behaviours of a Duffing system. At the jump-up or jump-down frequency, the output of a Duffing system changes drastically when there is a small change in the excitation frequency. Based on the harmonic balance approach, Brennan *et al.* [2008] have provided a good summary of the calculations of these jump frequencies of a lightly damped Duffing oscillator and Kovacic *et al.* [2008] have also studied the resonance response of a Duffing system without the

linear stiffness term.

Although not very mathematically rigorous, the harmonic balance approach provides outline sketches of nonlinear systems. The accuracy could be greatly improved by including the second harmonics [Mickens, 2010]. As more high harmonics are included, the number of harmonic coefficients increases and so does the number of balancing equations. Using the Duffing equation in Eq. (2.7) as an example, the harmonic balance method gives a set of four simultaneous equations containing cubic power terms of a_1,a_3,b_1 and b_3 when $Q = 3$. A detailed example can be found in [Peng *et al.*, 2008].

Not only the number of simultaneous equations increases with Q, the order of the power terms also increase. These equations then become tedious, sometimes difficult to solve, particularly when the system has more than one nonlinear term or has a higher degree of freedom. To find the final solutions, it is often resorted to numerical methods [Chen & Liu, 2007; Hayashi *et al.*, 1964; Lim & Wu, 2003; Lim *et al.*, 2006; Nayfeh & Mook, 1995; Peleg, 1979; Potts, 1981, 1982; Wu *et al.*, 2003].

Aiming to improve the efficiency of a high order harmonic balance method, some algorithms have been developed to simplify the calculation. MacDonald [1993] have compared two different methods, preliminary rationalization and obtaining Fourier coefficients by integration, when applying the harmonic balance method to different types of nonlinear systems. The strengths of these methods depend on the system type but it also found that the results for a system with fifth order nonlinearity were not satisfactory. Later, a new formulation of the harmonic balance method developed by Thomas *et al.* [2002] and Hall *et al.* [2002], named the high dimensional harmonic balance method, was introduced to improved computational efficiency [Liu *et al.*, 2006]. Lim & Wu [2003] have reduced the complexity by combining the harmonic balance method with linearisation.

Apart from the harmonic balance methods, two alternative groups of methods that calculate approximations to steady-state periodic solutions are explained in detail in [Mickens, 2010]. One is the parameter expansion, a type of perturbation method where a systems parameter is represented by a series expansion of another parameter the formulation of which requires skills and experience [He, 2002, 2006; Mickens, 1999; Senator & Bapat, 1993]. The other types are the direct and ex-

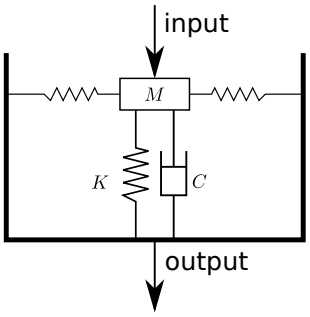

Figure 2.4: Nonlinear vibration isolator with auxiliary springs

tended iteration techniques which involve breaking down a nonlinear problem into a sequence of linear ones in small time steps [Lim & Wu, 2002; Mickens, 1987, 2005]. These methods cannot capture the transient solution so systems that possess limit cycles should be studied using the averaging methods instead. All these techniques, including the averaging methods which can be used to find transient solutions [Bogoliubov, 1961; Cveticanin, 2009; Krylov & Bogoliubov, 1947], provided better understanding of nonlinear vibration problems but they may be less intuitive when applied to parameter design, particularly when the system has high level of nonlinearity.

2.3.2 Nonlinear damping

The second type of nonlinear vibration isolation system analysis approaches focuses on the damping nonlinearities. While a spring, be it linear or nonlinear, provides a restoring force, damping removes energy from the system and hence is crucial to the vibration isolation performance.

The concept of nonlinear damping was first introduced in 1971 by Ruzicka & Derby [1971]. A vibration isolator with a damping force that is proportional to the velocity raised to an arbitrary power has been studied. The results show that it is possible to reduce the resonance without causing detrimental effects on the high frequency transmissibility, which overcomes the limitation of a linear vibration isolation system. Hundal [1981] have studied the response of a shock isolator that has a standard linear spring in parallel with a quadratic damper under a base acceleration excitation of rectangular pulses, and have found that the optimum quadratic

damping ratio depends on the pulse durations. Ravindra & Mallik [1993] later studied the effects of Coulomb damping on a hardening Duffing-type system and then showed that nonlinear viscous damping can completely eliminate the chaotic responses caused by the nonlinear spring [Ravindra & Mallik, 1995]. Using the perturbation method, Chandra Shekhar *et al.* [1998] have concluded that the displacement transmissibility is worsened by cubic damping, which is later confirmed by Milovanovic *et al.* [2009] using the harmonic balance method. Chandra Shekhar *et al.* [1999] have extended their studies to the effects of nonlinear damping on different types of vibration isolators and shock absorbers. It is also worth noting that natural inherent nonlinear damping characteristics in structures have been studied by Jeary [1996].

All the above mentioned results are based on various output approximation methods and numerical methods. In 2009, Lang *et al.* [2009] use a Volterra based method to analytically demonstrate the effects of cubic damping on the force transmissibility of a sdof vibration isolation system and the conclusions are consistent with the previous studies. This work is very important to future studies of nonlinear vibration isolation systems as the rigorous theoretical techniques, which will be detailed in the following section, were applied for the first time.

2.4 Output frequency response function approach

A general background of frequency domain analysis method based on the Volterra series model will be described, followed by its application to the nonlinear vibration isolation systems.

2.4.1 Generalised frequency response function

In contrast to linear systems, transferring energy between frequencies is a key property of nonlinear systems. When excited by a sinusoidal signal, a nonlinear system, in general, produces an output consisting of harmonic frequency components as well as the fundamental frequency component of the input signal. If the input is multi-tone, for example $A\sin\omega_1 t + B\sin\omega_2 t$, the output may contain the fundamental frequencies ω_1, ω_2 plus their harmonics $n\omega_1$, $n\omega_1$ and also some com-

binational frequencies such a $\omega_1 + \omega_2$ and $\omega_2 - \omega_1$. In order to relate the input and the output of a nonlinear system, Vito Volterra developed an expression for a nonlinear model in the late 1880s

Similar to a Taylor series where a nonlinear function is expressed as a power series, a Volterra series represents the output of a nonlinear system as a sum of convolution integrals [Maia *et al.*, 1997; Rugh, 1981; Schetzen, 1980]. A memoryless nonlinear function, whose output at time t is a function of the input at time t but not its history, can be expressed by a Taylor series which is a polynomial sum of the input.

$$y(t) = \sum_{n=0}^{\infty} c_n u^n(t) \tag{2.10}$$

A linear and causal system with memory is given by a convolution of the impulse response $h(t)$ and the input signal $u(t)$.

$$y(t) = \int_{-\infty}^{\infty} h(\tau) u(t-\tau) d\tau \tag{2.11}$$

The Volterra series combines equations (2.10) and (2.11) to approximate about a neighbourhood of the zero equilibrium nonlinear systems that are causal and have fading memory [Boyd & Chua, 1985] as follows.

$$y(t) = \sum_{n=1}^{\infty} \int_{-\infty}^{\infty} \cdots \int_{-\infty}^{\infty} h_n(\tau_1, \ldots, \tau_n) \prod_{i=1}^{n} u(t-\tau_i) d\tau_i \tag{2.12}$$

where $h_n(\tau_1, \ldots, \tau_n)$ is the n-th order impulse response called the Volterra kernel. A linear system described by Eq. (2.11) is a special case of the generalised equation (2.12) where all $h_n(\tau_1, \ldots, \tau_n)$'s are zero except when $n = 1$. Eq. (2.12) is an infinite sum of all high order impulse responses and an Nth order nonlinear Volterra system can therefore be written as

$$y(t) = \sum_{n=1}^{N} \int_{-\infty}^{\infty} \cdots \int_{-\infty}^{\infty} h_n(\tau_1, \ldots, \tau_n) \prod_{i=1}^{n} u(t-\tau_i) d\tau_i. \tag{2.13}$$

It is well known that signals in the time domain can be converted into the

frequency domain by Fourier transform. Convolution in the time domain is equivalent to multiplication in the frequency domain. A familiar form of Eq. (2.11) in the frequency domain is given by

$$Y(j\omega) = H(j\omega)U(j\omega) \tag{2.14}$$

where $U(j\omega)$ and $Y(j\omega)$ are the system input and output spectra, the Fourier transforms of the input $u(t)$ and output $y(t)$ in the time domain respectively. $H(j\omega)$, the system frequency response function, is the Fourier transform of the impulse response $h(t)$.

$$H(\omega) = \int_{-\infty}^{\infty} h(t)\ e^{-2\pi j\omega t}\, dt, \tag{2.15}$$

By using multi-dimensional transformations, George [1959] applied the convolution theorem to the kernels of a nonlinear system and obtained the nth order generalised frequency response function (GFRF)

$$H_n(j\omega_1, \ldots, j\omega_n) = \int_{-\infty}^{\infty} \cdots \int_{-\infty}^{\infty} h_n(\tau_1, \ldots, \tau_n) e^{-j(\omega_1\tau_1 + \cdots + \omega_n\tau_n)} d\tau_1 \cdots d\tau_n \tag{2.16}$$

The GFRFs describe generic nonlinear systems independent of their inputs hence are very important to the analysis of nonlinear systems that can be represented by a Volterra series model. The expression relating $Y(j\omega)$ and $U(j\omega)$ will be given by the output frequency response function described below.

2.4.2 Output frequency response function

Extending the simple relationship between the input and output frequency characteristics of linear systems given by Eq. (2.14), Lang & Billings [1996, 1997] studied the output frequency spectrum of nonlinear systems given a general input expressed by

$$u(t) = \frac{1}{2\pi} \int_0^{\infty} |U(j\omega)| \cos\left(\omega t + \angle U(j\omega)\right) d\omega \tag{2.17}$$

in the time domain. The derived Nth order output spectrum is given by

$$\begin{cases} Y(j\omega) = \sum_{n=1}^{N} Y_n(j\omega) \qquad \forall\omega \\ Y_n(j\omega) = \dfrac{1/\sqrt{n}}{(2n)^{n-1}} \displaystyle\int_{\omega_1+\cdots+\omega_n=\omega} H_n(j\omega_1,\ldots,j\omega_n) \prod_{i=1}^{n} U(j\omega_i) d\sigma_{n\omega} \end{cases} \tag{2.18}$$

where $H_n(j\omega_1,\ldots,j\omega_n)$ is the nth order GFRF as in Eq. (2.16) and $\int_{\omega_1+\cdots+\omega_n=\omega}(\cdot)d\sigma_{n\omega}$ denotes the integration of $(\cdot)$ over the n-dimensional hyperplane $\omega_1+\cdots+\omega_n=\omega$. An explicit expression describing the output frequencies of system (2.13) for a given frequency range of the input is also derived by Lang & Billings [1996, 1997] which provides important details of the frequency domain properties of nonlinear systems. Building upon this, the relationship between the system parameters and the output frequency spectrum called the output frequency response function (OFRF) is derived for nonlinear systems which can be described by a polynomial form differential equation model

$$\sum_{m=1}^{M} \sum_{\substack{p=0 \\ p+q=m}}^{m} \sum_{l_1,\cdots,l_{p+q}=0}^{L} c_{pq}(l_1,\cdots,l_{p+q}) \prod_{i=1}^{p} \frac{d^{L_i}y(t)}{dt^{L_i}} \prod_{i=p+1}^{p+q} \frac{d^{L_i}u(t)}{dt^{L_i}} = 0 \tag{2.19}$$

where M is the maximum degree of nonlinearity in terms of the input $u(t)$ and the output $y(t)$, L is the maximum order of derivatives of $u(t)$ and $y(t)$ and $c_{pq}(\cdot)$ are the coefficients of the polynomial [Lang *et al.*, 2007]. Eq. (2.19) can represent a wide range of physical systems, one example of which is given by the Duffing system in Eq. (2.7) in Section 2.3.1. For a particular input, there exists a polynomial expression of the output spectrum $Y(j\omega)$ in terms of the model parameters given by

$$Y(j\omega) = \sum_{j_1=0}^{m_1} \sum_{j_2=0}^{m_2} \cdots \sum_{j_{S_N}=0}^{m_{S_N}} \rho_{j_1,\cdots,j_{S_N}}(\omega) {x_1}^{j_1} \ldots {x_{S_N}}^{j_{S_N}}, \tag{2.20}$$

where $x_1,\ldots,x_{S_N}$ are the system parameters that define the system nonlinearity and m_i is the maximum power of x_i for $j=1,\ldots,S_N$. $\rho_{j_1,\cdots,j_{S_N}(\omega)}$, functions of ω, are the coefficients of the terms ${x_1}^{j_1}\ldots{x_{S_N}}^{j_{S_N}}$ and their values depend on the

input signal and the linear parameters of the system.

Eq. (2.20), known as the output frequency response function, can significantly facilitate the understanding and the design of nonlinear systems, and the results can readily be extended to the multi-input multi-output nonlinear systems studies by Swain & Billings [2001]. The application of this analytical approach to vibration isolation system will be discussed in the next section.

2.4.3 Application of the OFRF approach

The OFRF of a nonlinear system provides an explicit relationship between the output spectrum and the parameters that define the system nonlinearities so is very useful for analysing the effects of these nonlinear parameters on the output spectrum. These advantages have been exploited by the analytical study in [Lang *et al.*, 2009]. The derivative of the force transmissibility, expressed in the form given by Eq. (2.20), with respect to the cubic damping ratio was found to be negative around the resonant region, which means the resonant peak is reduced by an increase in the cubic damping coefficient. It was also found that the coefficients of the cubic damping ratio in the OFRF expression is insignificantly small when the frequency is far from the resonant frequency. These findings provide a concrete theoretical proof for the same conclusions reached by other approximation methods.

This OFRF analysis approach has a wide engineering application as most systems in the real world are nonlinear. Laalej & Lang [2010] have used this technique to analyse a vibration isolation system that has a magnetorheological (MR) damper installed in parallel with a linear spring and shows the effects of the MR damper parameters on the vibration isolation performance. Other applications include the study of the nonlinearity effects on the frequency response of a passive engine mount [Peng *et al.*, 2008] and a multi-degree-of-freedom structures with a nonlinear viscous damping device [Peng *et al.*, 2011].

Although not applicable to nonlinear systems which exhibit chaos or subharmonics, the OFRF based approach provides a more accurate and comprehensive description of nonlinear systems as opposed to the traditional harmonic balance method and other approximation methods.

Figure 2.5: a LORD RD-1005-3 MR damper

2.5 Semi-active nonlinear vibration isolation system

There are a number of semi-active damping devices that have been used for vibration control [Spencer Jr & Sain, 1997]. The variable-orifice damper has a valve that alters the size of the orifice which changes the resistance of the damping fluid in order to provide different damping characteristics. The mechanism of a mechanical valve has a potential reliability concern. Therefore, the controllable-fluid dampers have become more popular as the property of the fluid can be altered by an electric or magnetic field without needing any moving parts. The electrorheological (ER) dampers and the magnetorheological (MR) dampers function in a very similar way. MR dampers contain fluids consisting of soft magnetic particles. When a magnetic field is applied via a current, inter-particle bonds arise which causes resistance to the flow. The fluid then becomes more viscous which leads to an increase in the damping force produced by the MR damper. This phenomenon has been explained in detail by several authors [Bossis *et al.*, 2003; Ginder *et al.*, 1996; Stanway, 2004; Weiss *et al.*, 1994]. As the damping properties can be easily altered by the applied current, MR dampers, now commercially available, have potential in a wide range of engineering applications. A picture of a LORD RD-1005-3 MR damper is provided in Fig. 2.5 which is manufactured by LORD Corporation.

A number of studies have been conducted to improve vehicle suspension performance using MR dampers to reduce vibration transmitted from the road to the occupants of the rider. Using an MR damper to implement skyhook damping is also a popular research area [Batterbee & Sims, 2005; Lai & Liao, 2002; Lee & Choi, 2000; Yao *et al.*, 2002]. Other approaches include neural network control [Guo *et al.*, 2004] and H-infinity control [Du *et al.*, 2005]. These designs focus

on the low frequency range to alleviate vibrations from the road to the rider and rely on the measurement of the absolute displacement (or velocity) of the sprung mass. In these cases, the damper is used as a semi-active device which gives a force that is dependent on the system outputs. In other words, the damper is acting as an actuator in a feedback-control loop as illustrated in Fig. 2.1(a). The complex nonlinear characteristics of the MR damper must be taken into account when designing this kind of feedback-control loop and more challenging nonlinear multi-input-multi-output problems have to be considered when more than one control loop is involved.

Jansen & Dyke [2000] carried out a thorough review on different control strategies for MR dampers including the decentralised bang-bang control [McClamroch & Gavin, 1995] and the clipped-optimal control method [Dyke *et al.*, 1996]. Similar approaches using MR dampers were employed in structural vibration control [Xu *et al.*, 2003; Yi *et al.*, 2001]. Others have opted for adaptive fuzzy control [Kim *et al.*, 2009; Zhou *et al.*, 2003].

Spencer & Nagarajaiah [2003] have given some latest full-scale applications of MR dampers including the Nihon-Kagaku-Miraikan building in Japan and the cable-stayed Dongting Lake Bridge in China [Chen *et al.*, 2003; Duan *et al.*, 2006]. In these studies, the controller calculates the force required from the MR damper to reduce the vibration of a structure based on sensor measurements of the structural responses. The MR dampers therefore are performing the role of an actuator. Another interesting development is the smart passive system based on an MR damper incorporated with an electromagnetic induction unit, proposed by Cho *et al.* [2005], which have better performances than the clipped-optimal controlled system during severe earthquakes.

Ultimately, MR dampers are passive energy dissipating devices. When placed in a feedback control loop, it is very difficult to produce a performance that matches a fully active actuator. It is more natural to treat them as passive dampers as proposed by Laalej *et al.* [2012]. This new structure includes an MR damper into the plant as shown in Fig. 2.1(b) instead of placing it in the feedback path. In some separate studies, Sims *et al.* [1999, 2000] showed that the force-velocity relationship of an electrorheological damper can be shaped into a quadratic or a higher-order polynomial function by feedback control. Based on a mathematical model of an

MR damper, Laalej *et al.* [2012] have shown that this feedback control technique can be applied to MR dampers to produce the desirable damping characteristics.

2.6 Summary

Vibration control is required to prevent noise, in the form of displacement or force, transmitting from one interface to another. It is necessary to protect machinery from engine vibration and passenger in vehicles from road noise. Building protection against seismic activities is also of paramount importance.

The control strategies are often divided into three broad groups: (a) active, (b) passive and (c) semi-active. Relying on external power and real time measurements, active control may provide a very good performance if the model of the plant and the sensors are accurate. Passive control does not input any energy to the system, so there is no risk of inducing instability. Without a feedback control loop, passive devices, such as springs and dampers, are added to the plant. This is a more robust solution as it does not depend on an accurate model of the plant. The semi-active approach uses passive devices that have controllable properties to take the best of both active and passive methods. Similar to passive control, semi-active control does not input any energy to the system but has the freedom of changing the plants characteristics in real time operation.

The foundation of passive vibration control theories is based on a simple linear mass-spring-damper system. The properties of a basic linear force vibration isolation system as well as a displacement vibration isolation system have been discussed in Section 2.2. The main weaknesses of linear vibration isolators are their fixed cut-off frequency and their inability to suppress vibration over a wide frequency range. To improve the performance of a simple linear vibration isolator, stiffness nonlinearity has been introduced. Section 2.3.1 is concerned with a general form of a Duffing system where a cubic spring nonlinearity has been added to a linear vibration isolation system. Nonlinear stiffness may occur naturally in the plant or it may be introduced to reshape the transmissibility curve to achieve better isolation over the low frequency range. The most common method for analysing nonlinear Duffing system is the harmonic balance method. Another way to alter the transmissibility curve is the adoption of nonlinear damping.

The properties of nonlinear viscous damping have been discussed in Section 2.3.2. In a force vibration isolation system, nonlinear viscous damping is preferable to linear damping as the resonance can be reduced without causing any undesirable effects to other frequency ranges. These effects have been analysed by various nonlinear methods, the most notable of which is the output frequency response function (OFRF) based approach in Section 2.4.3. Developed from the frequency response of a Volterra series model, the OFRF method can be applied to a vibration control problem to express the force or displacement transmissibility of a nonlinear system as a polynomial function of the nonlinear damping coefficient. The effects of these nonlinear parameters on the vibration isolation performance can therefore be analytically analysed.

Finally, some practical applications of semi-active vibration control have been covered in Section 2.5. One particular semi-active device, the magnetorheological (MR) damper, is especially popular recently because of its reliability and flexibility. The damping properties of MR dampers can be varied almost instantly by the supply current. Together with a good control design, MR dampers offer more functionality than conventional linear viscous dampers. Their applications range from vehicle suspension to full-scale structural protection.

The literature mentioned in this chapter has covered the recent research on linear and nonlinear vibration control. Some further development based on these results will be addressed in the thesis. First, the recently developed OFRF approach will be applied to analyse more general nonlinear vibration isolation systems, which include both nonlinear damping and nonlinear stiffness. This would provide a solid theoretical support for the application of these nonlinear vibration isolation systems in practice. Then, these theoretical findings will be verified by experimental studies. Last but not least, the design method for nonlinear vibration isolation systems according to some frequency domain requirements will be investigated.

Chapter 3

Analysis of nonlinearly damped force vibration isolation systems

A wide range of physical systems can be modelled by the Duffing equation. Duffing himself gave a few examples relating to the motion of a pendulum and an electrical circuit [Duffing, 1918]. More examples including beams with nonlinear stiffness and nonlinear cable vibrations are explained in Kovacic and Brennan's book [2011]. The Duffing oscillator has been studied by a large number of authors since it was first published in 1918 [Duffing, 1918]. To understand the chaotic dynamics caused by the nonlinear stiffness term in the Duffing equation, researchers are challenged to consider a range of nonlinear system analytical and numerical methods.

Damping plays a very important role in the continuity of the output frequency response of the Duffing system. Traditionally, the Duffing equation has included only a linear viscous damping term but the idea of nonlinear damping has also been explored. Ravindra & Mallik [1994b; 1994c; 1995] have conducted a stability analysis using the harmonic balance method and their studies have concluded that nonlinear damping could be used as a mechanism to suppress chaos. Energy dissipation in a nonlinearly damped Duffing oscillator was also studied by Trueba *et al.* [2000] and Baltanas *et al.* [2001]. Because the OFRF provides an explicit analytical relationship between the system output frequency response and the system parameters of interests, this concept has already been used to analytically study the beneficial effects of nonlinear damping on a vibration isolation system

that has a linear spring [Lang *et al.*, 2009].

The chapter is concerned with the analysis of a nonlinear vibration isolation that has a nonlinear Duffing stiffness with an additional nonlinear damping term using the OFRF approach. For a single-tone sinusoidal input, the explicit relationships between the nonlinear terms, namely nonlinear stiffness and damping coefficients, and the output spectra are derived to form a basis for the theoretical analysis. Then, the rigorous analytical evaluations show the effects of these two nonlinear terms on the output spectra over different frequency ranges and reveal the potential problems and benefits of applying these nonlinearities to vibration isolation applications. Also supported by simulation studies, the results show that the beneficial effects of nonlinear viscous damping on a vibration isolator with a linear spring in [Lang *et al.*, 2009] are transferable to a Duffing system and that nonlinear stiffness can be used in conjunction with nonlinear damping such that the ability to suppress the output displacement can be exploited with minimum negative effects on the output force.

3.1 Nonlinearly damped Duffing system

Consider a single-degree-of-freedom mass-spring system with a nonlinear restoring force and a nonlinear viscous damping force depicted in Fig. 3.1 driven by an sinusoidal input force $F_{in}(t) = A_F \sin(\bar{\omega}t)$ with amplitude A_F and frequency $\bar{\omega}$. The dynamic relationship between the input force and the output force $F_{out}(t)$ is represented by

$$\begin{cases} M\ddot{z}(t) + C\dot{z}(t) + C_3[\dot{z}(t)]^3 + Kz(t) + K_3[z(t)]^3 = F_{in}(t) \\ F_{out}(t) = C\dot{z}(t) + C_3[\dot{z}(t)]^3 + Kz(t) + K_3[z(t)]^3 \end{cases} \tag{3.1}$$

where M is the mass, C the linear viscous damping constant, C_3 the cubic viscous damping constant, K the linear stiffness, K_3 the cubic stiffness, $z(t)$, $\dot{z}(t)$ and $\ddot{z}(t)$ are the displacement, velocity and acceleration of the moving mass respectively. It is assumed that the base is perfectly fixed to ground. When $K_3 = C_3 = 0$, System (3.1) is equivalent to a simple linear vibration isolator. When $K_3 > 0$ and $C_3 = 0$, System (3.1) is called the hardening Duffing system as it has a cubic

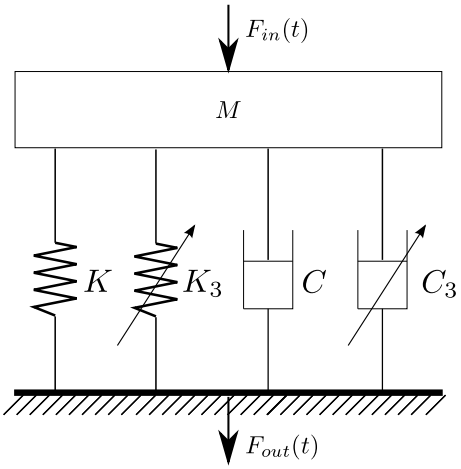

Figure 3.1: A Duffing system with additional nonlinear viscous damping.

restoring force that may naturally exist in many structures. When $K_3 = 0$ and $C_3 > 0$, System (3.1) is equivalent to the one studied in [Lang *et al.*, 2009; Ravindra & Mallik, 1994c]. The combined effects of these two nonlinear forces ($K_3, C_3 > 0$) will be theoretically studied in the frequency domain for the first time.

To analyse the effects of the nonlinear spring and damping characteristics for all systems that can be modelled by the generic system in Fig. 3.1, Eq. (3.1) is transformed into a more meaningful dimensionless form given by

$$\begin{cases} \ddot{y}_1(\tau) + y_2(\tau) = u(\tau) = \sin(\Omega\tau) \\ y_2(\tau) = y_1(\tau) + \gamma_3[y_1(\tau)]^3 + \xi_1\dot{y}_1(\tau) + \xi_3[\dot{y}(\tau)]^3 \end{cases} \tag{3.2}$$

where

$$\omega_0 = \sqrt{\frac{K}{M}}, \tag{3.3}$$

$$\tau = \omega_0 t, \tag{3.4}$$

$$\Omega = \frac{\bar{\omega}}{\omega_0}, \tag{3.5}$$

$$y_1(\tau) = \frac{Kz(t)}{A_F}, \tag{3.6}$$

$$\gamma_3 = \frac{K_3 {A_F}^2}{K^3}, \tag{3.7}$$

$$\xi_1 = \frac{C_1}{\sqrt{KM}}, \tag{3.8}$$

$$\xi_3 = \frac{C_3 {A_F}^2}{\sqrt{(KM)^3}}. \tag{3.9}$$

The first output $y_1(\tau)$ is the normalised displacement of the mass. $Y_1(j\omega)$, the Fourier transform of $y_1(\tau)$ represents the displacement spectrum of System (3.1) driven by the normalised frequency Ω. It can be shown that the second output

$$y_2(\tau) = \frac{F_{out}(t)}{A_F}. \tag{3.10}$$

relates the amplitude of the input force and output force. $Y_2(j\omega)$, the Fourier transform of $y_2(\tau)$ is the ratio of the amplitude of the fundamental harmonic of the output force to the amplitude of the input force and is equivalent to the definition of force transmissibility denoted by

$$T_F(\Omega) = \left| \frac{\mathcal{F}\{F_{out}(t)\}|_{\omega=\bar{\omega}}}{\mathcal{F}\{F_{in}(t)\}|_{\omega=\bar{\omega}}} \right| = \left| \frac{\mathcal{F}\{F_{out}(t)\}|_{\omega=\bar{\omega}}}{A_F} \right| = |\mathcal{F}\{y_2(\tau)\}|_{\omega=\Omega}| = |Y_2(j\Omega)| \tag{3.11}$$

where $\mathcal{F}\{\cdot\}$ is the Fourier transform operation. The output spectra of System (3.2), $Y_1(j\omega)$ and $Y_2(j\omega)$, also known as the output frequency responses, will be examined in the following sections to reveal how the spring and damping nonlinearities affect the displacement frequency response and force transmissibility of System (3.1).

3.2 Output spectra of the nonlinearly damped Duffing system

To facilitate the analysis of System (3.2), a frequency domain method based on the OFRF approach will be applied to find expressions for the output spectra as a polynomial in terms of the nonlinear stiffness and the nonlinear damping coefficient. However, before applying this powerful technique, it is essential to ensure that the system under study must be a polynomial type nonlinear differential model with a stable zero equilibrium that can be modelled by the Volterra series. In this

section, a condition for System (3.2) such that the OFRF approach requirements are satisfied will be first established. Then, the output spectra of System (3.2) will be expressed as functions of the system nonlinear parameters.

The jump and chaotic characteristics caused by the nonlinear stiffness term in a Duffing system may be suppressed and even eliminated by sufficient levels of damping [Ravindra & Mallik, 1993, 1994c]. To establish the legitimate range for the linear damping coefficient, ξ_1 and the nonlinear damping coefficient, ξ_3, so that the system does not exhibit any of these undesirable behaviours, the harmonic balance method is applied to System (3.2).

When System (3.2) is excited by a sinusoidal force $u(\tau) = \sin(\Omega\tau)$, the first order harmonic balance method approximates the first output $y_1(\tau)$ by a truncated Fourier series

$$y_1(\tau) = B\sin(\Omega\tau + \psi) \tag{3.12}$$

where B is the magnitude of the output displacement, Ω is the excitation frequency and ϕ is the phase difference between the input and the output signal. Substituting Eq. (3.12) into System (3.2) and equating the coefficients of $\sin(\Omega t)$ and $\cos(\Omega t)$ yields

$$\left(\frac{3\xi_3 B^3\Omega^3}{4} + \xi_1 B\Omega\right)^2 + \left(\frac{3\gamma_3 B^3}{4} - B\Omega^2 + B\right)^2 - 1 = 0 \tag{3.13}$$

where higher order harmonics are neglected.

Eq. (3.13) can be written as a third order polynomial in Ω^2 given by

$$\mathcal{G}(B,\Omega) = a_3(\Omega^2)^3 + a_2(\Omega^2)^2 + a_1(\Omega^2) + a_0 = 0 \tag{3.14}$$

where a_i i=0,1,2,3 are functions of B, γ_3, ξ_1 and ξ_3. This can be solved numerically to create the amplitude-frequency plots in Fig. 3.2. For a Duffing system that can be represented by a convergent Volterra series over the whole frequency range, B is a single-valued function of Ω and the gradient $dB/d\Omega$ is a continuous function. That is, Eq. (3.13) only gives one unique real value of B for any given Ω. $dB/d\Omega$ is always finite and only changes sign once at the maximum value of B. If the system

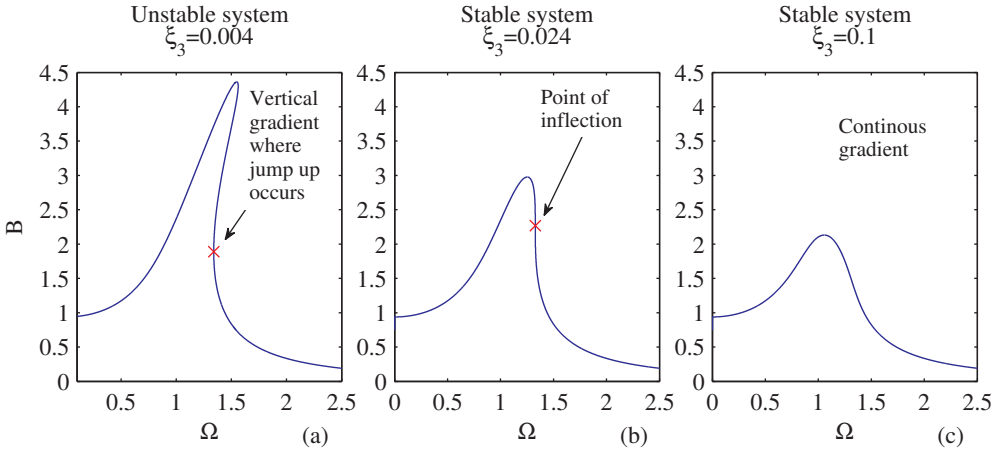

Figure 3.2: The effects of nonlinear viscous damping on jump avoidance. Numerical solutions of Eq. (3.13) where γ_3=0.1, ξ_1=0.01 and ξ_3=0.004, 0.024, 0.1

exhibits jumps, the jump-up frequency can be determined by setting the derivative of Ω with respect to B to zero as it occurs when the amplitude-frequency plot has a vertical tangent [Brennan *et al.*, 2008], i.e. $\frac{d\Omega}{dB} = 0$. For a system that is on the verge of showing jump behaviours, the point where the vertical tangent occurs is also an inflection point denoted by (Ω_c, B_c) where the gradient goes through infinity without changing sign [Malatkar & Nayfeh, 2002], i.e. $\frac{d\Omega}{dB}\Big|_{B=B_c} = 0$ and $\frac{d^2\Omega}{dB^2}\Big|_{B=B_c} = 0$. Therefore, if the output magnitude of System (3.2) is continuous over the whole frequency range, γ_3, ξ_1, ξ_3 must have values in the range given in Proposition 3.1.

Proposition 3.1. *If the output spectrum of System* (3.2) *is a continuous function of frequency* Ω*, then Eq.* (3.13) *must give only one real positive solution for* B *for any* Ω*, and there exist*

$$\gamma_3 \leqslant \gamma_{3c}, \quad \xi_1 \geqslant \xi_{1b} \quad \textit{and} \quad \xi_3 \geqslant \xi_{3c} \tag{3.15}$$

such that

$$\mathcal{R}\{\mathcal{G}', \mathcal{G}''\}\,|_{B=B_c,\gamma_3=\gamma_{3c},\xi_1=\xi_{1b},\xi_3=\xi_{3c}} = 0. \tag{3.16}$$

$\mathcal{G}'$ *and* $\mathcal{G}''$ *are the first and second derivatives of* $\mathcal{G}(B,\Omega)$ *with respect to* B *and*

$\mathcal{R}\{\mathcal{G}', \mathcal{G}''\}$ is the resultant of polynomials $\mathcal{G}'$ and $\mathcal{G}''$, where the resultant of two polynomials, for example,

$$\hat{A}(x) = \sum_{k=1}^{\hat{m}} \hat{a}_k x^k \quad \textit{and} \quad \hat{B}(x) = \sum_{k=1}^{\hat{n}} \hat{b}_k x^k \tag{3.17}$$

is defined as the determinant

$$\mathcal{R}\left\{\hat{A}, \hat{B}\right\} = \left|\begin{array}{cccccccc}
\hat{a}_{\hat{n}} & \hat{a}_{\hat{n}-1} & \hat{a}_{\hat{n}-2} & \cdots & \hat{a}_1 & \hat{a}_0 & & \\
 & \hat{a}_{\hat{n}} & \hat{a}_{\hat{n}-1} & \cdots & \hat{a}_2 & \hat{a}_1 & \hat{a}_0 & \\
 & & & \cdots & & & & \\
 & & & \hat{a}_{\hat{n}} & \hat{a}_{\hat{n}-1} & \cdots & \hat{a}_2 & \hat{a}_1 & \hat{a}_0 \\
\hat{b}_{\hat{m}} & \hat{b}_{\hat{m}-1} & \hat{b}_{\hat{m}-2} & \cdots & \hat{b}_1 & \hat{b}_0 & & \\
 & \hat{b}_{\hat{m}} & \hat{b}_{\hat{m}-1} & \cdots & \hat{b}_2 & \hat{b}_1 & \hat{b}_0 & \\
 & & & \cdots & & & & \\
 & & & \hat{b}_{\hat{m}} & \hat{b}_{\hat{m}-1} & \cdots & \hat{b}_2 & \hat{b}_1 & \hat{b}_0
\end{array}\right| \begin{array}{l} \left.\vphantom{\begin{array}{c}a\\a\\a\\a\end{array}}\right\} \hat{n} \textit{ rows} \\ \left.\vphantom{\begin{array}{c}a\\a\\a\\a\end{array}}\right\} \hat{m} \textit{ rows} \end{array}$$

and the remaining entries all equal to zero [Apostol, 1970].

Proof. See Ref. [Malatkar & Nayfeh, 2002].

□

Proposition 3.1 states a necessary condition for System (3.2) to be modelled by a convergent Volterra series for all excitation frequencies. γ_{3c}, ξ_{1b}, ξ_{3c} are the critical values for this condition. These three parameters are interdependent. Thus, when two of the three parameters are fixed, the remaining parameter can be determined by solving Eqs. (3.14), (3.16) and $\mathcal{G}''(B_c, \Omega_c) = 0$.

Under the condition in Proposition 3.1 where System (3.2) is stable at the zero equilibrium and can be described in the neighbourhood of the equilibrium by the Volterra series, the output spectra of the system can be represented using the OFRF as described in Proposition 3.2 below.

Proposition 3.2. *Under the condition in Proposition 3.1, the output spectra of*

System (3.2) *under a sinusoidal input* $u(\tau) = \sin(\Omega\tau)$ *are given by*

$$\begin{aligned} Y_J(j\omega) =& P^{(J)}_{0,0}(j\omega) + P^{(J)}_{1,0}(j\omega)\gamma_3 + P^{(J)}_{2,0}(j\omega)\gamma_3^2 \\ &+ \cdots + P^{(J)}_{0,1}(j\omega)\xi_3 + P^{(J)}_{1,1}(j\omega)\gamma_3\xi_3 + P^{(J)}_{2,1}(j\omega)\gamma_3^2\xi_3 \\ &+ \cdots + P^{(J)}_{0,2}(j\omega)\xi_3^2 + P^{(J)}_{1,2}(j\omega)\gamma_3\xi_3^2 + P^{(J)}_{2,2}(j\omega)\gamma_3^2\xi_3^2 \\ &+ \cdots P^{(J)}_{\lfloor (N-1)/2\rfloor,\lfloor (N-1)/2\rfloor}(j\omega)\gamma_3^{\lfloor (N-1)/2\rfloor}\xi_3^{\lfloor (N-1)/2\rfloor} \\ =& \sum_{\bar{n}=0}^{\lfloor (N-1)/2\rfloor}\sum_{\bar{m}=0}^{\bar{n}} P^{(J)}_{\bar{m},\bar{n}-\bar{m}}(j\omega)\gamma_3^{\bar{m}}\xi_3^{\bar{n}-\bar{m}} \qquad J = 1, 2 \end{aligned} \tag{3.18}$$

where N *is the maximum order of nonlinearity in the Volterra series representation of the system and* $\lfloor (N-1)/2 \rfloor$ *is the floor function indicating the largest integer less than or equal to* $(N-1)/2$. $P^{(J)}_{\bar{m},\bar{n}-\bar{m}}(j\omega)$*, the coefficient of the term* $\gamma_3^{\bar{m}}\xi_3^{\bar{n}-\bar{m}}$*, is a function of frequency* ω *that depends on the linear parameters of System* (3.2).

Proof. See Appendix A.

In Eq. (3.18), the output spectra of System (3.2), $Y_1(j\omega)$ and $Y_2(j\omega)$ are expressed analytically as a polynomial in terms of the two nonlinear characteristic parameters, γ_3 and ξ_3. This is the OFRF representation of the system output spectra and can obviously facilitate the analysis of the effects of γ_3 and ξ_3 on the system outputs in the frequency domain. Nonlinear terms are known to produce harmonics in the system outputs, which may have significant effects on the system performance as Rijlaarsdam *et al.* [2012, 2013] have proposed a frequency domain based method to minimise the energy level of the harmonics. The OFRF representation of $Y_J(j\omega)$ can be used to evaluate both the fundamental harmonic and the higher order harmonics. This can be achieved by substituting $\omega = p\Omega$ into Eq. (3.18) to yield

$$Y_J(jp\Omega) = \sum_{\bar{n}=0}^{\lfloor (N-1)/2\rfloor}\sum_{\bar{m}=0}^{\bar{n}} P^{(J)}{}_{\bar{m},\bar{n}-\bar{m}}(jp\Omega)\gamma_3^{\bar{m}}\xi_3^{\bar{n}-\bar{m}} \qquad J = 1, 2, \quad p = 1, 2, \cdots . \tag{3.19}$$

Instead of examining each of the higher harmonics individually, the overall characteristics can be represented by the total output energy defined as the sum of the

magnitude squared of the fundamental and all higher harmonics as

$$E_J(\Omega) = \sum_{p=1}^{\infty} |Y_J(jp\Omega)|^2, \quad J = 1, 2 \tag{3.20}$$

which obviously can also be written as a polynomial in γ_3 and ξ_3 using the OFRF concept.

Both the fundamental and higher order harmonic output spectra as described in Eq. (3.19) and the output energy given in Eq. (3.20) are the function of the nonlinear spring constant γ_3, the nonlinear damping constant ξ_3, and the excitation frequency Ω, which measures the vibration isolation performance of System (3.2). These expressions are significant as they can be used to analytically reveal the effects of each of the nonlinear parameters on the system vibration isolation performance. The lower the values of $|Y_J(j\Omega)|$ and $E_J(\Omega)$ are, the better the performance is. When compared with a linear system where $\gamma_3, \xi_3 = 0$, it can be concluded that γ_3 or ξ_3 has a desirable effect on the vibration isolation performance if the value of $|Y_J(j\Omega)|$ when $\gamma_3, \xi_3 > 0$ is smaller than $|Y_J(j\Omega)|$ when $\gamma_3, \xi_3 = 0$, i.e.

$$\left| Y_J(j\Omega)|_{\gamma_3,\xi_3>0} \right| < \left| Y_J(j\Omega)|_{\gamma_3,\xi_3>0} \right| \tag{3.21}$$

or

$$\frac{\partial |Y_J(j\Omega)|}{\partial \alpha} < 0 \qquad \alpha = \gamma_3, \xi_3. \tag{3.22}$$

The same comparison can be performed on $E_J(\Omega)$.

3.3 Effects of nonlinearities on the system performance

In this section, the properties of $Y_J(j\Omega)$ and $E_J(\Omega)$ will be examined over three frequency ranges, the resonant region where $\Omega \approx 1$ and two non-resonant regions where $\Omega \ll 1$ and $\Omega \gg 1$. The analysis will show the effects of γ_3 and ξ_3 on $Y_J(j\Omega)$

and $E_J(\Omega)$ to reveal the benefits of using both nonlinear stiffness and nonlinear damping in vibration isolation.

3.3.1 Effects of nonlinear stiffness

Proposition 3.3. *Under the same condition of Proposition 3.2, the following results are true for $\xi_1 > 0$ and $\bar{\xi}_3 \geqslant \xi_3 \geqslant 0$, where $\bar{\xi}_3$ is a positive number.*

(i) When $0 \leqslant \Omega < 1$, there exists a $\bar{\gamma}_3$ such that

$$\frac{\partial |Y_1(j\Omega)|^2}{\partial \gamma_3} < 0 \tag{3.23}$$

if $0 < \gamma_3 < \bar{\gamma}_3$.

(ii) When $\Omega \ll 1$

$$\left| Y_2(j\Omega)\big|_{\gamma_3=0} \right| \approx \left| Y_2(j\Omega)\big|_{\gamma_3 \geqslant 0} \right|. \tag{3.24}$$

(iii) When $\Omega \approx 1$, there exists a $\bar{\gamma}_3$ such that

$$\frac{\partial |Y_2(j\Omega)|^2}{\partial \gamma_3} > 0 \tag{3.25}$$

if $0 < \gamma_3 < \bar{\gamma}_3$.

(iv) When $\Omega \gg 1$

$$\left| Y_J(j\Omega)\big|_{\gamma_3=0} \right| \approx \left| Y_J(j\Omega)\big|_{\gamma_3 \geqslant 0} \right| \qquad J = 1, 2. \tag{3.26}$$

Proof. The complete proof is provided in Appendix B and a brief description of the procedure is given below.

First, express the derivative of $|Y_J(j\Omega)|^2$ as a polynomial in ξ_3 given by

$$\frac{\partial |Y_J(j\Omega)|^2}{\partial \gamma_3} = b_0^{(J)} + b_1^{(J)} \gamma_3 + b_2^{(J)} {\gamma_3}^2 \cdots \qquad J = 1, 2 \tag{3.27}$$

where $b_i, i = 0, 1, 2, \cdots$ are functions of $P^{(J)}_{\bar{m},\bar{n}-\bar{m}}(j\omega)$ and ξ_3. When $0 \leqslant \Omega < 1$, it is shown that $b_0^{(1)} < 0$ and conclusion (i) is implied. When $\Omega \approx 1$, it is shown that $b_0^{(2)} < 0$ and conclusion (iii) is implied.

Then, express $|Y_J(j\Omega)|^2$ as a polynomial in γ_3 given by

$$|Y_J(j\Omega)|^2 = c_0^{(J)} + c_1^{(J)}\gamma_3 + c_2^{(J)}{\gamma_3}^2 \cdots \qquad J = 1, 2 \tag{3.28}$$

where $c_i, i = 0, 1, 2, \cdots$ are functions of $P^{(J)}_{\bar{m},\bar{n}-\bar{m}}(j\omega)$ and ξ_3. When $\Omega \ll 1$ and it is shown that $c_i^{(2)} \approx 0, i = 1, 2, \cdots$ and conclusion (ii) is implied. When $\Omega \gg 1$ and it is shown that $c_i^{(J)} \approx 0, , i = 1, 2, \cdots, J = 1, 2$ and conclusion (iv) is implied.

The four results in Proposition 3.3 summarise the effects of the nonlinear stiffness ratio γ_3 on the displacement spectrum $Y_1(j\Omega)$ and the force spectrum $Y_2(j\Omega)$ of a Duffing system. Although not new, these results are deduced analytically using the recently developed OFRF approach based on Volterra models instead of methods that require approximations to be made or solutions to be found numerically. Analytic methods produce much more insight into what causes what and are an important advance to results in this field. In addition, the OFRF approach allows the examination of the effects of γ_3 in the presence of another nonlinear characteristic parameter ξ_3. All four results hold for $\xi_3 \geqslant 0$.

Proposition 3.3(i) indicates that an increase in γ_3 leads to a fall in the magnitude of $Y_1(j\Omega)$ when Ω is below the resonant frequency. This effect is unique to γ_3 as it cannot be achieved by adjusting the level of linear or nonlinear damping. Proposition 3.3(ii) indicates that γ_3 has no effect on $Y_2(j\Omega)$ when $\Omega \ll 1$ but Proposition 3.3(iii) shows a positive rise in the magnitude of $Y_2(j\Omega)$ in response to an increase in γ_3 at the resonant frequency. When Ω is large, Proposition 3.3(iv) shows that neither $Y_1(j\Omega)$ nor $Y_2(j\Omega)$ is affected by γ_3. These results highlight the pros and cons of using nonlinear stiffness in vibration isolation. On the one hand, the properties of nonlinear stiffness shown by Proposition 3.3(i), (ii) and (iv) are desirable as the transmissibilities are either reduced or maintained. On the other hand, the key problem is the rise in the magnitude of $Y_2(j\Omega)$ as described in Proposition 3.3(iii). In the next section, the effects of nonlinear damping on the output spectra will be analysed to show that it is possible to exploit the advantages of γ_3 while overcoming its weakness.

Stiffness or damping parameters	Effects on the outputs	$\Omega \ll 1$	$0 \leqslant \Omega < 1$	$\Omega \approx 1$	$\Omega \gg 1$
γ_3	$\frac{\partial\|Y_1(j\Omega)\|^2}{\partial\gamma_3}$		-ve		≈ 0
	$\frac{\partial\|Y_2(j\Omega)\|^2}{\partial\gamma_3}$	≈ 0		+ve	≈ 0
ξ_3	$\frac{\partial\|Y_J(j\Omega)\|^2}{\partial\xi_3}$ $J=1,2$	≈ 0		-ve	≈ 0
	$\frac{\partial\|E_J(\Omega)\|^2}{\partial\xi_3}$ $J=1,2$	≈ 0		-ve	≈ 0
ξ_1	$\frac{\partial\|Y_1(j\Omega)\|^2}{\partial\xi_1}, \frac{\partial\|E_1(\Omega)\|^2}{\partial\xi_1}$	≈ 0		-ve	≈ 0
	$\frac{\partial\|Y_2(j\Omega)\|^2}{\partial\xi_1}, \frac{\partial\|E_2(\Omega)\|^2}{\partial\xi_1}$	≈ 0		-ve	+ve

Table 3.1: Effects of γ_3, ξ_3 and ξ_1 on the output frequency spectra.

3.3.2 Effects of nonlinear damping

Proposition 3.4. *Under the same condition of Proposition 3.2, the following results are true for $\bar{\gamma}_3 \geqslant \gamma_3 \geqslant 0$ and $\xi_1 > 0$, where $\bar{\gamma}_3$ is a positive number.*

(i) When $\Omega \approx 1$, there exists a $\bar{\xi}_3$ such that

$$\frac{\partial|Y_J(j\Omega)|^2}{\partial\xi_3} < 0 \qquad J = 1,2 \tag{3.29}$$

if $0 < \xi_3 < \bar{\xi}_3$.

(ii) When $\Omega \ll 1$ or $\Omega \gg 1$

$$\left|Y_J(j\Omega)\big|_{\xi_3=0}\right| \approx \left|Y_J(j\Omega)\big|_{\xi_3>0}\right| \qquad J = 1,2. \tag{3.30}$$

Proof. The complete proof is provided in Appendix C and a brief description of the procedure is given below.

First, express the derivative of $|Y_J(j\Omega)|^2$ as a polynomial in γ_3 given by

$$\frac{\partial|Y_J(j\Omega)|^2}{\partial\xi_3} = b_0^{(J)} + b_1^{(J)}\xi_3 + b_2^{(J)}{\xi_3}^2\cdots \qquad J = 1,2 \tag{3.31}$$

where $b_i, i = 0,1,2,\cdots$ are functions of $P^{(J)}_{\bar{m},\bar{n}-\bar{m}}(j\omega)$ and γ_3. When $\Omega \approx 1$, it is shown that $b_0^{(1)} < 0$ and conclusion (i) is implied.

Then, express $|Y_J(j\Omega)|^2$ as a polynomial in ξ_3 given by

$$|Y_J(j\Omega)|^2 = c_0^{(J)} + c_1^{(J)}\xi_3 + c_2^{(J)}{\xi_3}^2 \cdots \qquad J = 1, 2 \tag{3.32}$$

where $c_i, i = 0, 1, 2, \cdots$ are functions of $P^{(J)}_{\bar{m},\bar{n}-\bar{m}}(j\omega)$ and γ_3. When $\Omega \gg 1$ and it is shown that $c_i^{(J)} \approx 0, , i = 1, 2, \cdots, J = 1, 2$ and conclusion (ii) is implied.

Proposition 3.4 extends the results in [Lang *et al.*, 2009] where $\gamma_3 = 0$ to a Duffing system where $\gamma_3 > 0$ and shows that the beneficial effects of nonlinear damping on a vibration isolation system with linear stiffness are transferable to a Duffing system. Proposition 3.4(i) indicates that an increase in the nonlinear damping ratio can reduce the resonant peaks of both output spectra $Y_1(j\Omega)$ and $Y_2(j\Omega)$ and Proposition 3.4(ii) indicates that the non-resonant regions where $\Omega \ll 1$ and $\Omega \gg 1$ of the output spectra are not affected by ξ_3. These results imply that the nonlinear damping parameter provides an effective way of reducing transmissibilities of System (3.2) at the resonance without causing detrimental effects over the other frequency ranges which gives a major advantage over linear damping when applied to vibration isolation.

The implications of Proposition 3.4 on the design of viscously damped vibration isolation systems is twofold. First, nonlinear damping should be considered when aiming to reduce transmissibilities of a nonlinear Duffing system as it is more effective than linear damping. Second, when designing a vibration isolation system, nonlinear damping can be used in conjunction with nonlinear stiffness such that the beneficial effects of these two nonlinear parameters can complement each other. Examples of the combined use of these two nonlinear parameters will be illustrated in Section 3.4.

3.3.3 Effects of nonlinear damping on the output energy

Proposition 3.5. *Under the same condition of Proposition 3.2, the following results are true for $\xi_1 > 0$ and $\bar{\gamma}_3 \geqslant \gamma_3 \geqslant 0$, where γ_3 is a positive number.*

(i) When $\Omega \approx 1$, there exists a $\bar{\xi_3}$ such that

$$\frac{\partial |E_J(\Omega)|^2}{\partial \xi_3} < 0 \qquad J = 1, 2 \tag{3.33}$$

if $0 < \xi_3 < \bar{\xi}_3$.

(ii) When $\Omega \ll 1$ *or* $\Omega \gg 1$

$$E_J(\Omega)\big|_{\xi_3=0} \approx E_J(\Omega)\big|_{\xi_3>0} \qquad J = 1, 2. \tag{3.34}$$

Proof. See Appendix D.

The results from Proposition 3.5 extend the findings in Proposition 3.4 to show that the effects of nonlinear damping on the total output energy is similar to those on the fundamental harmonic. Proposition 3.5(i) indicates that a positive change in ξ_3 leads to a reduction in the total output energy around the resonant region whereas Proposition 3.5(ii) states that the level of total output energy when the excitation frequency is much lower or much higher than the resonant frequency is hardly affected by ξ_3. The nonlinear damping parameter might cause an increase in the magnitude of some harmonics but Proposition 3.5 shows that the overall effect is negligible.

A summary of Propositions 3.3 to 3.5 is provided in Table 3.1. As explained in Section 3.2, the purpose of a vibration isolation system is to reduce signals transferring from one interface to another so the smaller the magnitudes of the output spectra the better. In other words, a parameter is judged to be beneficial to the vibration isolation performance if the partial derivative of the output spectra with respect to the parameter is negative. It can be seen from Table 3.1 that γ_3 is beneficial to $|Y_1(j\Omega)|$ below the resonant frequency but not to $|Y_2(j\Omega)|$ at resonance whereas ξ_3 is beneficial to both $|Y_1(j\Omega)|$ and $|Y_2(j\Omega)|$ as well as to $|E_1(\Omega)|$ and $|E_2(\Omega)|$ at resonance. These imply that the advantageous effects of γ_3 on $|Y_1(j\Omega)|$ below the resonant frequency can be exploited as long as ξ_3 is introduced to counteract the undesirable effects of γ_3 at resonance. For completeness, the effects of the linear damping parameter ξ_1 is also provided in the table. To avoid the detrimental effects of ξ_1 on the high frequency performance, the value of ξ_1 should be limited.

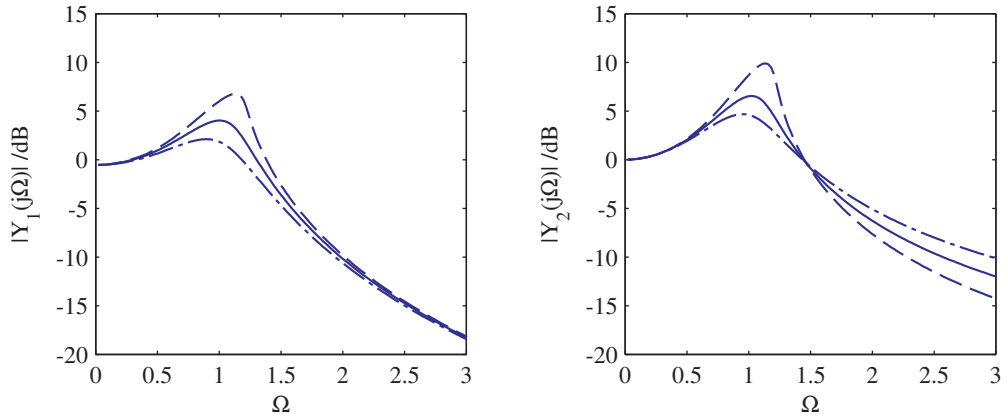

Figure 3.3: The effects of ξ_1 on the output spectra. $\gamma_3 = 0.1$, $\xi_3 = 0$. Dashed: $\xi_1 = 0.4$; Solid: $\xi_1 = 0.6$; Dot-dashed: $\xi_1 = 0.8$.

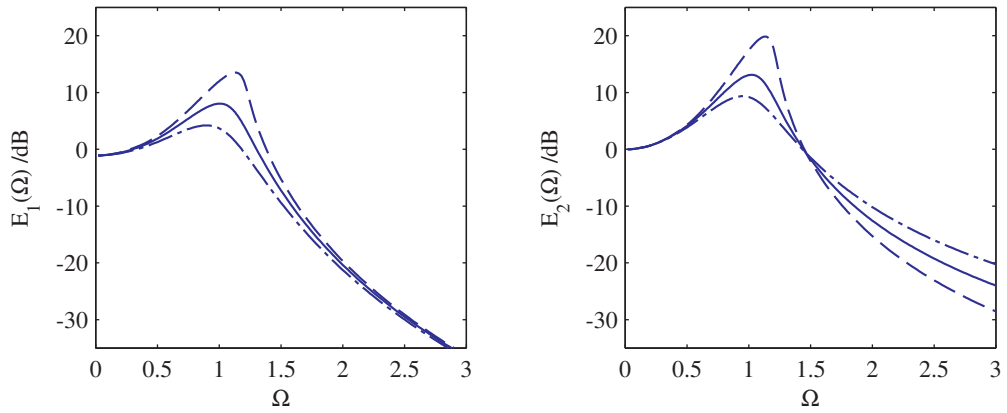

Figure 3.4: The effects of ξ_1 on the output energy spectra. $\gamma_3 = 0.1$, $\xi_3 = 0$. Dashed: $\xi_1 = 0.4$; Solid: $\xi_1 = 0.6$; Dot-dashed: $\xi_1 = 0.8$.

3.4 Simulation studies and discussions

To demonstrate the condition in Proposition 3.1 and the effects of nonlinear stiffness and nonlinear viscous damping on vibration isolation theoretically proven in Propositions 3.3-3.5, numerical simulation studies were conducted and results will be presented in this section.

3.4.1 Simulation studies

The three plots in Fig. 3.2 show the harmonic balance solutions of System (3.2) given by Eq. (3.13) for three different values of ξ_3 to demonstrate the effects of nonlinear damping on the jump phenomena when $\gamma_3 = 0.1$ and $\xi_1 = 0.01$. When the nonlinear damping is small ($\xi_3 = 0.004$), there is a vertical gradient at $\Omega = 1.34$, which is the jump-up frequency. The $B-\Omega$ curve in Fig 3.2(a) shows more than one value of B when $1.34 \leqslant \Omega \leqslant 1.55$, i.e. there are multiple solutions to Eq. (3.13). When ξ_3 reaches a critical value $\xi_{3c} = 0.024$ as shown in Fig 3.2(b), the point where the vertical gradient occurs ($\Omega = 1.33$) is also a point of reflection, which makes Eq. (3.13) give only one real positive B for any $\Omega \geqslant 0$. When $\xi_3 > \xi_{3c} = 0.024$, the output amplitude B becomes a continuously differentiable function of Ω as shown in Fig 3.2(c). These three examples illustrate how nonlinear damping can eliminate unwanted jumps in Duffing systems and the condition under which the elimination occurs.

The condition of System (3.2) such that a valid OFRF can be obtained is defined collectively by γ_{3c}, ξ_{1b} and ξ_{3c} and the elimination of jumps can be achieved by reducing γ_3, raising ξ_1 or ξ_3, or a combination of the above. When determining values for γ_{3c}, ξ_{1b} and ξ_{3c} using Eq. (3.16), two of the three parameters should be fixed so that the third one can be calculated. In the example given in Fig. 3.2, the value of $\xi_{3c} = 0.024$ is obtained for given $\gamma_{3c} = 0.1$ and $\xi_{1b} = 0.01$. Therefore when $\gamma_2 \leqslant 0.1$, $\xi_1 \geqslant 0.01$ and $\xi_3 \geqslant 0.024$, the system has a continuous output spectrum for all $\Omega \geqslant 0$ so that the OFRF approach can be applied to study the effects of the nonlinear characteristic parameters on the system output responses in the frequency domain.

The well-known effects of linear damping on the output spectra of a Duffing system without jumps are illustrated by Figs. 3.3 and 3.4. A relatively high level of linear damping is required to ensure that the condition in Proposition 3.1 is satisfied when $\gamma_3 = 0.1$ and $\xi_3 = 0$. At the resonant frequency where $\Omega \approx 1$, the magnitudes of $Y_J(j\Omega)$ and $E_J(\Omega)$, $J = 1, 2$ are reduced as a result of an increase in ξ_1. However, the impact of ξ_1 on the high frequency region where $\Omega \gg 1$ makes linear damping undesirable in a vibration isolation application as it increases the transmissibilities. The examples below will show that nonlinear

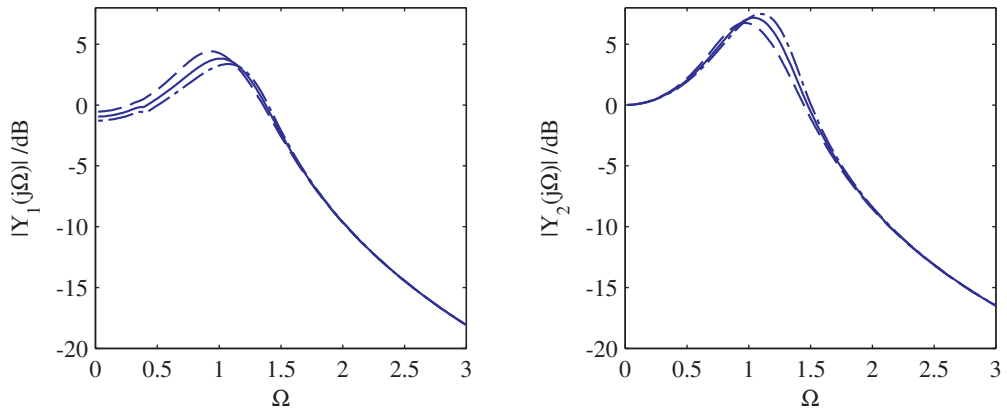

Figure 3.5: The effects of γ_3 on the output spectra. $\xi_1 = \xi_3 = 0.2$ and γ_3 taking the values of 0.1, 0.2 and 0.3. Dashed: $\gamma_3 = 0.1$; Solid: $\gamma_3 = 0.2$; Dot-dashed: $\gamma_3 = 0.3$.

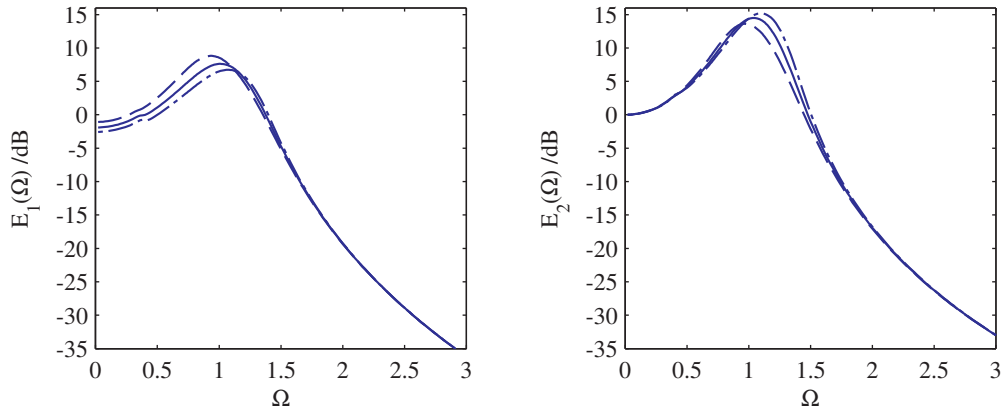

Figure 3.6: The effects of γ_3 on the output energy spectra. $\xi_1 = \xi_3 = 0.2$ and γ_3 taking the values of 0.1, 0.2 and 0.3. Dashed: $\gamma_3 = 0.1$; Solid: $\gamma_3 = 0.2$; Dot-dashed: $\gamma_3 = 0.3$.

damping is more effective in suppressing both the resonance and the responses over higher frequencies of a Duffing system.

Figs. 3.5 shows the effects of the nonlinear stiffness term on the output spectra of a nonlinearly damped Duffing system under a sinusoidal force excitation. The most interesting observation is the reduction in the magnitude of $Y_1(j\Omega)$, the displacement spectrum, when System (3.2) is forced to vibrate below the resonant frequency where $\Omega < 1$ as indicated by Proposition 3.3(i). This special effect is

beneficial to vibration isolation as the displacement of the moving mass is reduced, although the level of transmitted force remains the same, which is the result of Proposition 3.3(ii). As the value of γ_3 increases, it can be observed from Fig. 3.5 that the resonant peak of $Y_2(j\Omega)$ becomes more prominent, which is highly undesirable in vibration isolation. This is from result (iii) of Proposition 3.3. When $\Omega \gg 1$, all three curves representing the outputs of System (3.2) when γ_3 takes different values are overlapping, which indicates that γ_3 has insignificant effects on $Y_1(j\Omega)$ and $Y_2(j\Omega)$. This is exactly result (iv) of Proposition 3.3. Similar effects on the output energy spectra are observed in Fig. 3.6. When designing a vibration isolator involving nonlinear stiffness, the beneficial effects indicated by Proposition 3.3(i) and (iv) should be exploited if the detrimental effect around the resonant frequency given by Proposition 3.3(iii) can be managed.

The effects of nonlinear damping on a Duffing system under the excitation of a sinusoidal force in the case of $\gamma_3 = 0.1$, $\xi_1 = 0.1$ are illustrated by Figs. 3.7 and 3.8, and in the case of $\gamma_3 = 0.2$, $\xi_1 = 0.1$ by Figs. 3.9 and 3.10. All the figures clearly show that the increase of the nonlinear damping ratio ξ_3 causes a reduction of the resonance of all output spectra and output energy spectra when $\Omega \approx 1$ but these spectra remain almost unaffected by the change over the frequency ranges far away from the resonance where $\Omega \ll 1$ and $\Omega \gg 1$. The comparison of these results with Figs. 3.3 and 3.4 highlights the advantages of resonance suppression using nonlinear damping over linear damping in vibration isolation. Linear damping achieves the resonance suppression at a cost of the rise in the transmissibilities over the high frequency range whereas nonlinear damping can achieve the same level of suppression without introducing any significant alteration to the higher frequency transmissibilities. These are the results of Propositions 3.4 and 3.5.

A local maximum caused by the cubic nonlinear stiffness can be observed on each of the energy spectra at approximately one third of the resonant frequency in Fig. 3.10. These local maxima interrupt the continual increase of output energy as the excitation frequency increases from DC towards the resonant frequency. They are more prominent on the energy spectra than on the output frequency spectra in Fig. 3.9 which suggests that γ_3 affects the harmonics in the output more than the fundamental frequency component and confirms the validity of the use of the OFRF approach in the analysis of the system responses in these cases. Any

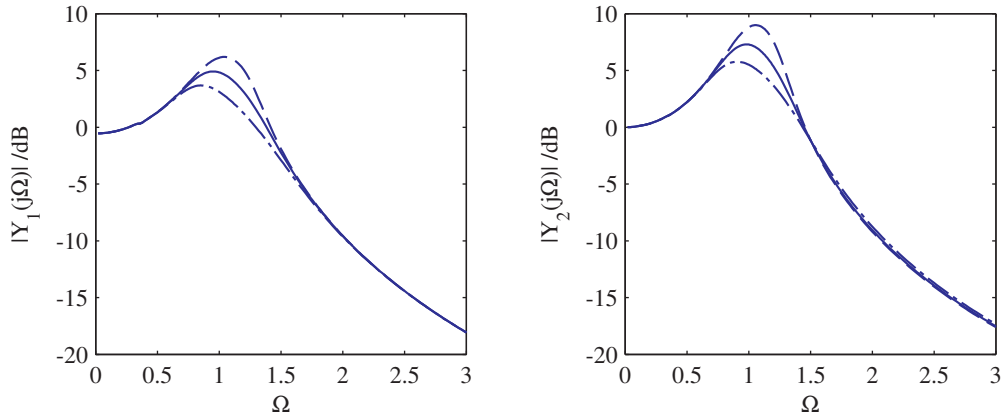

Figure 3.7: The effects of ξ_3 on the output spectra. $\xi_1 = 0.1$, $\gamma_3 = 0.1$. Dashed: $\xi_3 = 0.1$; Solid: $\xi_3 = 0.2$; Dot-dashed: $\xi_3 = 0.4$.

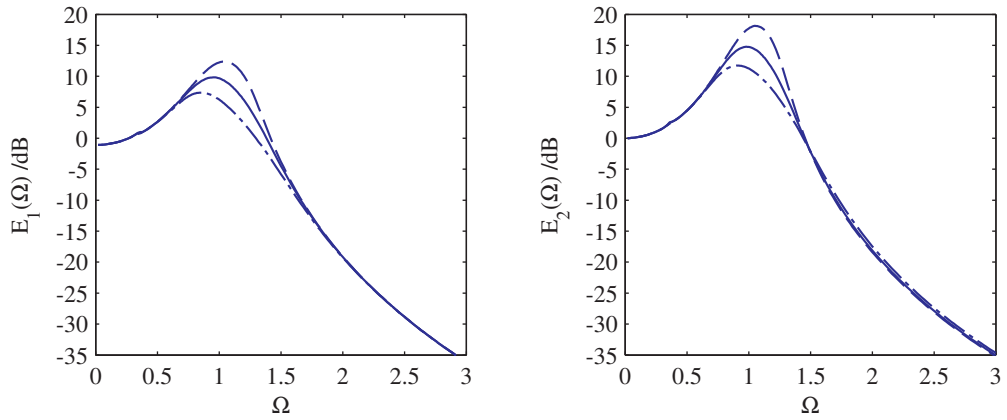

Figure 3.8: The effects of ξ_3 on the output energy spectra. $\xi_1 = 0.1$, $\gamma_3 = 0.1$. Dashed: $\xi_3 = 0.1$; Solid: $\xi_3 = 0.2$; Dot-dashed: $\xi_3 = 0.4$.

increase in the output energy is generally undesirable in vibration isolation but the zoomed-in views in Fig. 3.10 show that the effects of γ_3 on the output harmonics can be weakened by increasing nonlinear damping. This is another advantage of applying nonlinear damping to a Duffing system for vibration isolation.

3.4.2 Discussions

The properties of a nonlinearly damped Duffing system demonstrated by numerical studies in the above section can be exploited to design vibration isolation systems.

In such designs, first, the beneficial effects of nonlinear damping on the output spectra of a Duffing system illustrated above should be considered when aiming to suppress the resonant vibrations. For example, to reduce the transmissibility of a Duffing system that has a nonlinear stiffness ratio $\gamma_3 = 0.1$, a linear damping ratio $\xi_1 = 0.3$ and no nonlinear damping, it is best to introduce nonlinear damping ξ_3 instead of raising the value of ξ_1 because of its ability to reduce the transmissibility around the resonant frequency with little impact on the high frequency performance. In Fig. 3.11, the original system is given by the dotted lines and the same level of resonance suppression can be achieved by either increasing ξ_1 from 0.3 to 0.6 (dashed lines) or by introducing $\xi_3 = 0.16$ (solid lines). At $\Omega = 3$, the magnitude of $Y_2(j\Omega)$ increases from -15 to -12 dB as ξ_1 increases but it is maintained at about -15 dB when ξ_3 is introduced. It is very clear that nonlinear damping is preferable to linear damping when vibration isolation is required over a large range of frequencies.

Second, the beneficial effects of nonlinear stiffness on the displacement spectrum can be exploited when designing a vibration isolation system where the movement of the mass is of concern. As described by Proposition 3.3(i), the displacement of the mass in a Duffing system can be reduced by raising the nonlinear stiffness parameter when the excitation frequency is below the resonant frequency. However, some undesired consequences such as the increase in the resonant force transmissibility and the amplification of superharmonics must be minimised by increasing the nonlinear damping parameter. Fig. 3.12 shows two Duffing systems with a similar resonant peak in the force spectrum achieved through different means. The first system has $\xi_3 = 0.4$ and a weaker nonlinear stiffness term where $\gamma_3 = 0.17$. The displacement spectrum $Y_1(j\Omega)$ starts just below 0 dB at $\Omega = 0$. The second system has a much stronger nonlinear stiffness term where $\gamma_3 = 0.6$ so that $Y_1(j\Omega)$ starts at a smaller magnitude of about -2 dB at $\Omega = 0$. The undesirable effects of increasing γ_3 are concealed by raising ξ_3 to 0.6. It can also be observed that the system with a stronger nonlinear stiffness term has a $Y_1(j\Omega)$ which is approximately 2 dB lower than that of the system with a weaker nonlinear stiffness term at $\Omega = 1$. The force spectra $Y_2(j\Omega)$ of the two systems are similar although the system with a higher nonlinear stiffness parameter has its force transmissibility peak shifted a little to the right.

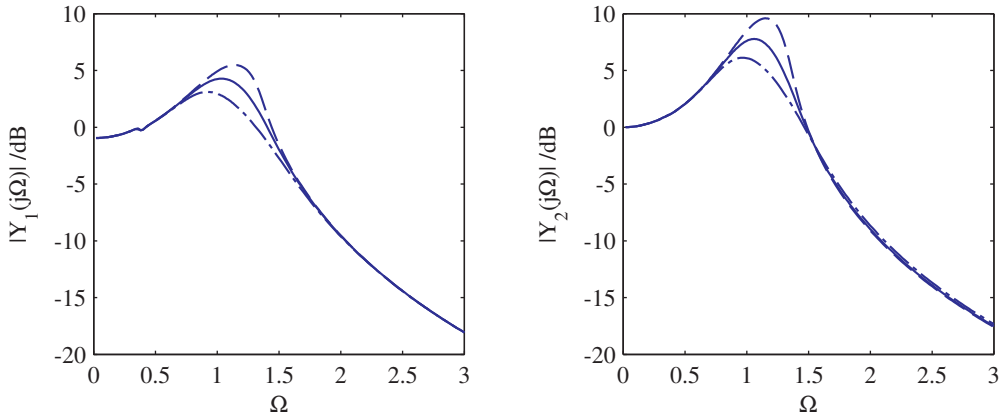

Figure 3.9: The effects of ξ_3 on the output spectra. $\xi_1 = 0.1$, $\gamma_3 = 0.2$. Dashed: $\xi_3 = 0.1$; Solid: $\xi_3 = 0.2$; Dot-dashed: $\xi_3 = 0.4$.

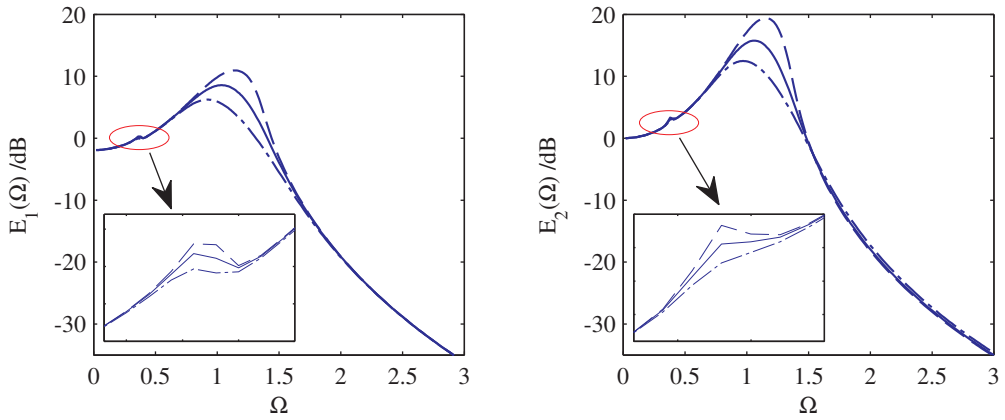

Figure 3.10: The effects of ξ_3 on the output energy spectra. $\xi_1 = 0.1$, $\gamma_3 = 0.2$. Dashed: $\xi_3 = 0.1$; Solid: $\xi_3 = 0.2$; Dot-dashed: $\xi_3 = 0.4$.

The comparison of the two Duffing systems in Fig. 3.12 shows that it is sometimes desirable to introduce nonlinear stiffness in vibration isolation provided that a suitable level of nonlinear damping is designed to compensate for the undesirable effects. The benefits introduced by nonlinear stiffness are not significant if only the force transmissibility is considered but the reduction in the displacement of the moving mass may be essential in some applications. Neither design has an absolute advantage over the other. The choice would depend on the objectives of the application and the implementation of the two nonlinear terms.

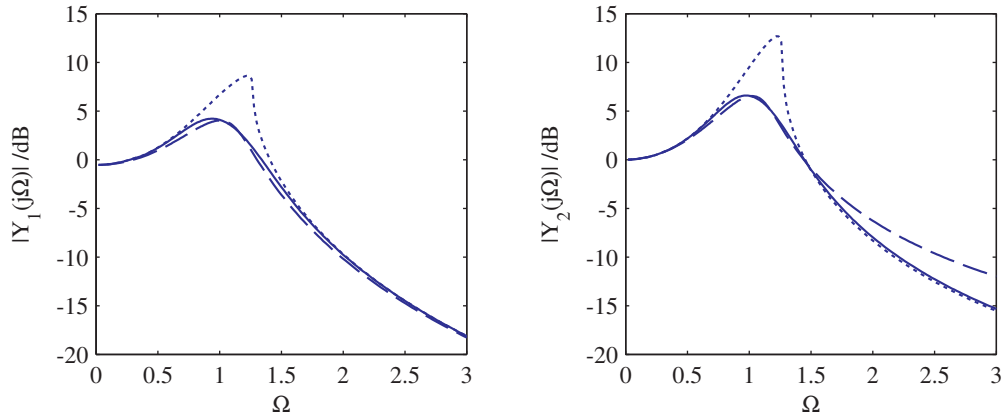

Figure 3.11: Comparison between linearly damped and nonlinearly damped Duffing systems where $\gamma_3 = 0.1$. Dotted: $\xi_1 = 0.3, \xi_3 = 0$; Dashed: $\xi_1 = 0.6, \xi_3 = 0$; Solid: $\xi_1 = 0.3, \xi_3 = 0.16$

3.5 Conclusions

The nonlinear stiffness term in the Duffing equation fascinates many researchers as it causes jump phenomenon when the level of damping is low. Either linear or nonlinear damping can be used to eliminate jumps, which is essential in almost all applications. To analyse the properties of the linearly or nonlinearly damped Duffing equation in the frequency domain, the perturbation method and the harmonic balance method are commonly used to find the amplitude-frequency relationship expressed in an implicit function where the higher harmonics are usually ignored to reduce the computational burden. The implicit function is usually a high order polynomial in amplitude (or frequency) but the relationship between the nonlinear parameters, namely the nonlinear stiffness and the nonlinear damping ratio, and the system output frequency responses is not clear.

The analysis in this chapter is based on the output frequency response function (OFRF) approach. Using this approach, the output spectra of a general polynomial form differential equation model, such as the Duffing equation, can be written down as a polynomial in the nonlinear parameters that define the system nonlinearity. This is a powerful method as the effects of the nonlinear parameters on the output spectra can be theoretically analysed without the need to ignore higher harmonics or to resort to numerical computation.

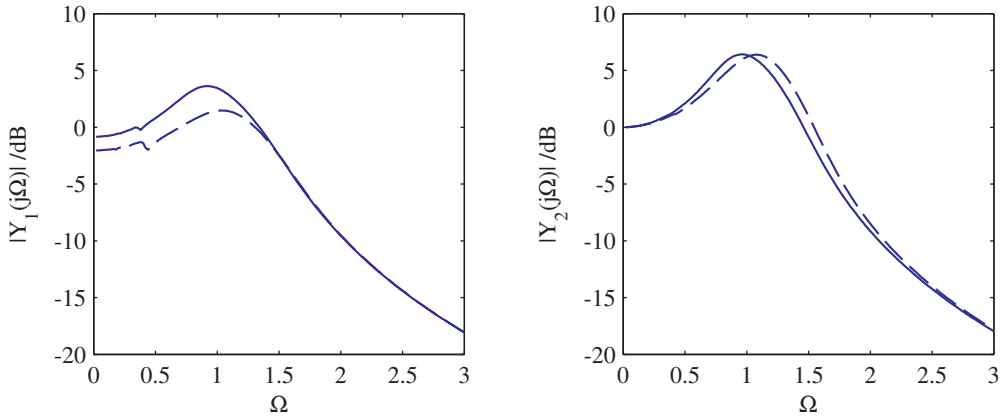

Figure 3.12: Comparison between two nonlinearly damped Duffing system with equivalent resonance where $\xi_1 = 0.001$. Solid: $\gamma_3 = 0.17, \xi_3 = 0.4$; Dashed: $\gamma_3 = 0.6, \xi_3 = 0.6$

In this chapter, in reference to a vibration isolation application, the OFRF approach has been applied to the nonlinearly damped Duffing equation under a sinusoidal input to reveal the effects of the nonlinear stiffness parameter, γ_3 and the nonlinear damping parameter, ξ_3, on the system output frequency responses. First, a condition was established using the harmonic balance method to determine the range of γ_3, ξ_1 and ξ_3 where the system exhibits no jumps so can be represented by a convergent Volterra series. Second, the OFRF's of the system outputs and the output energy spectra in the form of a polynomial in γ_3 and ξ_3 were deduced. Third, the effects of γ_3 and ξ_3 on the output spectra were analysed respectively. The Duffing stiffness is known for creating harmonics and increasing the height of the resonant peak, both of which are undesirable in vibration isolation. But the analysis shows the ability of Duffing stiffness to reduce the low frequency displacement, which has received little attention from other authors. The examination of the OFRF's also reveals that the nonlinear damping parameter can suppress the resonant peak without causing significant alterations in the output spectra and the output energy spectra in the non-resonant areas. This means that nonlinear damping is not only effective in counteracting the effects of the Duffing stiffness on the resonance, but is also capable of maintaining a good low frequency displacement performance introduced by the Duffing stiffness. Finally, simulation results

are provided to support the theoretical findings.

The results presented in this chapter have two major implications on the design of passive vibration isolation systems. First, nonlinear damping should be applied to systems that have a nonlinear stiffness, such as buckled beams, for it can achieve the same level of resonance suppression as linear damping but without causing any detrimental effects on the high frequency transmissibility. Second, the beneficial effects of nonlinear damping on both the output spectra and the output energy spectra should be exploited in the design of nonlinear vibration isolators. Additional nonlinear stiffness can be included if it is desirable to reduce the low frequency displacement. If this is the case, the level of nonlinear damping should be increased to compensate for the extra harmonics introduced by the nonlinear stiffness. The realisation and design of the nonlinearly damped force vibration isolation system studied in this chapter will be described in Chapters 5 and 6.

Chapter 4

Analysis of nonlinearly damped displacement vibration isolation systems

4.1 Introduction

The advantage of including nonlinear damping in a force vibration isolation system has been discussed in the previous chapter. Whilst linear systems have the same expression for both force and displacement transmissibility, the displacement transmissibility of vibration isolation systems with nonlinear viscous damping needs to be studied separately. When the force transmissibility is concerned, a cubic damping characteristic has been shown to be more effective than linear damping over a wide range of frequencies. However, when a base-excited vibration isolator is concerned, as Milovanovic *et al.* [2009] have pointed out, cubic damping was found to have very poor performance at high frequencies compared with a simple linear system despite offering good resonance suppression. It is therefore worth investigating whether other types of nonlinear viscous damping could provide a better overall performance.

Vibration isolation systems with a wider range of nonlinear damping where the damping force is proportional to the power of the velocity have been studied by Guo *et al.* [2012]. The power of the velocity, known as the damping exponent, has

a significant impact on the displacement transmissibility curve, especially over the high frequencies. Using numerical methods, it has been shown that, contrary to the force isolation system, a small damping exponent is beneficial to the displacement transmissibility. This result is important to the understanding of the properties of nonlinear damping but it lacks strong theoretical support.

In this chapter, a displacement vibration isolation system with a nonlinear viscous damping characteristic will be studied using the OFRF approach for the first time. The frequency response of systems with different damping exponents will be compared analytically over different frequency ranges to theoretically validate the results in Guo *et al.* [2012]. Simulation results will also be provided to confirm the theoretical findings.

4.2 Nonlinearly damped displacement vibration isolator

Consider the single-degree-of-freedom vibration isolation system consisting of a mass, a linear damper in parallel with a linear spring and an additional nonlinear viscous damper as shown in Fig. 4.1. The equation of motion of the system can be obtained as

$$M\ddot{z}(t) + Kz(t) + C\dot{z}(t) + F_c = -M\ddot{x}_{in}(t) \tag{4.1}$$

where $z(t) = x_{out}(t) - x_{in}(t)$, M is the mass, K is the spring stiffness, C is the linear damping constant, F_c is a nonlinear damping force defined by

$$F_c = \text{sign}[\dot{z}(t)]C_p|\dot{z}(t)|^p, \tag{4.2}$$

C_p is the nonlinear damping constant, $p > 0$ is the damping exponent and $x_{in}(t)$ is a sinusoidal input displacement given by $x_{in}(t) = A_D \sin(\bar{\omega}t)$ with frequency $\bar{\omega}$ and amplitude A_D. The resonant frequency ω_0 of the system is given by

$$\omega_0 = \sqrt{\frac{K}{M}}. \tag{4.3}$$

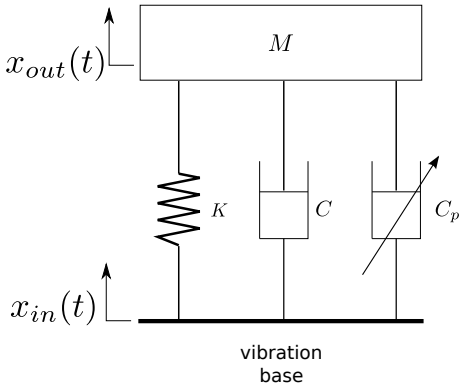

Figure 4.1: Displacement vibration isolation system with additional nonlinear damping.

When $F_c = 0$, Eq. (4.1) describes the motion of a simple well-known linear vibration isolation system.

To conduct a general analysis that is independent of the input magnitude, Eqs. (4.1) and (4.2) are converted into a non-dimensional form given by

$$\begin{cases} \ddot{y}_1(\tau) + \xi_1 \dot{y}_1(\tau) + \text{sign}[\dot{y}_1(\tau)]\xi_p |\dot{y}_1(\tau)|^p + y_1(\tau) = -\ddot{u}(\tau) \\ y_2(\tau) = u(\tau) + y_1(\tau) \end{cases} \tag{4.4}$$

where

$$\tau = \omega_0 t, \tag{4.5}$$

$$\Omega = \frac{\bar{\omega}}{\omega_0}, \tag{4.6}$$

$$u(\tau) = \frac{x_{in}(t)}{A_D}, \tag{4.7}$$

$$y_1(\tau) = \frac{z(t)}{A_D}, \tag{4.8}$$

$$\xi_1 = \frac{C}{\sqrt{KM}}, \tag{4.9}$$

$$\xi_p = \frac{C_2}{A_D} \left(\frac{A_D}{\sqrt{KM}} \right)^p. \tag{4.10}$$

From Eqs. (4.4), (4.7) and (4.8), it can be deduced that

$$y_2(\tau) = \frac{x_{out}(t)}{A_D} \tag{4.11}$$

which is the ratio of the amplitudes of the output and input displacements. Therefore, the displacement transmissibility in terms of the normalised frequency Ω of System (4.1), denoted by $T_D(\Omega)$, can be expressed as

$$T_D(\Omega) = \left| \mathcal{F}\left\{ \frac{x_{out}(t)}{A_D} \right\} \Big|_{\omega=\Omega} \right| = \left| \mathcal{F}\left\{ y_2(\tau) \right\} |_{\omega=\Omega} \right| = |Y_2(j\Omega)| \tag{4.12}$$

where $\mathcal{F}(\cdot)$ denotes the Fourier transform operation. $Y_2(j\Omega)$, the Fourier transform of $y_2(\tau)$ evaluated at the normalised excitation frequency, will be expressed as a polynomial in terms of the nonlinear damping coefficient, ξ_p, using the OFRF approach detailed in Chapter 2. This explicit expression of the displacement transmissibility will then undergo rigorous analytical analysis to reveal the effects of the damping exponent p as well as the damping coefficient ξ_p on the vibration isolation performance of System (4.1) in the following section.

4.3 OFRF representation of the displacement transmissibility

Let p be an odd integer which is larger than or equal to three, System (4.4) then becomes a general polynomial form differential equation model given by

$$\begin{cases} \ddot{y}_1(\tau) + \xi_1 \dot{y}_1(\tau) + \xi_p \dot{y}_1(\tau)^p + y_1(\tau) = -\ddot{u}(\tau) \\ y_2(\tau) = u(\tau) + y_1(\tau) \end{cases} \qquad p \in \{3, 5, 7, \cdots\} \tag{4.13}$$

which can normally be described in the neighbourhood of the equilibrium by the Volterra series and is stable at the zero equilibrium. The second output spectrum of System (4.13), a specific form of System (4.4), can be represented by a polynomial in terms of the nonlinear damping coefficient as described in Proposition 4.1 below.

Proposition 4.1. *The second output spectrum of System* (4.13) *under a sinusoidal*

input $u(\tau) = \sin(\Omega\tau)$ *can be expressed by*

$$\begin{aligned} Y_2(j\Omega) =& P_0(j\Omega) + P_1^{[p]}(j\Omega)\xi_p + P_2^{[p]}(j\Omega){\xi_p}^2 + \cdots + P_{\lfloor (N-1)/(p-1)\rfloor}^{[p]}(j\Omega){\xi_p}^{\lfloor (N-1)/(p-1)\rfloor} \\ =& P_0(j\Omega) + \sum_{\tilde{n}=1}^{\lfloor (N-1)/(p-1)\rfloor} P_{\tilde{n}}^{[p]}(j\Omega){\xi_p}^{\tilde{n}} \qquad N \geqslant p, \quad p \in \{3,5,7,\cdots\} \end{aligned} \tag{4.14}$$

where N *is the maximum order of nonlinearity in the Volterra series representation of the system and* $\lfloor\cdot\rfloor$ *is the floor function indicating the largest integer less than or equal to the operand.* $P_{\tilde{n}}^{[p]}(j\Omega)$*, the coefficient of the term* ${\xi_p}^{\tilde{n}}$*, is a function of frequency* Ω *that depends on the linear parameters of System* (4.4)*.*

Proof. Applying the OFRF procedure for multi-input-multi-output system detailed in Chapter 2 to System (4.13) the following generalized frequency response function (GFRF) between the input and the first and second outputs of System (4.13), respectively.

$$H_1^{(1)}(j\omega_1) = -\frac{(j\omega_1)^2}{(j\omega_1)^2 + j\xi_1\omega_1 + 1} = \frac{\omega_1^2}{(1-\omega_1^2) + j\xi_1\omega_1} = \frac{-\omega_1^2}{L(j\omega_1)} \tag{4.15}$$

$$H_2^{(2)}(j\omega_1) = 1 + H_1^{(1)}(j\omega_1) \tag{4.16}$$

$$H_n^{(2)}(j\omega_1, j\omega_2, \cdots, j\omega_n) = H_n^{(1)}(j\omega_1, j\omega_2, \cdots, j\omega_n) \tag{4.17}$$

$$\begin{aligned} H_n^{(1)}(j\omega_1, \cdots, j\omega_n) &= \xi_p \frac{\prod_{i=1}^{n}(j\omega_i)H_1^{(1)}(j\omega_i)}{L(j\omega_1 + \cdots + j\omega_n)} \\ &\text{for } n = (p-1)\tilde{n} + 1 \text{ where } \tilde{n} = 1 \end{aligned} \tag{4.18}$$

$$H_n^{(1)}(j\omega_1, \cdots, j\omega_n) = {\xi_p}^{\tilde{n}} \frac{\prod_{i=1}^{n}(j\omega_i)H_1^{(1)}(j\omega_i)}{L(j\omega_1 + \cdots + j\omega_n)} \sum_{Z=1}^{N_n} \prod_{i=1}^{\tilde{n}-1} \frac{\left(j\omega_{l_{i(1)}}^{Z} + \cdots + j\omega_{l_{i(j_i^{\tilde{n}})}}^{Z}\right)}{L\left(j\omega_{l_{i(1)}}^{Z} + \cdots + j\omega_{l_{i(j_i^{\tilde{n}})}}^{Z}\right)}$$

$$\text{for } n=(p-1)\tilde{n}+1 \text{ where } \tilde{n}=2,3,\cdots,\left\lfloor\frac{N-1}{p-1}\right\rfloor \tag{4.19}$$

and

$$H_n^{(1)}(j\omega_1,\cdots,j\omega_n)=0 \qquad \text{for other values of } n \tag{4.20}$$

where

$$L(j\omega_1+\cdots j\omega_n)=-\left[(j\omega_1+\cdots j\omega_n)^2+j\xi_1(j\omega_1+\cdots j\omega_n)+1\right] \tag{4.21}$$

$$j_i^{\tilde{n}}, \quad i=1,\ldots,\tilde{n}-1, \quad \in\{3,5,\ldots,(p-1)\tilde{n}-1\} \quad \text{for} \quad \tilde{n}\geqslant 2 \tag{4.22}$$

$$\omega^Z_{l_{i(\bar{j})}}, \quad i=1,\ldots,\tilde{n}-1, \quad \bar{j}=1,\ldots,j_i^{\tilde{n}}, \qquad \in\{\omega_1,\ldots,\omega_n\} \quad \text{for} \quad \tilde{n}\geqslant 2, \tag{4.23}$$

and N_n is an n dependent integer.

Substituting Eq. (4.15)-(4.20) into the general frequency response expression for systems under a sinusoidal input $u(\tau)=\sin(\Omega\tau)$ in Chapter 2 gives the second output spectrum as

$$Y_2(j\omega)=P_0(j\omega)+\sum_{\tilde{n}=1}^{\lfloor\frac{N-1}{p-1}\rfloor} P_{\tilde{n}}^{[p]}(j\omega){\xi_p}^{\tilde{n}} \qquad N\geqslant p, \quad p\in\{3,5,7,\cdots\} \tag{4.24}$$

where

$$P_0(j\omega)=\frac{1+j\xi_1\omega}{(j\omega)^2+j\xi_1\omega+1} \tag{4.25}$$

and

$$\begin{aligned} P_{\tilde{n}}^{[p]}(j\omega) &= \frac{1}{2^n}\sum_{\omega_1+\omega_2+\cdots+\omega_n=\omega} H_n^{(1)}(j\omega_1,\cdots,j\omega_n)A(\omega) \\ &= \frac{1}{2^n L(j\omega)}\sum_{\omega_1+\omega_2+\cdots+\omega_n=\omega}\left[\prod_{i=1}^{n}(j\omega_i)H_1^{(1)}(j\omega_i)A(\omega)\right]\sum_{Z=1}^{N_n}\prod_{i=1}^{\tilde{n}-1}\frac{\left(j\omega^Z_{l_{i(1)}}+\cdots+j\omega^Z_{l_{i(j_i^{\tilde{n}})}}\right)}{L\left(j\omega^Z_{l_{i(1)}}+\cdots+j\omega^Z_{l_{i(j_i^{\tilde{n}})}}\right)}. \end{aligned} \tag{4.26}$$

When $\omega = \Omega$, Eq. (4.24) becomes

$$Y_2(j\Omega) = P_0(j\Omega) + \sum_{\tilde{n}=1}^{\lfloor \frac{N-1}{p-1} \rfloor} P_{\tilde{n}}^{[p]}(j\Omega)\xi_p{}^{\tilde{n}} \qquad N \geqslant p, \quad p \in \{3, 5, 7, \cdots\} \tag{4.27}$$

where

$$P_0(j\Omega) = \frac{1 + j\xi_1\Omega}{(j\Omega)^2 + j\xi_1\Omega + 1} \tag{4.28}$$

and

$$\begin{aligned} P_{\tilde{n}}^{[p]}(j\Omega) &= \frac{\Omega^n \left| H_1^{(1)}(j\Omega) \right|^{n-1} H_1^{(1)}(j\Omega)}{2^n L(j\Omega)} \sum_{\omega_1+\omega_2+\cdots+\omega_n=\Omega} \sum_{Z=1}^{N_n} \prod_{i=1}^{\tilde{n}-1} \frac{\left(j\omega^Z_{l_{i(1)}} + \cdots + j\omega^Z_{l_{i(j_i^{\tilde{n}})}} \right)}{L\left(j\omega^Z_{l_{i(1)}} + \cdots + j\omega^Z_{l_{i(j_i^{\tilde{n}})}} \right)} \\ &= \frac{-\Omega^{3n}}{2^n L(j\Omega)^2 \left| L(j\Omega) \right|^{n-1}} \sum_{\omega_1+\omega_2+\cdots+\omega_n=\Omega} \sum_{Z=1}^{N_n} \prod_{i=1}^{\tilde{n}-1} \frac{\left(j\omega^Z_{l_{i(1)}} + \cdots + j\omega^Z_{l_{i(j_i^{\tilde{n}})}} \right)}{L\left(j\omega^Z_{l_{i(1)}} + \cdots + j\omega^Z_{l_{i(j_i^{\tilde{n}})}} \right)}. \end{aligned} \tag{4.29}$$

This completes the proof for Proposition 4.1. □

Proposition 4.1 provides an explicit relationship between $Y_2(j\omega)$, the second output spectrum of System (4.13), and a nonlinear damping characteristic defined by the damping exponent p and the damping coefficient ξ_p. The degree of the polynomial expression given by Eq. (4.14) depends on the N and p. Substituting Eq. (4.14) into Eq. (4.12) gives the displacement transmissibility of System (4.13) as

$$T_D(\Omega) = \left| P_0(j\Omega) + \sum_{\tilde{n}=1}^{\lfloor (N-1)/(p-1) \rfloor} P_{\tilde{n}}^{[p]}(j\Omega)\xi_p{}^{\tilde{n}} \right| \qquad N \geqslant p, \quad p \in \{3, 5, 7, \cdots\} \tag{4.30}$$

Eq. (4.30) is the OFRF representation of the displacement transmissibility which will facilitate the analysis of the effects of the nonlinear damping characteristic on the system vibration isolation performance in the frequency domain. This expression will be examined for different values of p in the next section.

4.4 Effects of damping exponent

In this section, the properties of the displacement transmissibility $T_D(\Omega)$ will be examined over two particular frequency ranges, the resonant region where $\Omega \approx 1$ and high frequency region where $\Omega \gg 1$. With the OFRF expression of the displacement transmissibility, it is possible to compare the vibration isolation performance of two systems that have different damping exponents. The analytical results will show that the nonlinear damping exponent, rather than the damping coefficient, plays a crucial role in improving the vibration isolation over a wide frequency range.

Proposition 4.2. *For $p_1 \in \{3, 5, 7, \cdots\}$ and $p_2 = p_1 + 2$, there exist a $\xi_{p_1} > 0$ and a $\xi_{p_2} > 0$ such that*

(i) when $\Omega \approx 1$,

$$T_D(\Omega)|_{p=p_1,\xi_1=\xi_{1'},\xi_p=\xi_{p_1}} = T_D(\Omega)|_{p=p_2,\xi_1=\xi_{1'},\xi_p=\xi_{p_2}}. \tag{4.31}$$

(ii) and when $\Omega \gg 1$

$$T_D(\Omega)|_{p=p_1,\xi_1=\xi_{1'},\xi_p=\xi_{p_1}} < T_D(\Omega)|_{p=p_2,\xi_1=\xi_{1'},\xi_p=\xi_{p_2}}. \tag{4.32}$$

Proof. Let $T^A(\Omega)$ denote the displacement transmissibility of System (4.13) where $p = p_1$, $\xi_1 = \xi_{1'}$ and $\xi_p = \xi_{p_1}$, and $T^B(\Omega)$ denote the displacement transmissibility of System (4.13) where $p = p_2 = p_1 + 2$, $\xi_1 = \xi_{1'}$ and $\xi_p = \xi_{p_2} = \xi_{p_1} - \delta$ where δ is finite and positive. For $N = 2p_1 - 1$, the polynomial expressions of $T^A(\Omega)$ and $T^B(\Omega)$, from Eq.(4.30), are

$$T^A(\Omega) = \left| P_0(j\Omega) + P_1^{[p_1]}(j\Omega)\xi_{p_1} + P_2^{[p_1]}(j\Omega)\,{\xi_{p_1}}^2 \right| \tag{4.33}$$

and

$$T^B(\Omega) = \left| P_0(j\Omega) + P_1^{[p_2]}(j\Omega)\,(\xi_{p_1} - \delta) \right| \tag{4.34}$$

respectively. Equating Eqs. (4.33) and (4.33) at $\Omega = 1$ yields a polynomial in ξ_{p_1} given by

$$c_4 {\xi_{p_1}}^4 + c_3 {\xi_{p_1}}^3 + c_2 {\xi_{p_1}}^2 + c_1 \xi_{p_1} + c_0 = 0 \tag{4.35}$$

where the coefficients

$$c_0 = \mathrm{Re}\left[P_0(j) P_1^{[p_2]}(-j)\right] \delta - \left|P_1^{[p_2]}(j)\right|^2 \delta^2 \tag{4.36}$$

$$c_4 = \left|P_1^{[p_2]}(j)\right|^2 \tag{4.37}$$

and c_1, c_2, c_3 are real functions of $P_0(j\Omega)$, $P_1^{[p_1]}(j\Omega)$, $P_2^{[p_1]}(j\Omega)$ and $P_1^{[p_2]}(j\Omega)$. Given that all the coefficients are real and c_4 is always positive, according to Descartes' rule of signs [Anderson *et al.*, 1998; Struik, 1969], Eq.(4.35) must have one or three positive real roots if c_0 is negative. Evaluating Eq. (4.28) at $\Omega = 1$ and Eq. (4.29) at $\Omega = 1$ where $\xi_1 = \xi_{1'}$, $p = p_2$ and $\bar{n} = 1$ provides

$$P(j) = \frac{1 + j\xi_{1'}}{j\xi_{1'}} \tag{4.38}$$

and

$$P_1^{[p_2]}(j) = \frac{-(1)^{3n}}{2^n L(j)^2 \left|L(j)\right|^{n-1}} = \frac{1}{2^{p_2} {\xi_{1'}}^{p_2+1}} \tag{4.39}$$

respectively. It can be obtained from Eqs. (4.36), (4.38) and (4.39) that

$$c_0 = \mathrm{Re}\left[\frac{1 + j\xi_{1'}}{j\xi_{1'}} \cdot \frac{1}{2^{p_2} {\xi_{1'}}^{p_2+1}}\right] \delta - \left|\frac{1}{2^{p_2} {\xi_{1'}}^{p_2+1}}\right|^2 \delta^2 < 0 \quad \Rightarrow \quad \delta > 2^{p_2} {\xi_{1'}}^{p_2+1}. \tag{4.40}$$

Therefore, if $\delta > 2^{p_2} {\xi_{1'}}^{p_2+1}$, there exists a ξ_{p_1} such that $T^A(\Omega) = T^B(\Omega)$ at $\Omega = 1$, which is the summary of Proposition 4.2(i).

When $\Omega \gg 1$,

$$P_0(j\Omega) \approx \frac{-j\xi_{1'}}{\Omega} \tag{4.41}$$

and

$$P_{\tilde{n}}^{[p]}(j\Omega) \approx \frac{-\Omega^{3n}}{2^n\Omega^4\Omega^{2(n-1)}} \sum_{\omega_1+\omega_2+\cdots+\omega_n=\Omega} \sum_{Z=1}^{N_n} \prod_{i=1}^{\tilde{n}-1} \frac{1}{L\left(j\omega_{l_{i(1)}}^Z + \cdots + j\omega_{l_{i(j_i^{\tilde{n}})}}^Z\right)}$$
$$= \frac{-\Omega^{3n}}{2^n\Omega^4\Omega^{2(n-1)}\Omega^{\tilde{n}-1}} \sum_{\omega_1+\omega_2+\cdots+\omega_n=\Omega} \sum_{Z=1}^{N_n} \prod_{i=1}^{\tilde{n}-1} \frac{\Omega}{L\left(j\omega_{l_{i(1)}}^Z + \cdots + j\omega_{l_{i(j_i^{\tilde{n}})}}^Z\right)}$$
$$= \frac{-\Omega^{p-1}}{2^{(p-1)\tilde{n}+1}} C_{p,\tilde{n}} \tag{4.42}$$

where

$$C_{p,\tilde{n}} = \sum_{\omega_1+\omega_2+\cdots+\omega_n=\Omega} \sum_{Z=1}^{N_n} \prod_{i=1}^{\tilde{n}-1} \frac{\Omega}{L\left(j\omega_{l_{i(1)}}^Z + \cdots + j\omega_{l_{i(j_i^{\tilde{n}})}}^Z\right)} \tag{4.43}$$

is a bounded constant which is dependent on $\tilde{n}$ and p but independent of Ω. Thus,

$$\begin{aligned} T^A(\Omega) =& |P_0(j\Omega)|^2 + \left|P_1^{[p_1]}(j\Omega)\right|^2 \xi_{p_1}^2 + \left|P_2^{[p_1]}(j\Omega)\right|^2 {\xi_{p_1}}^4 \\ &+ \mathrm{Re}\left[P_0(j\Omega)P_1^{[p_1]}(-j\Omega)\right] \xi_{p_1} + \mathrm{Re}\left[P_0(j\Omega)P_2^{[p_1]}(-j\Omega)\right] {\xi_{p_1}}^2 \\ &+ \mathrm{Re}\left[P_1^{[p_1]}(j\Omega)P_2^{[p_1]}(-j\Omega)\right] {\xi_{p_1}}^3 \\ \approx& \left|+P_1^{[p_1]}(j\Omega)\right|^2 \xi_{p_1}^2 + \left|P_2^{[p_1]}(j\Omega)\right|^2 {\xi_{p_1}}^4 + \mathrm{Re}\left[P_1^{[p_1]}(j\Omega)P_2^{[p_1]}(-j\Omega)\right] {\xi_{p_1}}^3 \\ =& \Omega^{2(p_1-1)} C_A \end{aligned} \tag{4.44}$$

where C_A is a bounded constant which is dependent on $P_1^{[p_1]}(j\Omega)$, $P_2^{[p_1]}(j\Omega)$ and ξ_{p_1} but is independent of Ω. Similarly,

$$T^B(\Omega) \approx \Omega^{2(p_2-1)} C_B \tag{4.45}$$

where C_B is a bounded constant which is dependent on $P_1^{[p_2]}(j\Omega)$ and ξ_{p_2} but is independent of Ω. Because $p_2 > p_1$, it can be concluded that $\Omega^{2(p_2-1)}C_B > \Omega^{2(p_1-1)}C_A$ for $\Omega \gg 1$. Therefore, $T^B(\Omega) > T^A(\Omega)$ is true and the second conclusion of Proposition 4.2 is reached. This completes the proof for Proposition 4.2.□

Proposition 4.2 compares two nonlinear vibration isolation systems with the same linear damping ratio but different damping parameters to provide a theoretical proof for the numerical results in [Guo *et al.*, 2012]. To demonstrate the effects of the damping exponent on the displacement transmissibility, consider System (4.13) with parameters taking values from the two following cases.

System(a): $p = p_1$, $\xi_1 = \xi_{1'} > 0$ and $\xi_p = \xi_{p_1} > 0$

System(b): $p = p_2$, $\xi_1 = \xi_{1'} > 0$ and $\xi_p = \xi_{p_2} > 0$

where $p_1 < p_2$. Proposition 4.2 states that, for some values of ξ_{p_1} and ξ_{p_2}, the two systems have the same displacement transmissibility at $\Omega \approx 1$ but System(a) has a smaller displacement transmissibility than System(b) when $\Omega \gg 1$. This result implies that, for two systems that are indifferent at $\Omega \approx 1$, the system with a lower damping exponent provides better vibration isolation at high frequencies. In other words, System(a) provides better vibration isolation than System(b) when the excitation frequency is large. Therefore, when designing a displacement vibration isolation system with a nonlinear viscous damping characteristic, a small damping exponent is preferable.

Proposition 4.2 is based on System (4.13), a specific form of System (4.4), where the damping exponent p is an odd integer larger than or equal to three. This limitation allows a simple expression of the displacement transmissibility in terms of ξ_p given by Eq. (4.30). It may be possible to extend this proposition for the general System (4.4) for all $p \in (0, \infty)$. A brief description of the method is provided below.

To satisfy the requirements of the OFRF approach, System (4.4) must be represented by a general polynomial form differential equation model, which means that the power of each term must be an integer. This can be achieved by approximating the odd damping function by a polynomial in $\dot{y}_1(\tau)$ given by

$$\text{sign}[\dot{y}_1(\tau)]\xi_p|\dot{y}_1(\tau)|^p = \xi_p \sum_{\bar{p}=0}^{\bar{P}} a_{\bar{p}} \dot{y}_1(\tau)^{2\bar{p}+1} \tag{4.46}$$

where $a_{\bar{p}}$ are coefficients that depend on p and $2\bar{P}+1$ is the degree of polynomial approximation. Substituting Eq. (4.46) into System (4.4) will transform

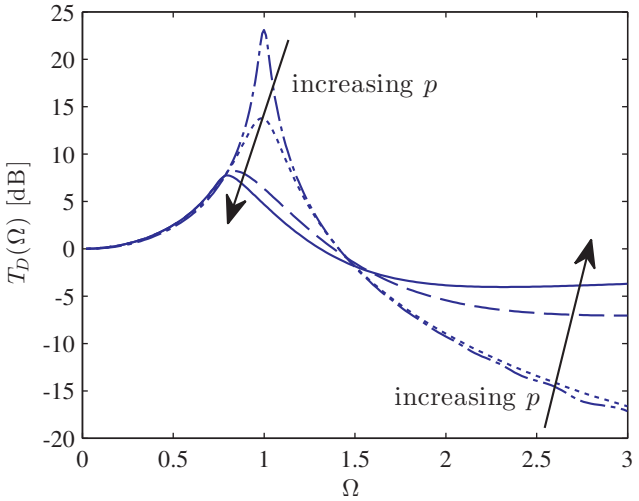

Figure 4.2: The effects of p on the displacement transmissibility. $\xi_1 = 0.01$ and $\xi_p = 0.2$. Solid: $p = 5$; Dashed: $p = 3$; Dotted: $p = 1$; Dot-dashed: $p = \frac{1}{2}$.

System (4.4) into a general polynomial form differential equation model that has P nonlinear terms. The OFRF of such system is more complicated than Eq.(4.30) due to the large number of nonlinear terms, but can be simplified as a function of ξ_p and $a_{\bar{p}}$, which will facilitate further analytical studies.

4.5 Simulation studies and discussions

To demonstrate the effects of the nonlinear damping exponent on vibration isolation theoretically proven in Proposition 4.2, results of numerical simulation conducted using MATLAB are presented in Figs 4.2 to 4.4.

Fig. 4.2 shows the simulation results of System (4.4) for a range of damping exponent p with the nonlinear damping coefficient ξ_p held constant. As the damping exponent increases, the resonant peak reduces whereas the high frequency transmissibility rises. These effects have been observed in Guo *et al.* [2012]. Because of the damping exponent causes the displacement transmissibility to change in opposite directions at the resonant region and over the high frequency range, it is difficult to conclude whether a nonlinear viscous damping characteristic given by Eq. (4.2) is beneficial to the overall vibration isolation performance.

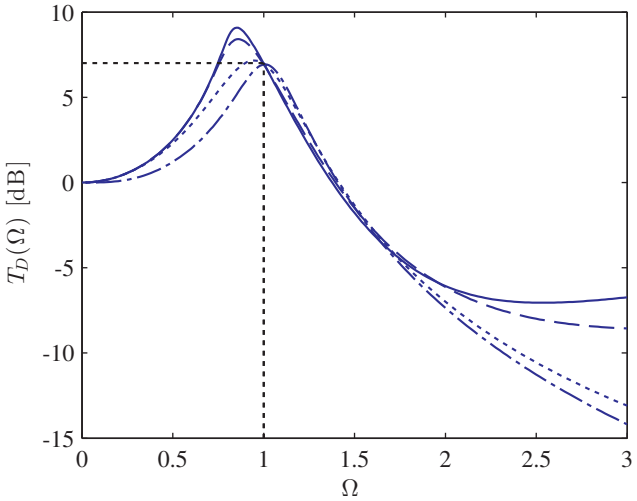

Figure 4.3: Comparison of systems where $\xi_1 = 0.1$ and $T_D(\Omega)|_{\Omega=1} = 7$ dB. Solid: $p = 5$, $\xi_5 = 0.034$; Dashed: $p = 3$, $\xi_3 = 0.13$; Dotted: $p = 1$, $\xi_1 = 0.4$; Dot-dashed: $p = \frac{1}{2}$, $\xi_{\frac{1}{2}} = 0.51$.

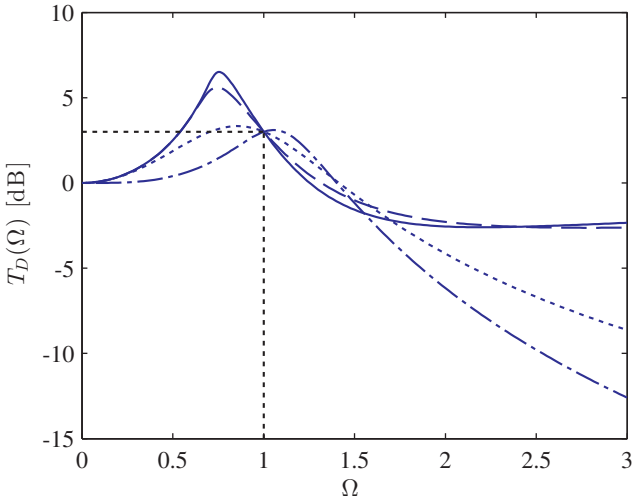

Figure 4.4: Comparison of systems where $\xi_1 = 0.01$ and $T_D(\Omega)|_{\Omega=1} = 3$ dB. Solid: $p = 5$, $\xi_5 = 0.825$; Dashed: $p = 3$, $\xi_3 = 1.06$; Dotted: $p = 1$, $\xi_1 = 0.49$; Dot-dashed: $p = \frac{1}{2}$, $\xi_{\frac{1}{2}} = 0.88$.

Proposition 4.2 compares nonlinear vibration isolation systems that have the same displacement transmissibility at the resonant region for positive odd p. The displacement transmissibility of System (4.4) where $p = 3$ and $p = 5$ are shown by the solid and the dashed lines in Fig. 4.3 respectively. These two curves intersect at $\Omega = 1$ and it is clear that the curve where $p = 3$ has a lower value when $\Omega = 3$. These numerical results validate Proposition 4.2.

To determine whether Proposition 4.2 is also true for non-integer values for p, Fig. 4.3 also includes the transmissibility curves for System (4.4) with $p = \frac{1}{2}$ and a purely linear system where $\xi_p = 1$ as a reference. The transmissibility of these two systems is again 6 dB at $\Omega = 1$ but $T_D(\Omega)$ of the former system is -14.2 dB which is more than 1 dB less than that of the latter system. This result extended Proposition 4.2 for $0 < p < 1$ and is very significant as it shows that System (4.4) can match the vibration isolation performance of its equivalent linear system around resonance while producing higher level of isolation when the excitation frequency is high.

Another set of results where all the curves intersect at $\Omega = 1$ are shown in Fig. 4.4. These systems have a damping exponent ranging from $\frac{1}{2}$ to 5. Among these systems which are indifferent at $\Omega \approx 1$, the transmissibility over the high frequencies falls with the value of the damping exponent p. This confirms the findings of Proposition 4.2 and also demonstrates that the system where $p = \frac{1}{2}$ gives the lowest transmissibility at high frequencies. It is worth noting that the frequency at which the maximum transmissibility occurs increases as a result of the reduction in p. The minor side-effect is relatively insignificant when compared with the improvement of the high frequency isolation performance.

4.6 Conclusions

Displacement vibration isolation systems are required in many applications. Being the only design parameter of a linear vibration isolation system in the non-dimensional form, the linear damping ratio defines the height of the resonance as well as the high frequency transmissibility. To dampen the resonance by increasing the linear damping ratio, the high frequency transmissibility suffers as a result. To overcome this limitation, the idea of nonlinear damping has been studied by

Ravindra & Mallik [1995].

Guo *et al.* [2012] have studied the effects of nonlinear viscous damping on vibration isolation systems by using the Ritz-Galerkin method to find approximate solutions. The numerical results show that a damping exponent that is larger than one is beneficial to a force vibration isolation system but more effective suppression of the displacement transmissibility over the whole frequency range is achieved by a small damping exponent. To provide a strong theoretical basis to support these findings, the nonlinear vibration isolation system has been re-examined using the OFRF approach in this chapter.

The frequency response of a single-degree-of-freedom vibration system with a nonlinear viscous damping characteristic under a sinusoidal displacement excitation has been studied analytically using the OFRF approach. To demonstrate the effects the damping exponent on the system vibration isolation performance, the displacement transmissibility over the whole frequency range is represented by an explicit function of the damping coefficient and the damping exponent in the form of a polynomial, which leads to the theoretical comparison of systems with different damping exponents. It has been shown that systems with different damping exponents can have the same transmissibility at the resonant frequency but the one with a smaller damping exponent produces much better vibration isolation at high frequencies.

The findings in this chapter has provided a theoretical analysis of a nonlinear displacement vibration isolation system for the first time. Supported by simulation studies, the results conclude that the beneficial effects of nonlinear damping should be exploited in the design of displacement vibration isolators to produce low transmissibility around the resonant frequency and the high frequency region simultaneously. With this strong theoretical basis, the proposed vibration isolation can be exploited for a wide range of engineering applications and one method of realisation will be discussed in Chapter 5.

Chapter 5

Semi-active implementation of nonlinear vibration isolation system and experimental studies

5.1 Introduction

Magnetorheological (MR) dampers are semi-active devices that have a fluid with viscosity controlled by the supply current. They have been applied to many vibration control problems such as the Nihon-Kagaku-Miraikan building in Japan [Spencer & Nagarajaiah, 2003] and the cable-stayed Dongting Lake Bridge in China [Chen *et al.*, 2003; Duan *et al.*, 2006]. In these studies, the controller calculates the force required from the MR damper to reduce the vibration of a structure based on sensor measurements of the structural responses, which means that the MR damper is used as a semi-active device to give a force that is dependant on the system outputs. In other words, the damper is acting as an actuator in a feedback-control loop as illustrated in Fig. 5.1(a). The complex nonlinear characteristics of the MR damper, as well as the controlled structure, must be taken into account when designing this kind of feedback-control loop and more challenging nonlinear multi-input-multi-output problems have to be considered when more than one control loops are involved.

The control problem of many of the above mentioned applications may be sim-

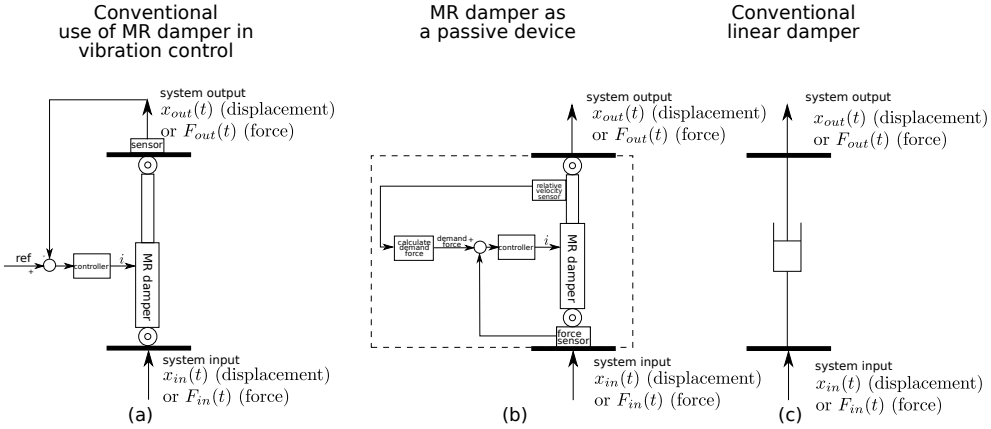

Figure 5.1: An illustration of two different approaches of using an MR damper for vibration isolation. (a) Conventional use of MR damper in vibration control (b) MR damper used as a passive damping device with a desired characteristic. (c) Conventional linear viscous damper

plified if the MR dampers are used as energy dissipating devices like conventional dampers but with a desired damping force-velocity relationship. Recently, a new structure of an MR damper based vibration control system was proposed by Laalej *et al.* [2012] where the MR damper is used as a damper rather than an actuator in a feedback-control loop. Fig. 5.1(b) illustrates this idea on a single-degree-of-freedom (sdof) vibration isolation system. Unlike the conventional approach in Fig. 5.1(a), the MR damper is under a closed-loop control which makes the MR damper behave as a viscous damper with a desired damping characteristic. In this new configuration, the MR damper and the feedback-controller form a stand-alone passive damping unit, indicated by the dashed box, which is an easy substitute of any two-terminal passive device such as the conventional linear viscous damper depicted by Fig. 5.1(c).

To benefit from the MR damper-based damping unit, the force-velocity relationship must be designed to produce a desired system performance. As illustrated by the theoretical studies in Chapters 3 and 4, a vibration isolation system with an appropriate nonlinear damping characteristic can provide a good level of isolation over all wide range frequencies, unlike its linear counterpart which has the classic trade-off between the resonant peak suppression and the high-frequency transmissibility. The studies in [Guo *et al.*, 2012; Laalej *et al.*, 2012; Lang *et al.*, 2009;

Ravindra & Mallik, 1994a] imply that an effective vibration isolation system could be created if an appropriate nonlinear damping characteristic is implemented using a feedback-controlled MR damper based on the new control system structure proposed in [Laalej *et al.*, 2012]. Sims *et al.* [1999, 2000] showed that the force-velocity relationship of an electrorheological damper can be shaped into a quadratic or a higher-order polynomial function by feedback-control. These results further confirm the feasibilities of such a nonlinear vibration isolation system.

This chapter will investigate the performance of vibration isolation using nonlinear damping implemented by a feedback-controlled MR damper by both simulation studies and experimental tests. The objectives are to validate the theoretical effects of nonlinear damping on vibration isolation in Chapters 3 and 4 by simulation and experiments, to verify the effectiveness of an MR damper based implementation of nonlinear damping and the corresponding vibration control system, and to demonstrate the potential applications of the new MR damper based vibration control ideas in engineering practice where it is essential to have high vibration isolation performance over a wide range of frequencies. First, the feedback-control of the MR damper using a mathematical model of the MR damper, which the simulation studies in this chapter are based on, will be described in Section 5.2. Then, the feedback-controlled MR damper with an appropriate nonlinear damping characteristic will be incorporated into a force vibration isolation system and a displacement vibration isolation system in Sections 5.3 and 5.4 respectively.

5.2 Feedback-controlled MR damper

Conventional fluid viscous dampers provide a force proportional to the velocity but there are no readily available dampers that could provide a nonlinear damping characteristic defined by Eq. (4.2) in Chapter 4, that is

$$F_c = \text{sign}[\dot{z}(t)]C_p|\dot{z}(t)|^p, \tag{5.1}$$

where C_p is the nonlinear damping constant, $p > 0$ is the damping exponent, z and $\dot{z}$ are the relative displacement and velocity of the damper's terminals respectively. To create this nonlinear damping characteristic, a feedback-controlled

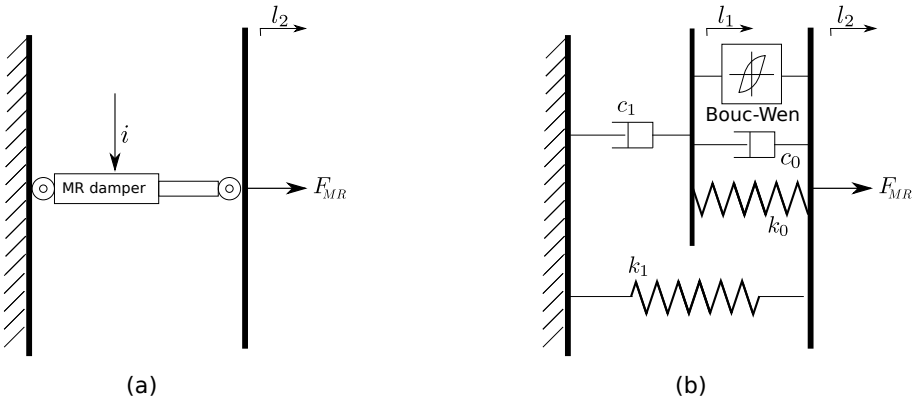

Figure 5.2: (a) A schematic diagram of an MR damper (b) Spencer model of an MR damper [Spencer *et al.*, 1997]

system can be designed to regulate the output force of a commercially available MR damper. In this section, a mathematical model of an MR damper will be introduced, followed by an implementation of the feedback-controlled system.

5.2.1 The Spencer model

A mathematical model of MR dampers which incorporates the Bouc-Wen hysteresis model [Wen, 1976] and a network of springs and dampers was proposed by Spencer *et al.* [1997]. The schematic of the model is shown in Fig. 5.2 and the dynamics is governed by equations

$$\begin{cases} \dot{w} = -\gamma|\dot{l_1} - \dot{l_2}| \cdot |w| \cdot w - \beta(\dot{l_1} - \dot{l_2})|w|^2 + B(\dot{l_1} - \dot{l_2}) \\ \dot{l_2} = \frac{1}{c_0+c_1}\left[\alpha w + c_o\dot{l_1} + k_0(l_1 - l_2)\right] \\ F_{MR} = -c_1\dot{l_2} - k_1(l_1 - l_0) \\ \alpha = \alpha_a + \alpha_b i \\ c_0 = c_{0a} + c_{0b} i \\ c_1 = c_{1a} + c_{1b} i \end{cases} \tag{5.2}$$

where i is the input current, F_{MR} is the MR damper damping force, l_1 and l_2 are the displacements defined in Fig. 5.2(b), l_0 is the initial displacement of spring k_1 and w, the hysteretic component, is an evolutionary variable that has a dimension

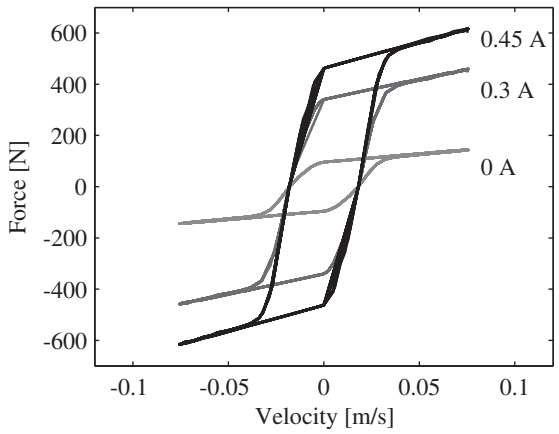

Figure 5.3: Characteristics of an MR damper under constant current excited by a 4 Hz, ±3 mm displacement input.

of length. The shape and size of the hysteresis loop is governed by γ, β and B. The values of the other twelve parameters c_{0a}, c_{0b}, c_{1a}, c_{1b}, k_0, k_1, B, α_a, α_b, β, γ and l_0 have been identified by Sapiński *et al.* [2010] by fitting the Spencer model [Spencer *et al.*, 1997] to the experimental data obtained from an MR damper RD-1005-3 manufactured by LORD Corporation. Under different constant supply currents to the MR damper, the force response was measured under sine, triangular and square displacement excitations with the fixed amplitude of 3 mm at frequencies of 1, 2.5, 3.3 and 5 Hz. The damper piston is at the mid-stroke position at the beginning of each test. In the identification process, the constrained nonlinear optimization with the `constr` procedure available in the Optimization Toolbox of MATLAB was used. The numerical values of model parameters were determined under the quality criterion assuming the form of an integral of the squared difference between the measured and predicted force responses. The results are given in Table 5.1. The value of k_1 is small relative to that of other parameters, which suggests that the stiffness of the MR damper is insignificant.

MR dampers have a highly nonlinear characteristic that depends on the applied current. In general, the damper provides a higher damping force as the current increases. Implemented in MATLAB/Simulink, the mathematical model described by Eq. (5.2) is used to produce the force-velocity relationship presented by the solid lines in Fig. 5.3. It can be observed that the inherent hysteretic effect of MR

Parameter	Value	Unit	Parameter	Value	Unit
c_{0a}	672	$\mathrm{Nsm^{-1}}$	B	121	-
c_{0b}	3152	$\mathrm{Ns(Am)^{-1}}$	α_a	6949	$\mathrm{Nm^{-1}}$
c_{1a}	227150	Ns/m	α_b	60789	N/(Am)
c_{1b}	1050000	Ns(Am)	β	212114	$1/\mathrm{m^2}$
k_0	732	N/m	γ	455707	$1/\mathrm{m^2}$
k_1	81	N/m	l_0	0	m

Table 5.1: MR damper parameters identified from experimental data in [Sapiński *et al.*, 2010]

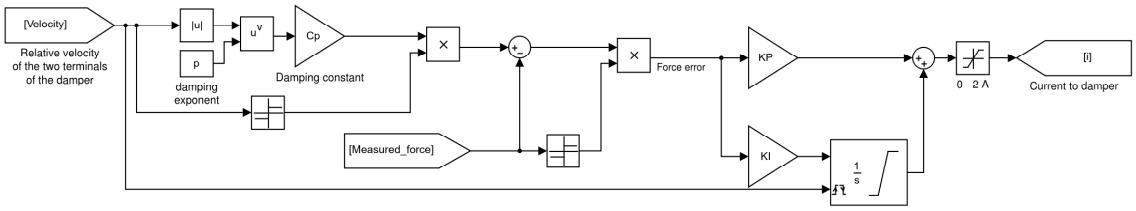

Figure 5.4: Simulink diagram of MR damper damping force controller

dampers dominates the force profile when the velocity is low but is less significant at higher velocities. When no supply current is supplied to the damper, the output force is 144 N at a velocity of 0.075 $\mathrm{ms^{-1}}$. This gives an approximate damping constant of 1920 $\mathrm{Nsm^{-1}}$.

5.2.2 Implementation of feedback-control

Feedback-control can be applied to an MR damper to create a two-terminal device in Fig. 5.1(b) which gives the nonlinear damping characteristic defined by Eq. (5.1). Sims *et al.* [2000] have shown that a proportional-integral feedback-controller with sign adjustments can shape the force-velocity relationship of electrorheological dampers into a linear or a higher order polynomial function. An implementation of this control strategy in MATLAB/Simulink is given in Fig. 5.4. The force controller manipulates the current supplied to the damper according to the error between the measured force and the demanded force, which is a function of the velocity defined by Eq. (5.1). The purpose of the sign adjustment is to ensure that no current is supplied when the signs of the measured and demanded forces do

not agree with that of the error and the integrator is reset every time the velocity changes direction. K_P and K_I, the proportional and integral gains respectively, are determined for each C_p.

To assess the quality of the nonlinear damping implementation, the controller in Fig. 5.4 is applied to the MR damper model given by Eq. (5.2) under a sinusoidal displacement input where $l_2(t) = A_D \sin(2\pi f t)$, where A_D is the amplitude of the displacement input and f in the input frequency in Hz. Note that temporal frequency with the unit Hz is used throughout this chapter as it is more suitable for practical implementation. The implementation of two types of nonlinear viscous damping characteristics, square-root damping and cubic damping, are presented below.

First, the steady-state results of this closed-loop controlled MR damper model under a displacement excitation where f takes the value of 2 Hz and 8 Hz respectively, are given both in the time domain and on the force-velocity plane in Fig. 5.5, where the parameters of the desired damping characteristic in (5.1) are chosen to be $p = \frac{1}{2}$ and $C_{\frac{1}{2}} = 700$ $\mathrm{Ns^{\frac{1}{2}}m^{-\frac{1}{2}}}$. The solid lines representing the demanded force closely resemble the dashed lines representing the output force of the MR damper model under closed-loop control. The discrepancies between the demanded and the achieved signals are mainly caused by the hysteresis of the damper which cannot be eliminated by simple feedback-control. This phenomenon is clearly observed in the force-velocity plane, especially when the amplitude of the input displacement is small as shown in Figs. 5.5(a) and (c).

Second, the simulation results of a cubic damping characteristic implementation where $p = 3$, $C_3 = 1 \times 10^5$ $\mathrm{Ns^3m^{-3}}$ and $f = 2$ Hz, is presented in Figs. 5.6(a)(c), and where $p = 3$, $C_3 = 200$ $\mathrm{kNs^3m^{-3}}$ and $f = 8$ Hz, in Figs. 5.6(b)(d). Behaviours similar to the square-root damping implementation are observed. The output force of the feed-back controlled MR damper is close to the demanded force when the velocity is high but the force-velocity relationship is dominated by the hysteretic effects when the velocity is small. The implementation is therefore only suitable for inputs with relatively large velocity so that most of the operation occurs away from the hysteresis region.

These two simulation examples have demonstrated the implementation of different nonlinear damping characteristics using a feedback-controlled MR damper.

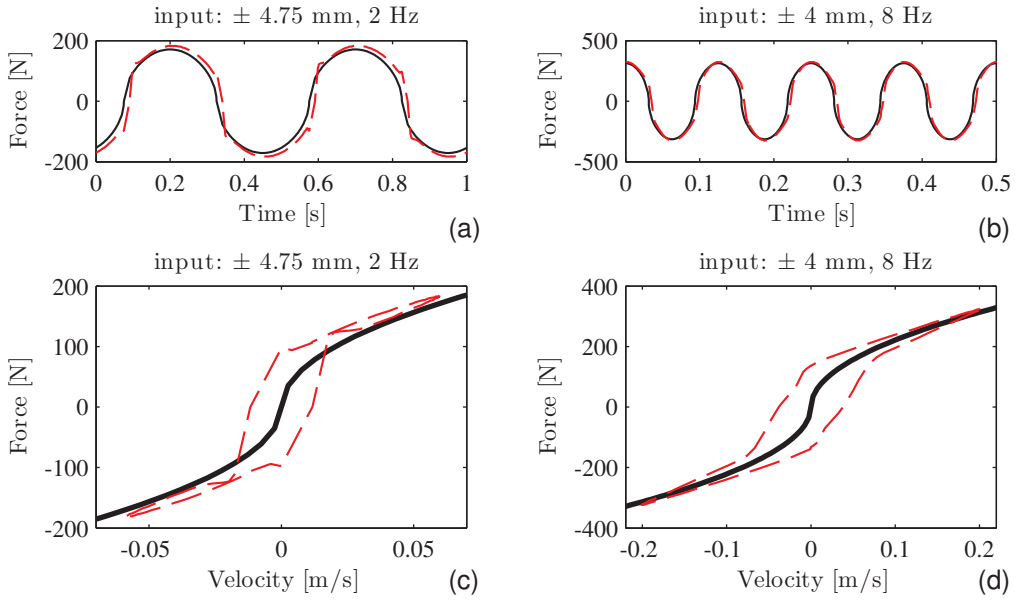

Figure 5.5: Simulation results of an MR damper based implementation of a square-root damping characteristic where $C_{\frac{1}{2}} = 700$ $\mathrm{Ns^{\frac{1}{2}}m^{-\frac{1}{2}}}$. Solid: demand force; Dashed: implemented force. (a),(c) A_D=4.75 mm and f=2 Hz. (b),(d) A_D=4 mm and f=8 Hz.

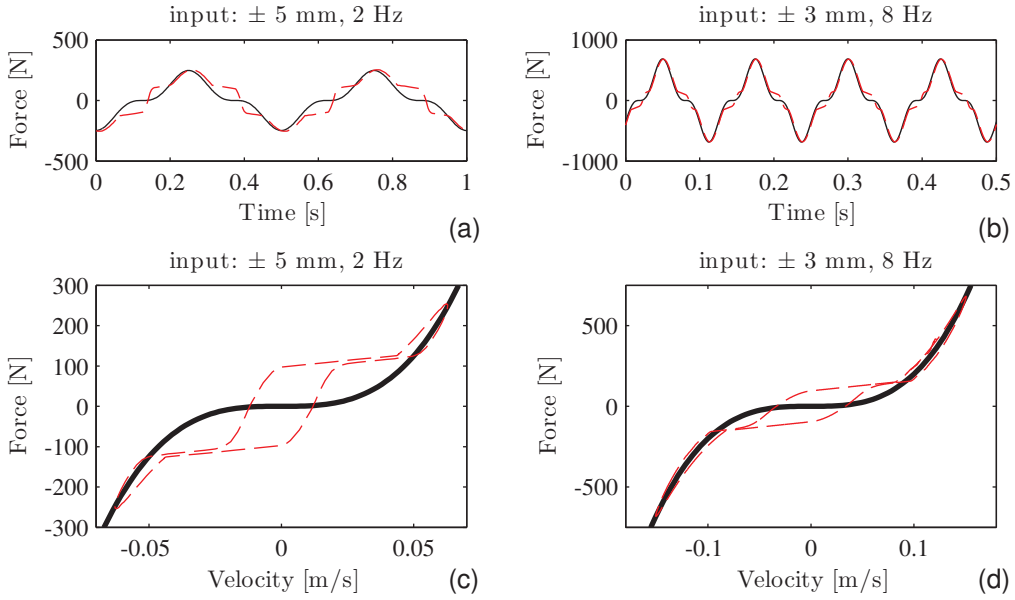

Figure 5.6: Simulation results of an MR damper based implementation of a cubic damping characteristic. Solid: demand force; Dashed: implemented force. (a),(c) $C_3 = 1\times10^5$ $\mathrm{Ns^3m^{-3}}$, A_D=5 mm and f=2 Hz. (b),(d) $C_3 = 200$ $\mathrm{kNs^3m^{-3}}$, A_D=3 mm and f=8 Hz.

Although the control method was originally designed for electrorheological (ER) dampers [Sims *et al.*, 2000], the simulation results have shown that the natural force-velocity relationship of an MR damper can be transformed into a desired nonlinear force-velocity function. The discrepancies between the implemented damping force and the theoretical nonlinear damping characteristic described by Eq. (5.1) is relatively small outside the hysteresis region. With these successful implementations of the desired nonlinear damping characteristics, the feedback-controlled MR damper will be incorporated into a force vibration isolation system and a displacement isolation system respectively to demonstrate their advantages over conventional linear dampers in experimental studies.

5.3 MR damper-based force vibration isolation

The theoretical benefits of cubic viscous damping have been discussed in Chapter 3. In a force vibration isolation system, it is preferable to apply cubic viscous damping to suppress the resonance as the low transmissibility over high frequencies is maintained. In this section, a theoretical cubic damping characteristic in a force vibration isolation system depicted by Fig. 5.7(a) will be implemented by a feedback-controlled MR damper as shown in Fig. 5.7(b) in an experiment.

The force vibration isolation system in Fig. 5.7(a) is equivalent to System (3.1) in Chapter 3 where $K_3 = 0$. The equation of motion is therefore

$$\begin{cases} M\ddot{z}(t) + C\dot{z}(t) + C_3[\dot{z}(t)]^3 + Kz(t) = F_{in}(t) = A_F \sin(2\pi f t) \\ F_{out}(t) = C\dot{z}(t) + C_3[\dot{z}(t)]^3 + Kz(t) \end{cases} \tag{5.3}$$

where C the linear viscous damping constant is assumed to be small, C_3 is the cubic viscous damping constant, $z(t)$, $\dot{z}(t)$ and $\ddot{z}(t)$ are the displacement, velocity and acceleration of the moving mass respectively. The mass M is 25 kg and the spring stiffness K is 250 kNm^{-1}. To realise this theoretical nonlinear vibration isolation, the dynamics of the cubic damping force $C_3[\dot{z}(t)]^3$ is replaced by the MR damper with its model given in Eq. (5.2) and the MR damping force controller is as described in Fig. 5.4.

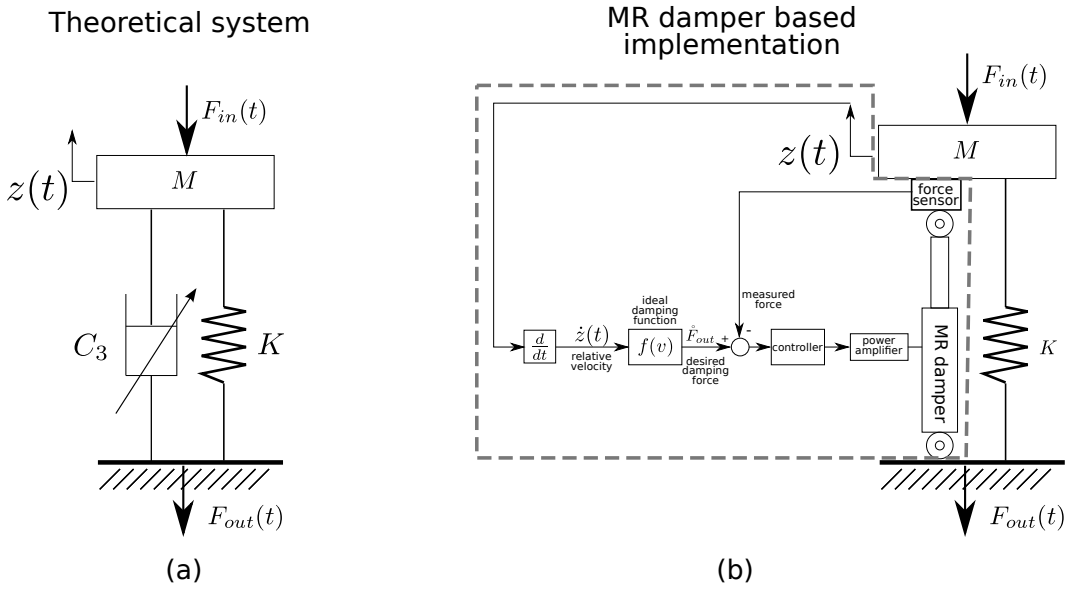

Figure 5.7: (a) Theoretical nonlinearly damped force vibration isolation system (b) MR damper based implementation of (a)

5.3.1 Experimental set-up

An experiment on the force transmissibility of a vibration isolation system with cubic damping force has been carried out. The test configuration, a physical realisation of the concept in Fig. 5.7, is shown in Fig. 5.8. The mass, excited by an inertial shaker (Data Physics Corporation IV46/PA100E), is allowed to move vertically, and is connected to a base via an MR damper (Lord RD-1005-3) placed in the centre of a spring. Force sensor① measures the input force applied to the mass while force sensor③ measures the output force applied to the base. The force transmissibility can be obtained from these two measurements. To control the output force of the MR damper, the controller takes readings from the velocity sensor to find the desired nonlinear damping force $\hat{F}_{out}(t) = C_3\dot{z}(t)^3$. The error between this desired force and the measurement from force sensor② is then sent to the controller in Fig. 5.4 to calculate the current supplied to the MR damper.

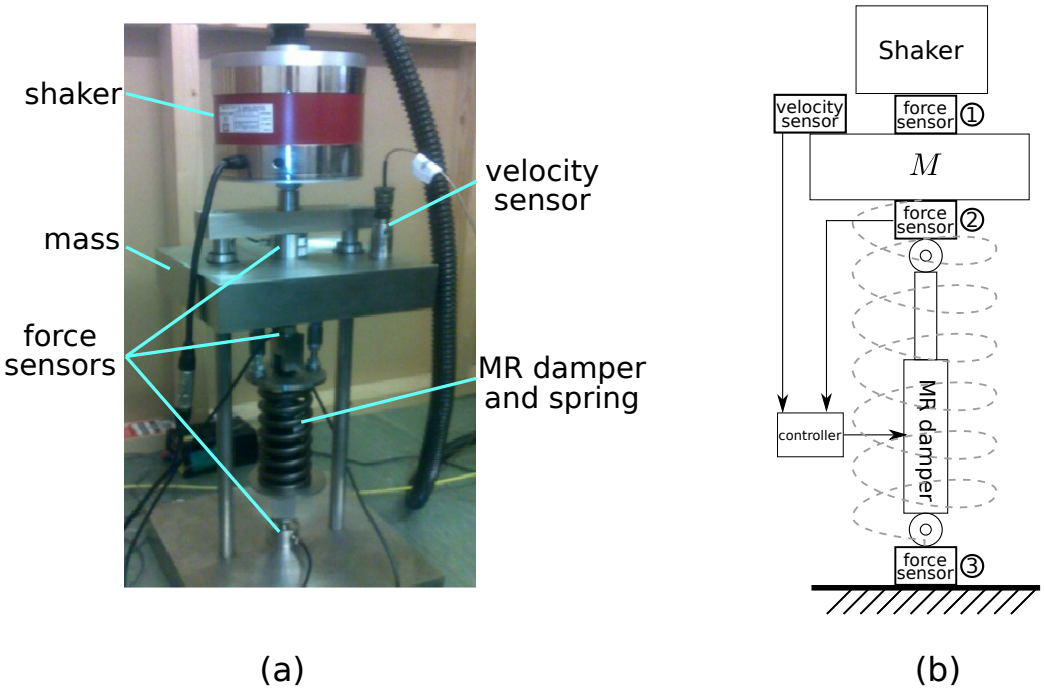

Figure 5.8: Experimental configuration of a force vibration isolation system (a) picture of the test equipment (b) schematic of the test set-up

5.3.2 Experimental results

The results in this section are obtained from MR damper based nonlinear vibration isolation system in Fig. 5.8 under an input force $F_{in}(t) = A_F \sin(2\pi ft)$ where A_F=220 N and f=25 Hz.

The experimental results of the implementation of a nonlinear damping force where $C_3 = 200$ kNs^{3}m^{-3} is shown in both the time domain and the force-velocity plan in Fig. 5.9. Due to the small input force, the amplitude of the velocity is rather small (< 0.1 ms^{-1}) so the MR damper is mostly operated within the hysteretic region. Nonetheless, during the part of a cycle where the force is increasing, the output force of the feedback controller MR damper is close to the ideal nonlinear demand force. The current signal in Fig. 5.9 explains why. When the demand force is increasing, the controller provides a suitable current increase to raise the viscosity of the MR fluid which increases the output force. But when the demand force is decreasing, the controller cannot further reduce the output force of the MR damper after cutting off the supply current.

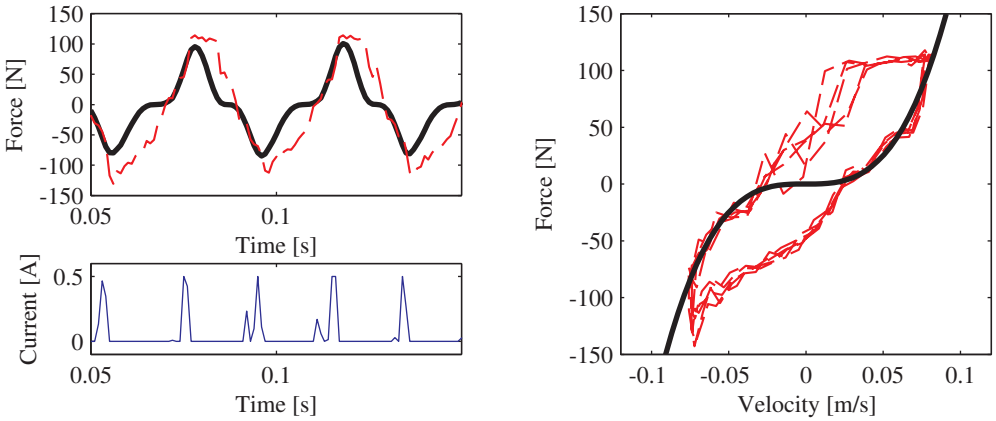

Figure 5.9: Experimental implementation of nonlinear cubic force where C_3 = 200 kNs^{3}m^{-3}. Black solid: demand force; red dashed: MR damper output force.

The force transmissibility of the MR damper based nonlinear vibration isolation system is shown in Figs. 5.10 and 5.11. A digital signal is applied to the inertial shaker to provide an input force to the system but such force is not under controlled loop control. The inertial shaker could unfortunately only provide a maximum force of 170 N according to its specifications and no alternatives were available when the experiments were conducted. To maximise the output force of the shaker, the excitation frequency is chosen to be 25 Hz, which is near the resonance frequency of the shaker. The input and output force measurements are shown in Figs. 5.10. The Fourier transform of these signals show that their amplitudes at 25 Hz are 140 N and 220 N respectively, which gives a transmissibility of -4 dB as shown in Fig. 5.11.

It is not possible to obtain more meaningful data points at other frequencies due to the deficiency of the shaker. At 25 Hz, the force transmissibility of the experimental vibration isolator is just below the theoretical force transmissibility curve of System (5.3) where C_3 = 200 kNs^{3}m^{-3} as shown in Fig. 5.11. This may be due to the imperfect sinusoidal input and energy lost to friction.

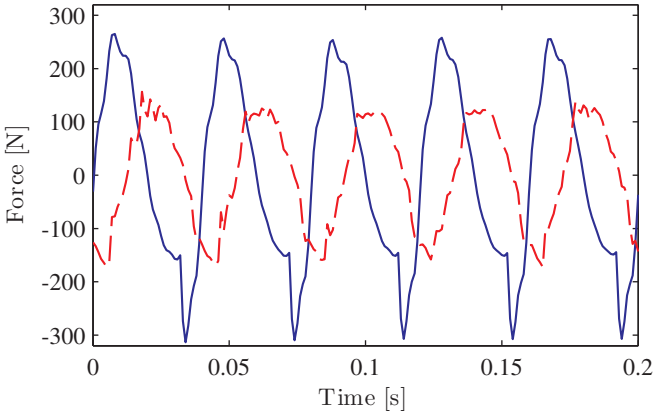

Figure 5.10: Experimental results of an MR based nonlinear vibration isolator. Solid: Input force measured by forces sensor①; Dashed: Output force measured by force sensor③.

5.3.3 Discussions

The above experiment has demonstrated the implementation of a cubic damping characteristic using a feedback controlled MR damper. As a semi-active system, the controller is actively engaged to produce the required nonlinear damping force for about half of each cycle. Fig. 5.11 also includes the transmissibility curve of a linear system, the maximum transmissibility of which matches that of the nonlinear system, to emphasise the advantage of cubic damping over linear damping over the high frequency range. And, more essentially, the experimental data point also stays underneath the transmissibility of this equivalent linear system to show that a feedback controlled MR damper could provide better vibration isolation than a conventional linear viscous damper.

The experiment can be improved by a more suitable force input. First, a more powerful input force is required to fully utilise the whole operating envelop of an MR damper which would lessen the effects of the hysteresis. Second, the input force should be under closed-loop control so that a constant sinusoidal amplitude is provided across a wide range of frequencies. An actuator under closed-loop control may be more suitable than inertial shakers. Finally, the experiment should be also be conducted for input forces with different amplitudes. This would provide a clear indication of the true beneficial operating range the proposed MR damping

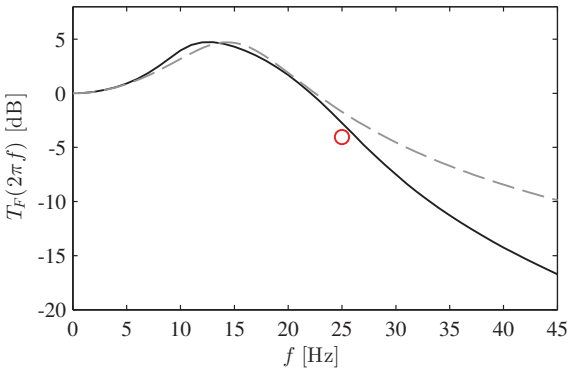

Figure 5.11: Force transmissibility. Solid: theoretical result of System (5.3) where $C = 0$ Nsm^{-1}, $C_3 = 200$ kNs^{3}m^{-3}, A_F=220 kN. Circles: experimental results. Dashed: theoretical result of System (5.3) where $C = 1.9$ kNsm^{-1}, $C_3 = 0$ Ns^{3}m^{-3}.

based vibration isolation system.

5.4 MR damper-based displacement vibration isolation

The theoretical study in Chapter 4 has shown that a displacement vibration isolation system with a small damping exponent can provide a lower transmissibility over high frequencies while matching the resonance suppression ability of an equivalent linear system. An experiment exploiting the semi-active property of an MR damper has been conducted to demonstrate these phenomena.

Again, consider the displacement isolation system described by System (4.1) in Chapter 4, which is the same as the system depicted by Fig. 5.12(a). Under the excitation of an input displacement $x_{in}(t) = A_D \sin(2\pi f t)$ with frequency f and amplitude A_D, the dynamics of this single-degree-of-freedom vibration isolation system consisting of a mass M=10 kg, a linear damper C in parallel with a linear spring K=1 MNm^{-1} with an additional nonlinear viscous damper is described by

$$M\ddot{z}(t) + Kz(t) + C\dot{z}(t) + \text{sign}[\dot{z}(t)]C_{\frac{1}{2}}|\dot{z}(t)|^{\frac{1}{2}} = -M\ddot{x}_{in}(t) \tag{5.4}$$

where $z(t) = x_{out}(t) - x_{in}(t)$ and $C_{\frac{1}{2}}$ is the square-root damping constant. Similar

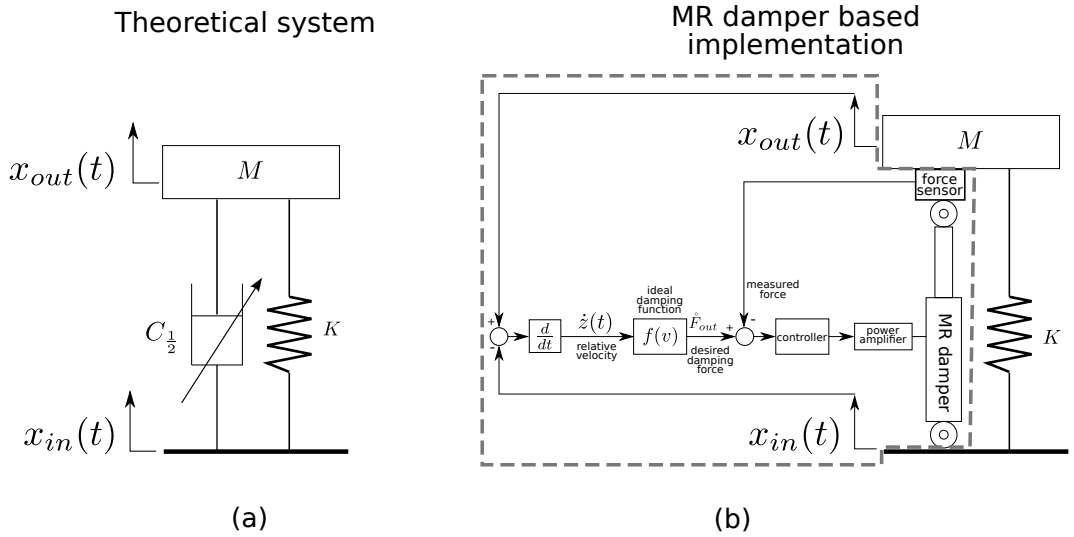

Figure 5.12: (a) Theoretical nonlinearly damped displacement vibration isolation system (b) MR damper based implementation of (a)

to the implementation of a nonlinear force vibration isolator in Section 5.3, the theoretical nonlinear square-root damping force $\text{sign}[\dot{z}(t)]C_{\frac{1}{2}}|\dot{z}(t)|^{\frac{1}{2}}$ will be replaced by a feedback controlled MR damper as shown in Fig. 5.12(b) in the experimental study.

5.4.1 Experimental configuration

A test configuration shown in Fig. 5.14 has been constructed according to Fig. 5.12(b). One end of the MR damper is connected to a displacement-controlled shaker (V780-HPA-K by Ling Dynamic Systems Limited) and the other to a 100 kg mass which can either be fixed rigidly to the ground so that $x_{out}(t) = 0$ (Config. 1) or be allowed to move freely in the horizontal direction (Config. 2). Config. 1 facilitates the testing of the MR damper in isolation while Config. 2, including a 1 MNm^{-1} spring installed in parallel to the damper, is for the vibration isolation test. The shaker supplies a sinusoidal displacement input at a given amplitude and frequency to one end of the damper while the force produced by the damper and the velocity of the other end of the damper are measured by a force sensor and a laser Doppler vibrometer (OFV-505 by Polytec) respectively. Although not shown in the figure, the experimental system also includes a PI controller designed to regulate the cur-

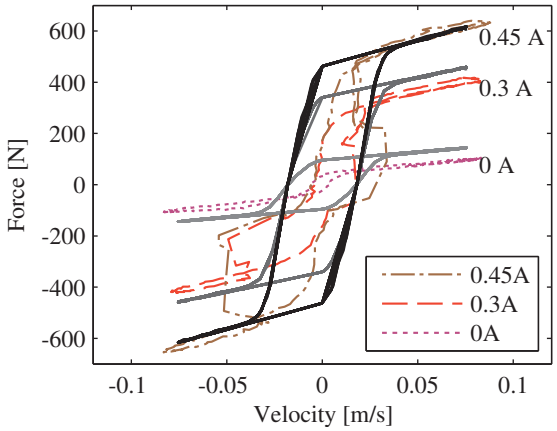

Figure 5.13: Force-velocity curves of an MR damper under constant current excited by a 4 Hz, ±3 mm displacement input. Grey solid: simulation data from RD-1005-3 damper model. Dotted, dashed, dot-dashed: experimental data where i_d=0, 0.3, 0.45 A respectively.

rent applied to the MR damper via an electronic board which provides the MR damper current i via a control voltage V.

As the RD-1005-3 damper is no longer in production, the experiments have been conducted on a new RD-8041-1 damper, also supplied by LORD corporation, which has very similar specifications. The two dampers have the same shaft diameters and their force-velocity curves supplied by the manufacturer are also identical despite that the RD-8041-1 damper has a slightly larger body diameter of 42.1 mm instead of 41.4 mm. As the values for the parameters in the Spencer model are available for the RD-1005-3 damper which is not the case for the RD-8041-1 damper, the experiment described below was conducted to investigate whether and the results that the Spencer model with parameters identified from an RD-8041-1 damper can still provide an adequate representation of the dynamics of the RD-8041-1 damper.

To see how well the mathematical model based on the RD-1005-3 damper agrees with the RD-8041-1 damper, a simple test is conducted on the MR damper alone in Config. 1 to generate the force-velocity curves which can be compared with the simulation results of a RD-1005-3 damper in Fig. 5.3. The spring is removed and the mass is locked into a fixed position such that the MR damper is at mid-stroke,

which gives $x_{out}(t) = 0$. The MR damper now has one end fixed to ground and another end connected to the shaker. With a constant supplied current, a sinusoidal displacement is applied by the shaker to generate experimental results presented by the dotted lines in Fig. 5.13. Outside the hysteresis region, the experimental data shows reasonably good agreement with the simulation data (solid lines). The shapes of the hysteresis are difficult to match and the discrepancies may be due to small amounts of air in the damper as Gordaninejad *et al.* [2002] have pointed out. Because the damper is being used as a passive device as opposed to an actuator in the feedback loop, the accuracy of the modelling becomes less important and it can be concluded that model Eq. (5.2) with parameters as determined in [Sapiński *et al.*, 2010] can give a good representation of the dynamics of the RD-8041-1 damper for the purpose of this study.

5.4.2 Experimental implementation of nonlinear damping

To verify the simulation results on the implementation of the nonlinear damping characteristic in Section 5.2.2, experimental studies were conducted using Config. 1. The force PI controller described above in Fig. 5.4 is implemented using Real-Time Windows Target, a MATLAB tool that sends and receives signals via an I/O board. When the force control loop is closed, the MR damper produces a nonlinear damping force as shown in Fig. 5.15. On the force-velocity plane, the experimental data lies in close proximity to the ideal nonlinear force function and shows even smaller hysteresis loops than the simulated data. These results further confirm that the nonlinear damping force-velocity relationship defined by Eq. (5.1) can be successfully realised by applying a closed-loop control for the damping force of an MR damper.

5.4.3 Implementation of a nonlinear displacement vibration isolation system

To observe the properties of a vibration isolation with a nonlinear damping force implemented by a feedback-controlled MR damper, Config. 2 of the experimental set-up will be used for simulation and experimental studies.

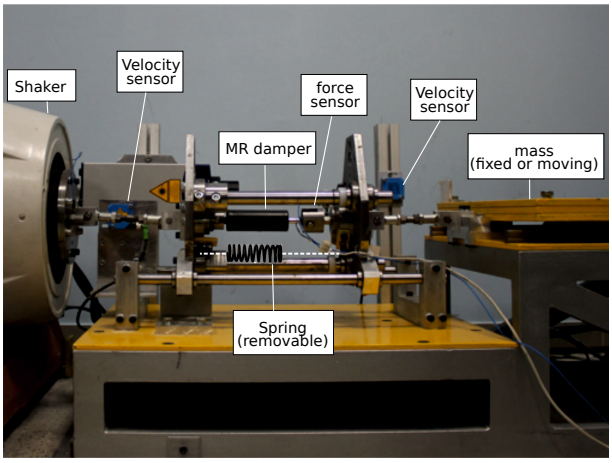

Figure 5.14: Experimental displacement vibration isolation system

First, the MR based vibration isolation system in Fig. 5.12(b) is simulated using Simulink/MATLAB. With the base subjected to a sinusoid with input amplitude of 3 mm and frequency ranging from 0 to 30 Hz, two sets of simulation results are obtained where the desired nonlinear damping force to be implemented by the feedback-controlled MR damper is a square-root function of $\dot{z}(t)$ and $C_{\frac{1}{2}}$ takes the values 700 and 1000 $\mathrm{Ns}^{\frac{1}{2}}\mathrm{m}^{-\frac{1}{2}}$ respectively. The results are given by the dot-dashed lines in Fig. 5.16 and 5.17. By comparing the system displacement transmissibility curves with that of System (5.4) given in solids lines, it can be observed that the feedback-controlled MR damper implemented nonlinear damping has the expected effects on the system transmissibility. In both cases, the resonant peaks are somewhat higher than the theoretical values but the high frequency data correlates well with the theoretical curves. The discrepancies are caused by the hysteresis in the MR damper as illustrated on the force-velocity plane in Section 5.2. When the input displacement amplitude is kept constant, higher velocities are achieved at higher frequencies hence the hysteretic effects becomes less significant. The higher frequency simulation data has better agreement with the theoretical values as a result. A linearly damped system with similar resonant peaks are included in Figs .5.16 and 5.17 for comparison. These results illustrate that the implementation of the desired nonlinear damping characteristic using a closed-loop controlled MR damper is effective in achieving lower transmissibility in a vibration isolation system, especially in the higher frequency region.

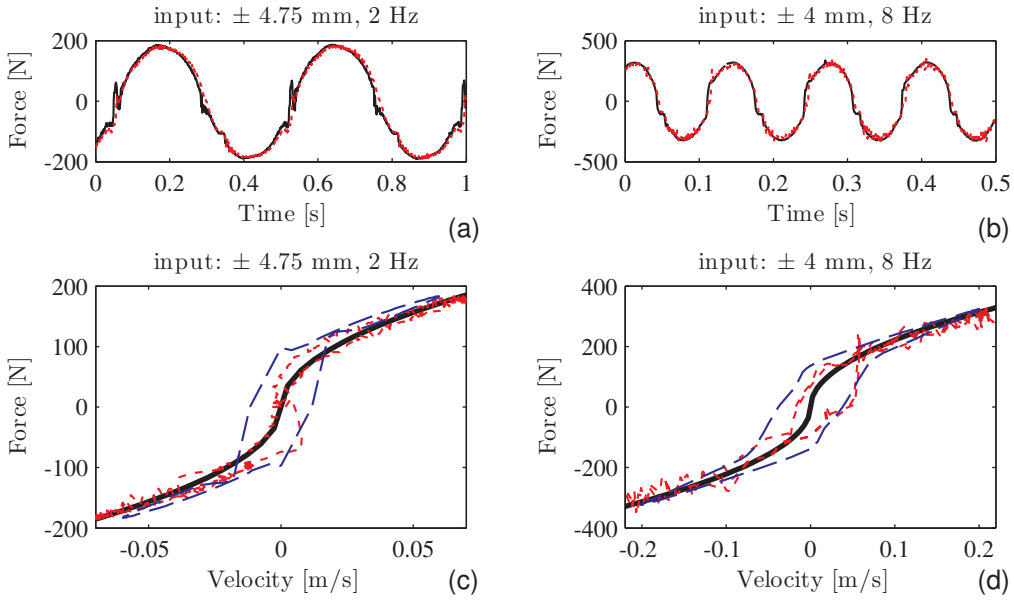

Figure 5.15: Experimental results of an MR damper based implementation of a square-root damping characteristic where $C_{\frac{1}{2}}$=700 $\mathrm{Ns}^{\frac{1}{2}}\mathrm{m}^{-\frac{1}{2}}$. Solid: demand force; Dashed: implemented force. (a),(c) A_D=4.75 mm and f=2 Hz. (b),(d) A_D=4 mm and f=8 Hz.

Then, the same sets of tests conducted are replicated on the experimental system in Fig. 5.14 where the spring is included and the mass is allowed to move freely in the horizontal direction. The shaker provides a sinusoidal displacement input $x_{in}(t) = A_D \sin(2\pi f t)$ to the base and $\dot{z}(t)$, the relative velocity of the two terminals of the MR damper, is given by the difference between the input and output velocity measured by the sensors. The experimental results are presented by the circles in Figs. 5.16 and 5.17. Each data point represents the steady-state transmissibility $T_D(2\pi f)$ at a particular frequency so the results are discrete. The frequency only goes up to 20 Hz because of the maximum speed limitation of the MR damper, beyond which damage could be done to the seals in the MR damper. In the two cases where $C_{\frac{1}{2}}$ takes values of 700 and 1000 $\mathrm{Ns}^{\frac{1}{2}}\mathrm{m}^{-\frac{1}{2}}$, the experimental data correlates well with the theoretical values as well as the simulation results. It is not surprising that the experimental data lies more closely to the theoretical curves than the simulation data does as the closed-loop MR damper has smaller hysteresis loops than Eq. (5.2) suggests (see Fig. 5.13). These results show the

effectiveness of using a feedback-controlled MR damper to implement a desired nonlinear damping characteristic and the good performance of the corresponding vibration isolation system.

To further illustrate the advantage of nonlinear damping in terms of the absolute displacement, Fig. 5.18 shows the 5 Hz and 12 Hz data points from Fig. 5.17 in the time domain. At 5 Hz and when a nonlinear force described by Eq. (5.1) with $C_{\frac{1}{2}} = 1000$ $\mathrm{Ns}^{\frac{1}{2}}\mathrm{m}^{-\frac{1}{2}}$ is implemented by the feedback-controlled MR damper, the amplitude of the periodic displacement signal is slightly larger than the sinusoidal output of a linear equivalent system where $C_1 = 4650$ Nsm^{-1}. At 12 Hz, the displacement amplitude of moving mass under nonlinear damping is much smaller than that of the system under linear damping. These results again demonstrate that a vibration isolation system with a nonlinear damping force implemented by a feedback-controlled MR damper achieves similar resonance suppression compared with an equivalent linear system does but it is much more effective in reducing vibration at high frequencies.

Note that the force and current controllers in Fig. 5.12(b) are tuned for each damping constant and have the same gain values for the whole experimental frequency range (0 to 20 Hz). When a higher damping constant is chosen, a control loop with a faster response time is needed to achieve the nonlinear force demand. It is important to stress that the controller gains are dependent on the MR damper and the designed damping characteristic but not other system parameters of the vibration isolation system. Unlike the conventional approach in Fig. 5.1(a), a change in the mass and/or the spring stiffness does not affect the choice of the controller gains.

Together with the controller which only takes measurements from the damper itself, the MR damper becomes a stand-alone nonlinear viscous damper with a specific damping constant, which makes it an easy substitution for a conventional linear viscous damper. When applying it to a vibration isolation application, no further monitoring is required once the force controller is tuned according to the chosen nonlinear damping constant and exponent. By replacing a linear damper in a vibration isolation system with this nonlinear viscous damping unit, the same level of resonant peak reduction can be achieved with much less detrimental effects on the high frequency region.

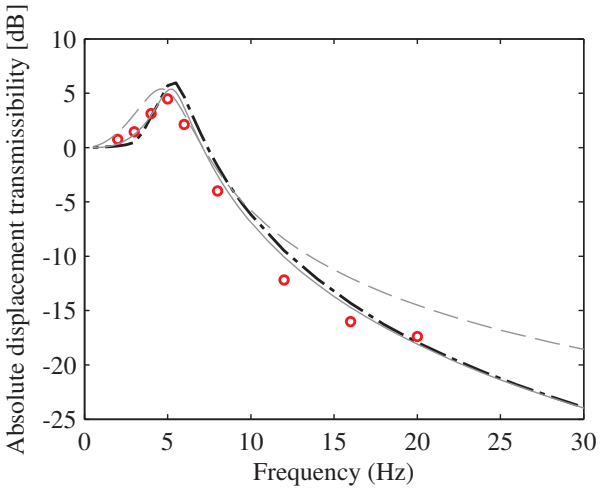

Figure 5.16: Displacement transmissibility curves. Solid: theoretical result of System (5.4) where $C_{\frac{1}{2}} = 700\ \mathrm{Ns}^{\frac{1}{2}}\mathrm{m}^{-\frac{1}{2}}$. Dot-dashed: simulation result with $C_{\frac{1}{2}} = 700\ \mathrm{Ns}^{\frac{1}{2}}\mathrm{m}^{-\frac{1}{2}}$ implemented by an MR damper. Circles: experimental results with $C_{\frac{1}{2}} = 700\ \mathrm{Ns}^{\frac{1}{2}}\mathrm{m}^{-\frac{1}{2}}$ implemented by an MR damper. Dashed: theoretical result of System (5.4) where $C_1 = 2100\ \mathrm{Nsm}^{-1}$.

5.5 Conclusions

There has been a growing use of MR dampers in vibration control. As the damping properties can be manipulated by a supplied current, MR dampers have been used in many semi-active applications such as vehicle suspension control and seismic protection. When employing an MR damper as an actuator in the feedback loop, an understanding of the highly nonlinear MR damper characteristics becomes essential which leads to the development of MR damper inverse models and other advanced MR damper control techniques. Using MR dampers in this manner also relies on the effective modelling of the controlled plant and accurate measurements of the system outputs. Therefore, there can be concerns associated with system stability and robustness if unmodelled dynamics and measurement errors become an issue.

In order to overcome these problems, the idea of using MR dampers as a damper as proposed by Laalej *et al.* [2012] has been adopted in this chapter. Like other conventional dampers, an MR damper under feedback damping force control behaves as a two-terminal passive damper which has a specific relative velocity and

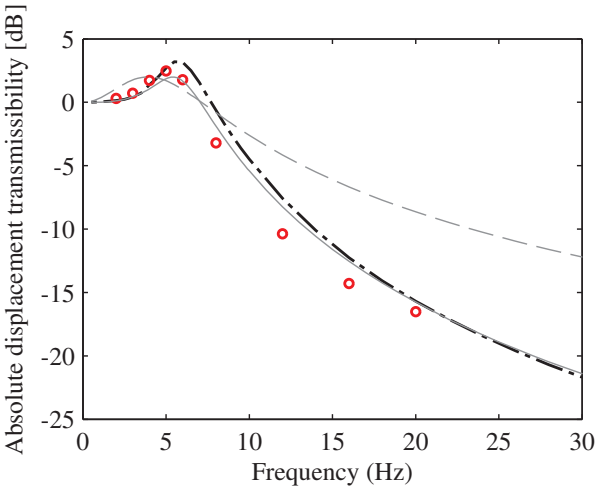

Figure 5.17: Displacement transmissibility curves. Solid: theoretical result of System (5.4) where $C_{\frac{1}{2}} = 1000\ \mathrm{Ns}^{\frac{1}{2}}\mathrm{m}^{-\frac{1}{2}}$. Dot-dashed: simulation result with $C_{\frac{1}{2}} = 1000\ \mathrm{Ns}^{\frac{1}{2}}\mathrm{m}^{-\frac{1}{2}}$ implemented by an MR damper. Circles: experimental data with $C_{\frac{1}{2}} = 1000\ \mathrm{Ns}^{\frac{1}{2}}\mathrm{m}^{-\frac{1}{2}}$ implemented by an MR damper. Dashed: theoretical result of System (5.4) where $C_1 = 4600\ \mathrm{Nsm}^{-1}$.

damping force relationship. In this configuration, the controller only requires measurements of the internal states of the damper hence it is independent of the plant dynamics. Because of its passive nature, this design is less susceptible to external disturbances and can be installed in any systems that require passive damping. The work presented in this chapter has realised this design to create a desired damping device for vibration isolation. This successful realisation has paved the way for an ideal vibration isolation system which has a nonlinear damping characteristic as shown by Guo *et al.* [2012]. Moreover, the implementation of nonlinear damping has validated the theoretical findings on nonlinear force vibration isolation system in Chapter 3 and on nonlinear displacement vibration isolation system in Chapter 4. By installing a closed-loop controlled MR damper in parallel with a spring in a sdof vibration isolation system, it has been shown, by both simulation and experimental studies, that a good level of vibration isolation is achieved around the resonant region as well as the high frequency region, which is a significant improvement on the performance of conventional linear dampers where resonant peaks are suppressed at the cost of a degraded high-frequency transmissibility.

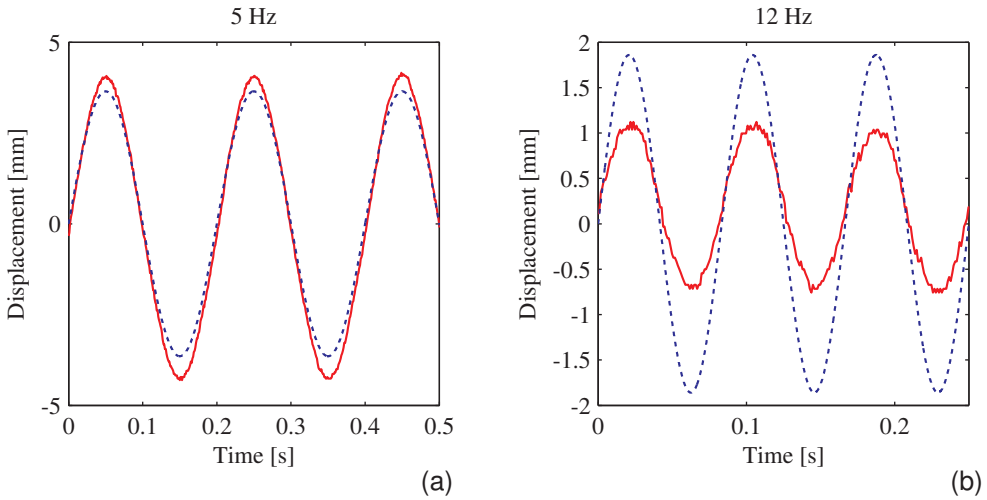

Figure 5.18: Comparisons of System (5.4) under linear and nonlinear damping at (a) 5 Hz and (b) 12 Hz. Blue dotted: C_1=4650 Nsm^{-1}, $C_{\frac{1}{2}}$=0 Ns$^{\frac{1}{2}}$m$^{-\frac{1}{2}}$; Red solid: experimental data with $C_{\frac{1}{2}}$ = 1000 Ns$^{\frac{1}{2}}$m$^{-\frac{1}{2}}$ implemented by an MR damper

The realisation of an ideal nonlinear damping characteristic using a commercially available MR damper under feedback-control offers an effective and easily implemented vibration isolation solution. Unlike other approaches, an extensive analysis of the plant dynamics or the MR damper itself is not necessary. Because the MR damper is acting as a passive device, it is robust enough for any changes in the system resonant frequency. Its damping properties can be adjusted by tuning the gains in the controller according to the desired damping constant and exponent (but not the plant parameters). As a self-contained two-terminal device, the feedback-controlled MR damper could offer instant enhancement to any existing vibration isolation system by replacing the conventional damper, although a very little power supply is required.

The results in this chapter may not only affect the way MR dampers are employed in vibration isolation applications but also their hardware design. A passive damper with a desired damping characteristic can become an off-the-shelf product if the MR damper and its controller are packaged into one unit. As Lam *et al.* [2010] suggested, a piezoelectric force sensor together with a linear variable differ-

ential transformer (LVDT) can be integrated into the MR damper so that it does not require any external sensing.

Chapter 6

Design methods of nonlinear vibration isolation systems

6.1 Introduction

As discussed in Chapter 2, an ideal vibration isolation system should have a low resonant peak, low high-frequency transmissibility and a large isolation range provided by a low cut-off frequency. Unlike a conventional linear system, vibration isolators with nonlinear components are difficult to design since traditional nonlinear approximation methods, such as the harmonic balance method, do not give any direct relationships between the nonlinear parameters and the output spectrum. It is only possible to find the output spectrum for given nonlinear parameters by numerically solving some implicit polynomial simultaneous equations. Recently, a new nonlinear analysis method based on the Volterra series, called the output frequency response function (OFRF) was proposed, which offers an explicit relationship between the parameters that define the system nonlinearity and the output spectrum [Lang *et al.*, 2007]. For a given output spectrum requirement, the OFRF method can be applied to determine the nonlinear parameters based on a set of simulation or experimental data.

In this chapter, a new type of nonlinear vibration isolation system which has both spring and damping nonlinearities will be investigated. These two nonlinearities complement each other to create a vibration isolator that has better per-

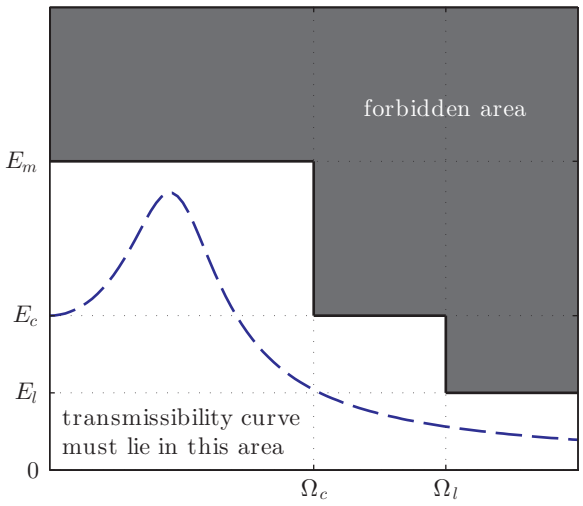

Figure 6.1: An illustration of the design requirements for sdof vibration isolation systems.

formance than a system with only one type of nonlinearity. Based on the OFRF approach, a systematic design procedure for this nonlinear vibration isolator is proposed. Simulation studies have been conducted to demonstrate the effectiveness of the design procedure as well as the vibration isolation performance of the designed system. The proposed method can also be applied to the design of other nonlinear systems that satisfy the modelling conditions of the OFRF approach.

6.2 Design requirements

The design requirements for a vibration isolator are usually some restrictions on the force transmissibility curve [Society of Automotive Engineers. Committee G-5: Aerospace Shock and Vibration, 1962, p 28]. Under a single-tone sinusoidal input excitation, the output of a nonlinear system contains frequencies at the excitation as well as many harmonics. The power transmissibility $E(\Omega)$, a function of the normalised frequency Ω is defined by

$$E(\Omega) = \frac{\int_0^T |F_{out}(t)|^2 \, dt}{\int_0^T |F_{in}(t)|^2 \, dt} \tag{6.1}$$

where T is an excitation period, $F_{in}(t)$ and $F_{out}(t)$ are the input and output forces respectively, and is therefore a more suitable metric for measuring the performance of a nonlinear vibration isolation system. The design may apply restrictions to the whole transmissibility curve but it is usually sufficient to specify the transmissibility at three critical points given by the following requirements.

(i) $\max_{\Omega} E(\Omega) \leqslant E_m$;

(ii) $E(\Omega) \leqslant E_c \qquad \Omega \leqslant \Omega_c$;

(iii) $E(\Omega) \leqslant E_l \qquad \Omega \leqslant \Omega_l$,

where E_m, E_c, E_l, Ω_c Ω_l are as illustrated in Fig. 6.1. Requirement (i) simply restricts the peak transmissibility which can be easily achieved by increasing either the linear or nonlinear damping ratio. Requirement (ii) defines the cut-off frequency Ω_c at which isolation begins. E_c is the cut-off amplitude which normally has a value of 1. In practical applications where the half-power point is important [SVS, 1969], E_c would take the value of $E_m/2$. As observed from Fig. 2.3 in Chapter 2, $E(\Omega)$ of a linear system is always 1 at $\Omega = \sqrt{2}$. If the requirement is more stringent, i.e. $E_c < 1$ or $\Omega_c < \sqrt{2}$ or both, auxiliary springs can be introduced to increase the isolation range. Requirement (iii) limits the transmissibility at a high frequency which can only be achieved by a low linear damping ratio. The power transmissibility curve of an ideal vibration isolation system must lie in the white area in Fig. 6.1 defined by E_m, E_c, E_l, Ω_c and Ω_l.

If these requirements cannot be achieved simultaneously by adjusting the linear damping ratio, the only design parameter in a non-dimensional linear vibration isolation system, adding stiffness and damping nonlinearities could be considered as solutions.

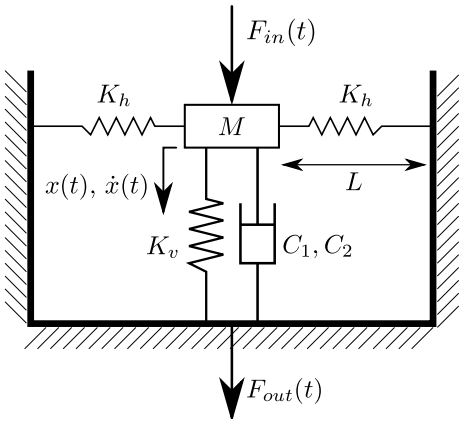

Figure 6.2: Single degree of freedom vibration isolation system with horizontal springs and a nonlinear damping characteristic.

6.3 Sdof vibration isolators with stiffness and damping nonlinearities

Energy transmissibility of a nonlinear vibration isolator

Fig. 6.2 shows a single-degree-of-freedom (sdof) vibration isolator that has a main vertical spring of stiffness K_v, two horizontal auxiliary springs of stiffness K_h and a nonlinear damping force given by the sum of a linear and a cubic function of the velocity. This vibration isolation system is an integration of the auxiliary spring design by Alabuzhev *et al.* [1989] and nonlinear viscous damping by Ravindra & Mallik [1995]. The equations of motion that relate the input force F_{in} and the output force $F_{out}(t)$ are given by

$$\begin{cases} M\ddot{z}(t) + C\dot{z}(t) + C_3[\dot{z}(t)]^3 + F_s[z(t)] = F_{in}(t) \\ F_{out}(t) = C\dot{z}(t) + C_3[\dot{z}(t)]^3 + F_s[z(t)] \end{cases} \tag{6.2}$$

where M is the mass, C the linear viscous damping constant, C_3 the cubic viscous damping constant, $z(t)$, $\dot{z}(t)$ and $\ddot{z}(t)$ are the displacement, velocity and acceleration of the moving mass respectively. The total vertical spring force acting on the

mass, provided by the primary and auxiliary springs, is given by

$$F_s[z(t)] = K_v z(t) + 2K_h \left(1 - \frac{L_0}{[z(t)^2 + L^2]^{\frac{1}{2}}}\right) z(t) \tag{6.3}$$

where L_0 is the natural length of the horizontal springs, each of which has a length of L in the horizontal position.

To conduct a general analysis, the system dynamics described by Eq. (6.2) under the excitation of a sinusoidal input

$$F_{in}(t) = A\sin(\bar{\omega}t) \tag{6.4}$$

can be transformed into a non-dimensional form given by

$$\begin{cases} \ddot{y}(\tau) + \xi_1 \dot{y}(\tau) + \xi_3[\dot{y}(\tau)]^3 + f_s[y(\tau)] = \sin(\Omega\tau) \\ f_{out}(\tau) = \xi_1 \dot{y}(\tau) + \xi_3[\dot{y}(\tau)]^3 + f_s[y(\tau)] \end{cases} \tag{6.5}$$

where

$$\omega_0 = \sqrt{\frac{K_v}{M}}, \tag{6.6}$$

$$\tau = \omega_0 t, \tag{6.7}$$

$$\Omega = \frac{\bar{\omega}}{\omega_0}, \tag{6.8}$$

$$y(\tau) = \frac{K_v z(t)}{A}, \tag{6.9}$$

$$\xi_1 = \frac{C}{\sqrt{K_v M}}, \tag{6.10}$$

$$\xi_3 = \frac{C_3 A^2}{\sqrt{(K_v M)^3}}. \tag{6.11}$$

$$\tag{6.12}$$

The non-dimensional spring force is given by

$$f_s[y(\tau)] = \frac{F_s[x(t)])}{A} = 2ky(\tau) + \left(1 - \frac{2k}{\sqrt{l^2 + \tilde{f}^2 y(\tau)^2}}\right) y(\tau) \tag{6.13}$$

where $k = K_h/K_v$ is the ratio of the stiffness of the auxiliary springs and the main spring, $l = L/L_0$ is the ratio of the length of the auxiliary springs in the horizontal position to their natural lengths and $\tilde{f}$ is a dimensionless parameter given by $A/(K_v L_0)$.

Rewriting Eq. (6.5) into a single-input-two-output system gives

$$\begin{cases} \ddot{y}_1(\tau) + y_2(\tau) = u(\tau) \\ y_2(\tau) = f_{out}(\tau) = \xi_1 \dot{y}_1(\tau) + \xi_3[\dot{y}_1(\tau)]^3 + f_s[y_1(\tau)] \end{cases} \tag{6.14}$$

where

$$u(\tau) = \sin(\Omega\tau) \tag{6.15}$$

$$y_1(\tau) = y(\tau) \tag{6.16}$$

and

$$y_2(\tau) = f_{out}(\tau) = \xi_1 \dot{y}(\tau) + \xi_3[\dot{y}(\tau)]^3 + f_s[y(\tau)]. \tag{6.17}$$

From Eqs. (6.2) and (6.5) to (6.11), it can be shown that

$$\frac{F_{out}(t)}{A} = f_{out}(\tau) = y_2(\tau). \tag{6.18}$$

The power transmissibility $E(\Omega)$ as detailed in Eq. (6.1) is now expressed in terms of the non-dimensional output $y_2(\tau)$, that is

$$E(\Omega) = \frac{\int_0^T |F_{out}(t)|^2 \, dt}{\int_0^T |F_{in}(t)|^2 \, dt} = \frac{\Omega}{\pi} \int_0^{2\pi/\Omega} |y_2(\tau)|^2 \, d\tau \tag{6.19}$$

where $T = 2\pi/\bar{\omega}$. Assuming that $y_2(\tau)$ takes the form of

$$y_2(\tau) = \sum_{q=1}^{\infty} b_q \sin(q\Omega\tau + \phi_p) \qquad b_q = 0 \text{ for even } q \tag{6.20}$$

and according to Parseval's theorem, the power transmissibility can also be repre-

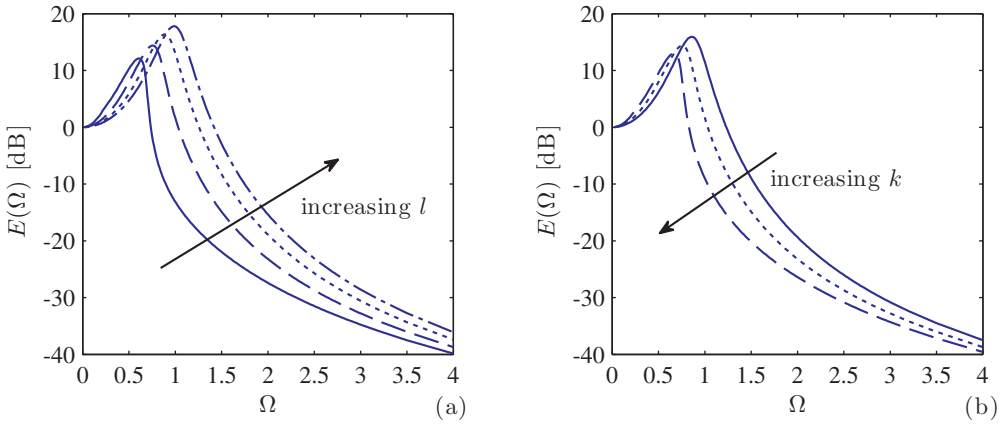

Figure 6.3: The power transmissibility of System (6.14) under linear damper. (a) $k = 1$, $\xi_1 = 0.4$, $\xi_3 = 0$ and $l = 0.7$ (solid), 0.8 (dashed), 0.9 (dotted), 1 (dot-dashed). (b) $l = 0.8$, $\xi_1 = 0.4$, $\xi_3 = 0$ and $k = 0.5$ (solid), 1 (dashed), 1.5 (dotted).

sented in the frequency domain as

$$E(\Omega) = \frac{\Omega}{\pi} \int_0^{2\pi/\Omega} |y_2(\tau)|^2 \, d\tau = \sum_{p=1}^{\infty} b_q^2 = \sum_{q=1}^{\infty} \left| \, Y_2(j\omega)|_{\omega=q\Omega} \, \right|^2 \tag{6.21}$$

where $Y_2(j\omega)$ is the Fourier transform of $y_2(\tau)$. Eq. (6.21) shows that the power transmissibility is equivalent to the squared sum of all the coefficients of the Fourier transform of the time signal. Therefore, the aggregate effects of the stiffness and damping nonlinearities on the output harmonics can be reflected on the power transmissibility.

6.3.1 Effects of spring nonlinearity on the power transmissibility

When $\xi_3 = 0$, the system described by Eq. (6.14), denoted by System (6.14) hereafter, is equivalent to the nonlinear isolator with high-static-low-dynamic-stiffness proposed by Alabuzhev *et al.* [1989]. The two auxiliary springs provide an elastic force acting in the opposite direction to that provided by the main spring. Therefore the vertical stiffness is reduced which leads to a reduction in the linear natural frequency. Fig. 6.3 shows the effects of the two auxiliary spring parameters l and

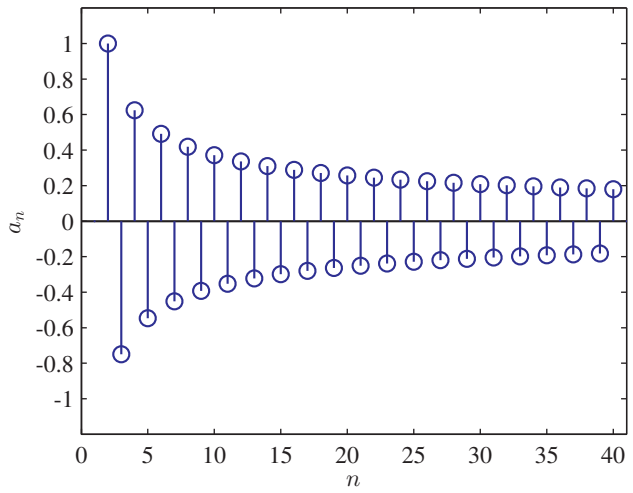

Figure 6.4: Coefficients of the Taylor series expansion of the nonlinear vertical spring force in Eq. (6.22).

k on the power transmissibility respectively, which can be explained by the Taylor approximation of the vertical spring force

$$f_s[y(\tau)] \approx \hat{f}_s[y(\tau)] = \frac{F_s[z(t)]}{A} = \left[1 - 2k\left(\frac{1-l}{l}\right)\right] y(\tau) + \sum_{n=2}^{N_T} a_n \left(\frac{k}{l}\right)\left(\frac{\tilde{f}}{l}\right)^{2n-2} y(\tau)^{2n-1} \tag{6.22}$$

where k and l must satisfy

$$2k\left(\frac{1-l}{l}\right) < 1 \tag{6.23}$$

to avoid negative stiffness and a_n is a coefficient that only depends on n. When $l = 1$ (i.e. the auxiliary springs are not compressed when they are in the horizontal position), the coefficient of $y(\tau)$ is one which means that the resonance occurs at $\Omega = 1$. To shift the resonant peak towards a lower frequency, l must be less than one. This is the effect demonstrated by Fig. 6.3(a). In addition, the coefficient of $y(\tau)$ can be further reduced by increasing k as shown in Fig. 6.3(b).

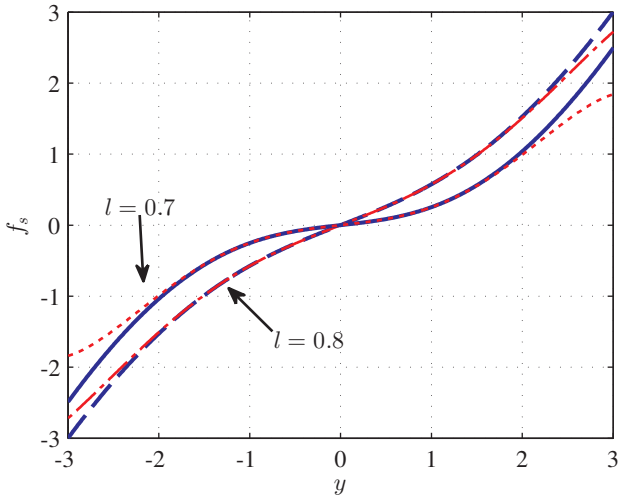

Figure 6.5: Nonlinear spring force (Eq. (6.13)) versus displacement where $\tilde{f} = 0.2$, $k = 1$ and l= 0.7 (dashed) , 0.8 (solid). Fifth order Taylor approximation given by Eq. (6.24) where $l = 0.7$ (dotted) and 0.8 (dot-dashed).

The unfortunate side effect of the horizontal springs, as pointed out by Carrella *et al.* [2012], is the introduction of nonlinear stiffness in the vertical direction which results in higher harmonics in the output and the bending of the resonant peak towards the high frequencies. The Taylor approximation in Eq. (6.22) shows that a small l and a large k are beneficial to reducing the coefficient of $y(\tau)$, which lowers the resonant frequency, but the coefficients of $y(\tau)^{2n+1}$ are raised as a result. When the level of damping is low, the jump behaviours, where a small change in the excitation frequency leads to a sudden change in the output magnitude, can be observed when the coefficients of $y(\tau)^{2n+1}$ are sufficiently large. This is the trade-off of including horizontal auxiliary springs in a vibration isolation system design.

Fig. 6.4 shows the values of a_n for $n = 2, 3, \cdots 40$. The magnitude of a_n reduces with the increase of n so the effects are dominated by the first few terms where n is small. The other interesting observation is that a_n has alternating signs. When n is even(odd), a_n is positive(negative) and creates a hardening(softening) nonlinearity which bends the resonant peak towards high(low) frequencies assuming $\tilde{f} < l$. Consequently, the peak bending effect caused by a_n is diminished by the peak

bending effect in the opposite direction caused by a_{n+1}. Because $|a_n| > |a_{n+1}|$ for $n = 2, 3, \cdots N_T$ and $a_n > 0$ for even n, the resonant peak is moved slightly towards high frequencies. If only a_2 is considered while a_n for $n = 3, 4, \cdots$ are assumed to be zero, as in [Carrella *et al.*, 2012], the peak bending effect would be greatly overestimated. For this reason, when approximating the nonlinear spring force with a Taylor series, N_T should be an odd number which is equal to or larger than three. In this study, N_T is assumed to be 3 so that Eq. (6.22) becomes

$$f_s[y(\tau)] = \gamma_1 y(\tau) + \gamma_2 y(\tau)^3 + \gamma_3 y(\tau)^5 \tag{6.24}$$

where

$$\gamma_1 = 1 - 2k\left(\frac{1-l}{l}\right) \tag{6.25}$$

$$\gamma_2 = \frac{\tilde{f}^2 k}{l^3} \tag{6.26}$$

$$\gamma_3 = -\frac{3\tilde{f}^4 k}{4l^5}. \tag{6.27}$$

γ_1 must have a value between 0 and 1, so Eq. (6.25) gives the following relationship between k and l:

$$\frac{2k}{1+2k} < l \leqslant 1. \tag{6.28}$$

Fig. 6.5 compares the approximated nonlinear spring force in Eq. (6.24) with the actual force in Eq. (6.13) where $\tilde{f} = 0.2$. The fifth order Taylor expansion provides good approximation for $y(\tau)$ between -2 and 2. The approximation accuracy would further improve as $\tilde{f}$ decreases.

6.3.2 Effects of damping nonlinearity on the power transmissibility

To exploit the benefits of horizontal springs in a vibration isolator design, nonlinear damping can be introduced to suppress the undesired harmonics and jumps. The theoretical study of a vibration isolation system with a linear spring by Lang *et al.*

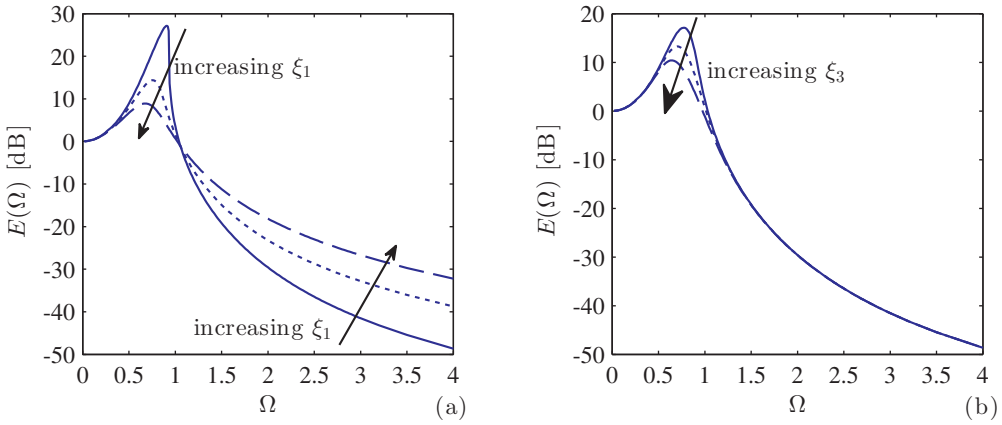

Figure 6.6: The power transmissibility of System (6.14) under (a) linear damper where $k = 1$, $l = 0.8$ and $\xi_3 = 0$. Solid: $\xi_1 = 0.2$; dotted: $\xi_1 = 0.4$; dashed: $\xi_1 = 0.6$; (b) nonlinear damper where $k = 1$, $l = 0.8$ and $\xi_1 = 0.1$. Solid: $\xi_3 = 0.02$; dotted: $\xi_3 = 0.05$; dashed: $\xi_3 = 0.1$.

[2009] has shown that the resonant peak can be reduced by nonlinear viscous damping which has little effect on the non-resonant areas. This overcomes the well-known problem of linear damping which increases transmissibility at high frequencies. Fig. 6.6(a) shows the detrimental effect of linear damping on the high frequency power transmissibility of System (6.14) which can be eradicated by nonlinear damping as shown in Fig. 6.6(b). Motivated by these observations, the present study is concerned with the design of a vibration isolation system that has a large isolation range provided by the auxiliary springs as demonstrated in Fig. 6.3, and a low high-frequency transmissibility maintained by a nonlinear damping.

6.4 Analysis of the system power transmissibility using the OFRF

To design a nonlinear vibration isolation system according to the requirements which limit the transmissibility at certain excitation frequencies, the relationship between the system parameters and the power transmissibility must be first established. In this section, the OFRF approach will be applied to System (6.14)

to express its power transmissibility as a polynomial function of the nonlinear parameters, which will be used to reformulate the OFRF estimation method for the power spectrum.

6.4.1 The OFRF representation of the system power transmissibility

Assume System (6.14) with a nonlinear spring force that can be approximated by Eq. (6.24) has a stable zero equilibrium and therefore can be represented by the Volterra series. The output frequency response of the system $Y_2(j\omega)$ can be written as [Lang *et al.*, 2007]

$$Y_2(j\omega) = \sum_{j_2=0}^{N_2} \sum_{j_3=0}^{N_3} \sum_{j_d=0}^{N_D} P_{j_2,j_3,j_d}(j\omega) {\gamma_2}^{j_2} {\gamma_3}^{j_3} \xi_3^{j_d} \tag{6.29}$$

which is a polynomial function of the model parameters that define the system nonlinearity. $P_{j_2,j_3,j_d}(j\omega)$, the polynomial coefficient, is a function of frequency and the linear system parameters, γ_1 and ξ_1. N_2, N_3 and N_D are the orders of the polynomial with respect to γ_2, γ_3 and ξ_3 respectively. Substituting Eq. (6.29) into Eq. (6.21) gives the power transmissibility as a polynomial function of γ_2, γ_3 and ξ_3

$$E(\Omega) = \sum_{p=1}^{\infty} \left| \, Y_2(j\omega)|_{\omega=p\Omega} \, \right|^2 = \sum_{j_2=0}^{M_2} \sum_{j_3=0}^{M_3} \sum_{j_d=0}^{M_D} Q_{j_2,j_3,j_d}(j\Omega) {\gamma_2}^{j_2} {\gamma_3}^{j_3} \xi_3^{j_d} \tag{6.30}$$

where M_2, M_3 and M_D are the orders of the polynomial with respect to γ_2, γ_3 and ξ_3 respectively. $Q_{j_2,j_3,j_d}(j\Omega), j_2 = 0, 1, \cdots M_2, j_3 = 0, 1, \cdots M_3, j_d = 0, 1, \cdots M_d$ are determined by $P_{j_2,j_3,j_d}(j\Omega), j_2 = 0, 1, \cdots N_2, j_3 = 0, 1, \cdots N_3, j_d = 0, 1, \cdots N_D$. When all the nonlinear terms are zeros ($\gamma_2, \gamma_3, \xi_3 = 0$), System (6.14) is simply a linear vibration isolation system with a linear damping ξ_1 and a linear stiffness γ_1, the power transmissibility of which is given by

$$E(\Omega)|_{\gamma_2,\gamma_3,\xi_3=0} = |P_{0,0,0}(j\Omega)|^2$$

$$= Q_{0,0,0}(j\Omega) = \left| \frac{\gamma_1 + j\xi_1\Omega}{\gamma_1 + j\xi_1\Omega + (j\Omega)^2} \right|^2 = \frac{{\gamma_1}^2 + (\xi_1\Omega)^2}{(\gamma_1 - \Omega^2)^2 + (\xi_1\Omega)^2} \tag{6.31}$$

reaching a maximum at $\Omega \approx \sqrt{\gamma_1}$.

6.4.2 OFRF estimation method

The power transmissibility written in the form given by Eq. (6.30) is not only useful for theoretical analysis, but also applicable to the estimation of the transmissibility for any given values of system parameters. At each frequency, there is $\bar{M}$ number of coefficients $Q_{j_2,j_3,j_d}(j\Omega)$ where

$$\bar{M} = (M_2 + 1)(M_3 + 1)(M_D + 1). \tag{6.32}$$

If there are $\bar{M}$ sets of known $E(\Omega)$ and the corresponding values of γ_2, γ_3 and ξ_3 denoted by the subscripts $(1), (2), \cdots, (\bar{M})$, the values of $Q_{j_2,j_3,j_d}(j\Omega)$ can be estimated by

$$\begin{bmatrix} \hat{Q}_{0,0,0}(\Omega) \\ \vdots \\ \hat{Q}_{M_2,M_3,M_D}(\Omega) \end{bmatrix} = {X_{\bar{M}}}^{-1} \begin{bmatrix} E_{(1)}(\Omega) \\ E_{(2)}(\Omega) \\ \vdots \\ E_{(\bar{M})}(\Omega) \end{bmatrix} \tag{6.33}$$

where

$$X_{\bar{M}} = \begin{bmatrix} ({\gamma_2}_{(1)}{}^0 {\gamma_3}_{(1)}{}^0 {\xi_3}_{(1)}{}^0) & \cdots & \cdots & ({\gamma_2}_{(1)}{}^{M_2} {\gamma_3}_{(1)}{}^{M_3} {\xi_3}_{(1)}{}^{M_D}) \\ \vdots & & \vdots & \vdots \\ ({\gamma_2}_{(\bar{M})}{}^0 {\gamma_3}_{(\bar{M})}{}^0 {\xi_3}_{(\bar{M})}{}^0) & \cdots & \cdots & ({\gamma_2}_{(\bar{M})}{}^{M_2} {\gamma_3}_{(\bar{M})}{}^{M_3} {\xi_3}_{(\bar{M})}{}^{M_D}) \end{bmatrix}. \tag{6.34}$$

Having obtained $\hat{Q}_{j_2,j_3,j_d}(j\Omega)$, the estimated values for $Q_{j_2,j_3,j_d}(j\Omega)$, the results can be substituted back into Eq. (6.30) to estimate $\hat{E}(\Omega)$ for other given γ_2, γ_3 and ξ_3,

i.e.

$$\hat{E}(\Omega) = \sum_{j_2=0}^{M_2} \sum_{j_3=0}^{M_3} \sum_{j_d=0}^{M_D} \hat{Q}_{j_2,j_3,j_d}(\Omega) {\gamma_2}^{j_2} {\gamma_3}^{j_3} \xi_3^{j_d}. \tag{6.35}$$

Eq. (6.35) is crucial to the design approach for a nonlinear vibration isolation system in this paper. Given the explicit relationship between $E(\Omega)$ and the nonlinear parameters γ_2, γ_3 and ξ_3, Eq. (6.35) provides a straightforward method to find the appropriate values for the nonlinear parameters to satisfy a particular requirement for $E(\Omega)$.

6.5 Design of vibration isolators with spring and damping nonlinearities

6.5.1 Design steps

The design of k, l, ξ_1 and ξ_3, the four parameters of the vibration isolation system depicted by Fig. 6.2 can be conducted in two stages. The linear parameters are first designed then held constant when the OFRF estimation method is applied for the nonlinear parameter design. It is straightforward to apply this strategy to design the linear and nonlinear damping coefficients, ξ_1 and ξ_3, as they are independent variables but special attention must be paid to the design of the auxiliary springs, defined by k and l, as both the linear and nonlinear stiffness force are affected. To separate the linear and nonlinear effects of the auxiliary springs, γ_1, γ_2 and γ_3 are written as functions of k and l given by Eqs. (6.25) to (6.27). After the linear stiffness coefficient γ_1 is determined, the OFRF estimation method can be applied to determine γ_2 and γ_3, subject to the constraint given by the relationship between k and l , that is Eq. (6.25).

The brief outline of the design process is given below. First, the linear parameters, γ_1 and ξ_1, are chosen according to requirements (ii) and (iii). Then, the OFRF estimation method is applied to find the nonlinear parameters γ_2, γ_3 and ξ_3 to satisfy requirement (i). Finally, the values of k and l are deduced from γ_1, γ_2 and γ_3. The parameters are selected in a sequential manner so the whole

process has to be iterated if the final design violates any of the requirements. To reduce or eliminate the amount of iterations required, estimation error margins are incorporated into the design. The detailed design procedure can be described as follows.

1. Choose the values of $\hat{f}$, M_2, M_3 and M_D.

   The value of $\hat{f}$ must be smaller than 0.2 so that the nonlinear stiffness force f_s can be accurately approximated by Eq. (6.24). M_2, M_3 and M_D define the orders of the polynomial representation in Eq. (6.30). Similar to the degree of polynomial curve fitting, the values of M_2, M_3 and M_D should be sufficiently high in order to accurately represent the power transmissibility but not too high to avoid Runge's phenomenon and excessive computation.

2. Find γ_1.

   Assuming that the system only have linear forces (i.e. $\gamma_2, \gamma_3, \xi_3 = 0$), find γ_1 according to requirements (i) and (ii). For this purpose, two simultaneous equations from Eq. (6.31) are obtained at $\Omega = \sqrt{\gamma_1}$ and $\Omega = \Omega_c$ where $E(\Omega)$ takes the value of E_m and E_c, respectively, to yield

   $$E_m = \frac{{\gamma_1}^2 + (\xi_1\sqrt{\gamma_1})^2}{(\gamma_1 - \sqrt{\gamma_1}^2)^2 + (\xi_1\sqrt{\gamma_1})^2} = \frac{\gamma_1 + \xi_1^2}{\xi_1^2} \tag{6.36}$$

   and

   $$E_c = \frac{{\gamma_1}^2 + (\xi_1\Omega_c)^2}{(\gamma_1 - \Omega_c^2)^2 + (\xi_1\Omega_c)^2}. \tag{6.37}$$

   The solution of γ_1, subject to the constraint $0 < \gamma_1 < 1$ of the equations, is the result of the determined γ_1. Note that if $E_c = 1$, γ_1 is simply determined by

   $$\gamma_1 = \frac{\Omega_c^2}{2}. \tag{6.38}$$

   In addition, the solution ξ_1 to the simultaneous equations is not relevant here and is discarded.

3. Find ξ_1.

   Again, assuming that the system only have linear forces, solve

   $$E(\Omega_l)|_{\gamma_2,\gamma_3,\xi_3=0} = E_l \tag{6.39}$$

   for ξ_1 according to requirement (iii). The solution gives the maximum value for ξ_1 as an increase in ξ_1 leads to an increase in $E(\Omega_l)$. To allow for the effects of the nonlinear stiffness and damping terms, reduce ξ_1 by 10%.

4. Find $\bar{M}$ different sets of values for the nonlinear parameters γ_2, γ_3 and ξ_3.

   Because γ_2 and γ_3 are functions of k and l, the relation of which are constrained by the choice of γ_1, the values of γ_2 and γ_3 are related. Rearranging Eq. (6.25) to give

   $$k = \frac{l\,(1-\gamma_1)}{2\,(1-l)} \tag{6.40}$$

   and substituting Eq. (6.40) into Eq. (6.26) and Eq. (6.27) gives

   $$\gamma_2 = \frac{\hat{f}^2(1-\gamma_1)}{2l^2(1-l)} \tag{6.41}$$

   and

   $$\gamma_3 = -\frac{3\hat{f}^4(1-\gamma_1)}{8l^4(1-l)} \tag{6.42}$$

   respectively. As the values of $\hat{f}$ and γ_1 have been determined, Eqs. (6.41) and (6.42) represent the nonlinear stiffness coefficients γ_2 and γ_3 as functions of l only. All parameters affecting the linear forces are now fixed, so the power spectrum only depends on l and ξ_3.

   Then, select $\bar{M}$ different sets of values of l and ξ_3, denoted as $l_{(J)}$ and $\xi_{3(J)}$ for $J = 1, 2, \cdots \bar{M}$ respectively. This populates the first three columns in Table 6.1. The values of γ_2 and γ_3, which are functions of l, in the last two columns are calculated using Eqs. (6.41) and (6.42).

Set	ξ_3	l	γ_2	γ_3
1	$\xi_{3_{(1)}}$	$l_{(1)}$	$\gamma_2(l_{(1)})$	$\gamma_3(l_{(1)})$
2	$\xi_{3_{(2)}}$	$l_{(2)}$	$\gamma_2(l_{(2)})$	$\gamma_3(l_{(2)})$
3	$\xi_{3_{(3)}}$	$l_{(3)}$	$\gamma_2(l_{(3)})$	$\gamma_3(l_{(3)})$
$\vdots$	$\vdots$	$\vdots$	$\vdots$	$\vdots$
$\bar{M}$	$\xi_{3_{(\bar{M})}}$	$l_{(\bar{M})}$	$\gamma_3(l_{(\bar{M})})$	$\gamma_3(l_{(\bar{M})})$

Table 6.1: Values of nonlinear parameters for the OFRF estimation.

5. Generate power spectra.

   Obtain the power spectrum $E(\Omega)$ for γ_2, γ_3 and ξ_3 taking values from each row in Table 6.1 over the required frequency range $\Omega \in \{\Omega_1, \Omega_2, \cdots, \Omega_S, \Omega_c, \Omega_l\}$ either by simulation or by experiment. These are denoted as $E_{(i)}(\Omega)$ for $i = 1, 2, \cdots, \bar{M}$.

6. Check if the jump phenomenon is observed in any of the power spectra.

   If the power transmissibility curve $E_{(i)}(\Omega)$ shows any discontinuities, increase the value of $\xi_{3_{(i)}}$ and regenerate the spectrum. Iterate this step until all power spectra are continuous functions.

7. Estimate the coefficients $\hat{Q}_{j_2,j_3,j_d}(\Omega)$ in the power spectrum using Eq. (6.33).

8. Find $\hat{\Omega}_{max}$.

   $\hat{\Omega}_{max}$ is the frequency at which the maximum estimated transmissibility occurs and can be obtained from Eq. (6.35) where $\xi_3 = \max\left(\{\xi_{3_{(1)}}, \xi_{3_{(2)}}, \cdots, \xi_{3_{(\bar{M})}}\}\right)$, γ_2 and γ_3 are deduced from Eqs. (6.41) and (6.42) where l takes any value within the range $\{l_{(1)}, l_{(2)}, \cdots, l_{(\bar{M})}\}$, i.e.

$$\hat{\Omega}_{max} = \arg\max_{\Omega} \hat{E}(\Omega) \tag{6.43}$$

   where (in the expression of $\hat{E}(\Omega)$) $\xi_3 = \max\left(\{\xi_{3_{(1)}}, \xi_{3_{(2)}}, \cdots, \xi_{3_{(\bar{M})}}\}\right)$ and $l \in \left[\min\left(\{l_{(1)}, l_{2_{(2)}}, \cdots, l_{2_{(\bar{M})}}\}\right), \max\left(\{l_{(1)}, l_{2_{(2)}}, \cdots, l_{2_{(\bar{M})}}\}\right)\right]$.

9. Find ξ_3.

Solve Eq. (6.35) at $\Omega = \hat{\Omega}_{max}$ as below.

$$\hat{E}(\hat{\Omega}_{max}) = \sum_{j_d=0}^{M_D} \underbrace{\left[\sum_{j_2=0}^{M_2} \sum_{j_3=0}^{M_3} \hat{Q}_{j_2,j_3,j_d}(\hat{\Omega}_{max}) {\gamma_2}^{j_2} {\gamma_3}^{j_3} \right]}_{\text{only depends on } \iota} \xi_3^{j_d} = 0.95 E_{Rmax}. \quad (6.44)$$

E_{Rmax} is multiplied by a factor of 0.95 to compensate for the uncertainty of $\hat{\Omega}_{max}$.

10. Calculate k.

    Calculate the value for k by substituting γ_1 and l into Eq. (6.40). The design parameters k, l and ξ_3 are found.

11. Check the solutions against the requirements.

    If requirement (i) is violated, repeat from Step 8 with the designed ξ_3 to get a better estimation of $\hat{\Omega}_{max}$.

    If requirement (ii) is violated, repeat from Step 8 with a smaller value of l which would increase the isolation range. If requirement (ii) cannot be satisfied with the smallest possible value for l, repeat from Step 2 with a smaller value of γ_1.

    If requirement (iii) is violated, repeat from Step 3 with a smaller value of ξ_1.

The above design process, summarised by the flow chart in Fig. 6.7, has provided a systematic way of deducing the linear and nonlinear parameters of the proposed vibration isolation system according to the design requirements. As the design requirements only restrict the performance at three critical points, multiple solutions can be found. In Step 8, the value for l is chosen from the data range that was used to find the polynomial coefficients of the power transmissibility expression in order to achieve good approximation of the power transmissibility. There is a natural trade-off between k, the stiffness ratio of the auxiliary springs to the primary spring, and l, ratio of the length of the auxiliary springs in the horizontal position to their natural lengths, as their relationship is limited by γ_1 as in Eq. (6.25). To achieve the same isolation range by holding γ_1 constant, the auxiliary springs are either lightly compressed (large l) but with a high stiffness

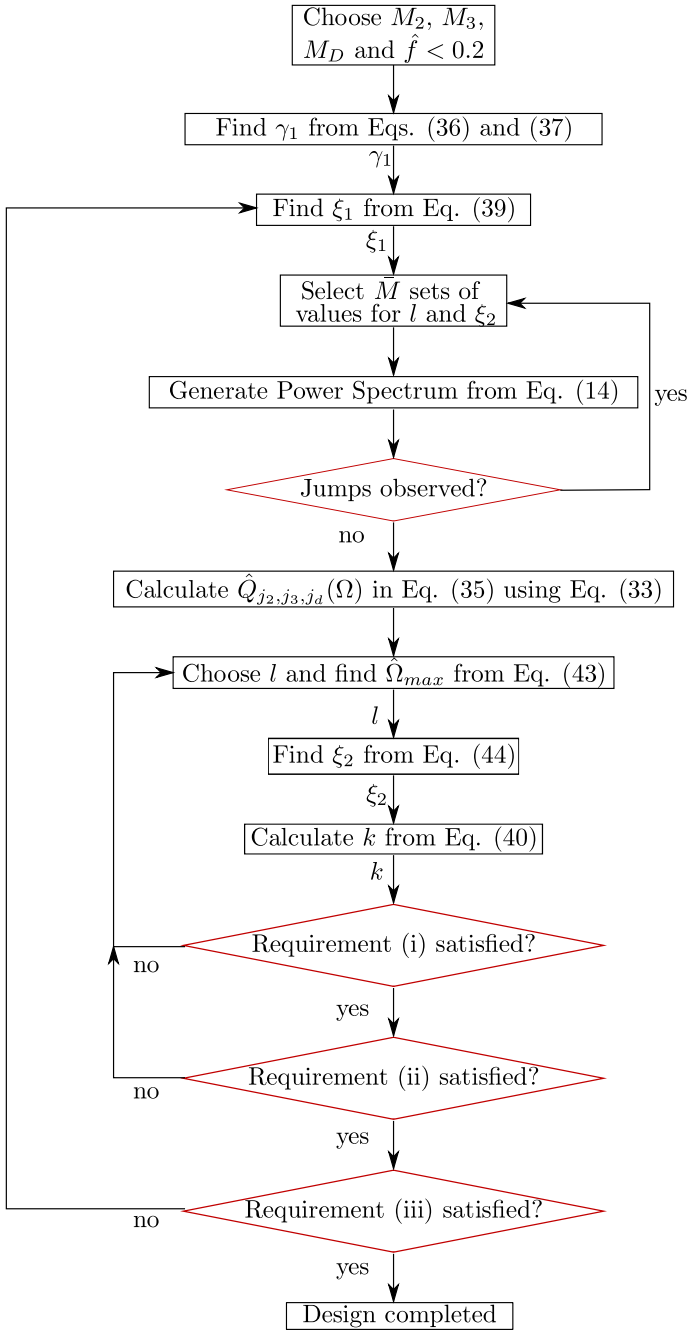

Figure 6.7: Nonlinear vibration isolator design procedures

(large k) or highly compressed (small l) but have a low stiffness (small l). The choice of l and the corresponding k are viewed as indifferent as far as the requirements are concerned as they produce the same isolation range, but extreme values

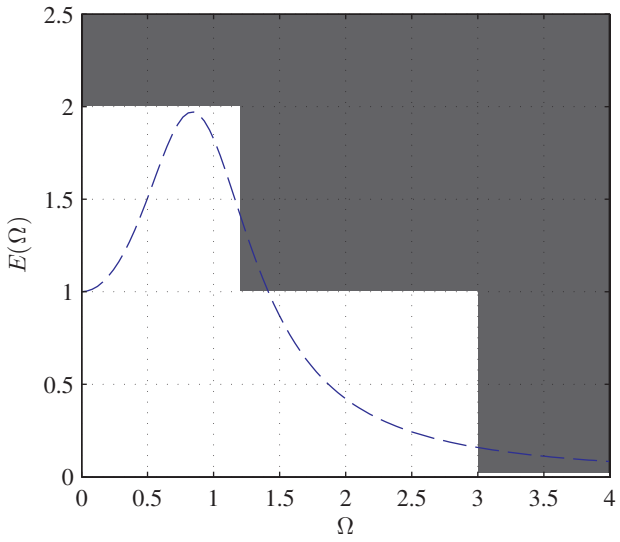

Figure 6.8: Vibration isolator design requirements. Dashed line: power transmissibility curve of System (6.14) where $\gamma_1 = 1, \xi_1 = 1.1$ and all other nonlinear terms are zero.

should be avoided as neither highly compressed auxiliary springs nor ones with very high stiffness are desirable in practice.

6.6 Numerical studies

6.6.1 Design process

In this section, a numerical example of the design of a nonlinear vibration isolator in the form of Eq. (6.2) following the procedure in Section 6.5.1 will be conducted to demonstrate the effectiveness of the proposed design approach. The objective of the design is to derive parameters for System (6.14) such that the requirements in Section 6.2 are satisfied. In this numerical example, a graphical representation of the requirements is given in Fig. 6.8 where $E_m = 2$, $E_c = 1$, $E_l = 0.02$, $\Omega_c = 1.2$ and $\Omega_l = 3$. The force transmissibility curve must lie in the white area. It is clear that these requirements cannot be simultaneously achieved by a linear vibration isolator as shown by the dashed line in Fig. 6.8 where $\gamma_1 = 1, \xi_1 = 1.1, \gamma_2, \gamma_3, \xi_3 = 0$. The linear damping ratio ξ_1 is selected to reduce the resonant peak to below 2 specified

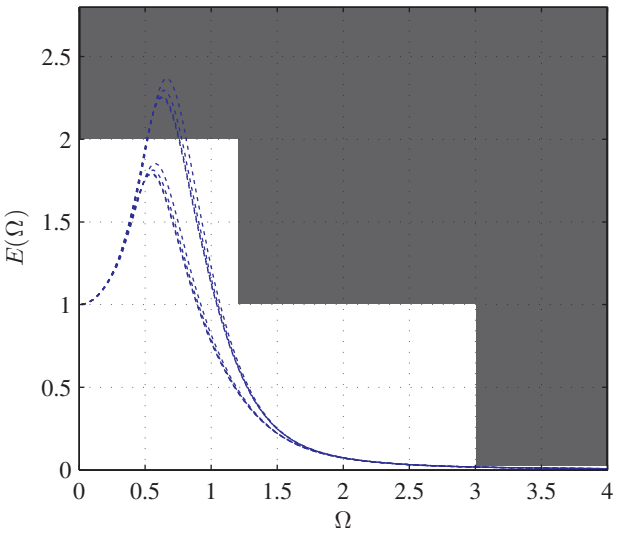

Figure 6.9: The power transmissibility of System (6.14) where $\xi_1 = 0.28$, $\gamma_1 = 0.72$, k, l and ξ_3 takes values from Table 6.2.

by requirement (i) but requirements (ii) and (iii) are violated as a result. Nonlinear parameters must therefore be introduced.

The parameters of System (6.14) are designed according to the method in Section 6.5.1 as below.

1. Take $\hat{f} = 0.1$, and $M_2, M_3, M_D = 1$ first.

2. As $E_c = 1$, Eq. (6.38) gives the value of γ_1 as $= 1.2^2/2 = 0.72$.

3. The solution of Eq. (6.39) where $\gamma_1 = 0.72$, $\gamma_2, \gamma_3, \xi_3 = 0$ at $\Omega = \Omega_l = 3$ gives $\xi_1 = 0.31$. Reducing it by 10% gives $\xi_1 = 0.28$.

4. $\bar{M} = (M_2 + 1)(M_3 + 1)(M_D + 1) = 2 \times 2 \times 2 = 8$. Eight sets of values for l and ξ_3 are given in the second and the third columns in Table 6.2. The corresponding values for γ_2, γ_3 in the last two columns are calculated using Eqs. (6.41) and (6.42).

5. System (6.14) with parameters taking values from Table 6.2 is simulated to produce the power transmissibility curves $E_{(i)}(\Omega), i = 1, 2, \cdots, 8$ in Fig. 6.9.

6. All the curves in Fig. 6.9 are continuous functions and no jumps are observed.

Set	ξ_3	l	γ_2	γ_3
1	$\xi_{3(1)} = 0.3$	$l_{(1)} = 0.70$	$\gamma_2(l_{(1)}) = 0.0952$	$\gamma_3(l_{(1)}) = -0.0146$
2	$\xi_{3(2)} = 0.3$	$l_{(2)} = 0.80$	$\gamma_2(l_{(2)}) = 0.1094$	$\gamma_3(l_{(2)}) = -0.0128$
3	$\xi_{3(3)} = 0.3$	$l_{(3)} = 0.90$	$\gamma_2(l_{(3)}) = 0.1728$	$\gamma_3(l_{(3)}) = -0.0160$
4	$\xi_{3(4)} = 0.3$	$l_{(4)} = 0.95$	$\gamma_2(l_{(4)}) = 0.3102$	$\gamma_3(l_{(4)}) = -0.0258$
5	$\xi_{3(5)} = 0.6$	$l_{(5)} = 0.70$	$\gamma_2(l_{(5)}) = 0.0952$	$\gamma_3(l_{(5)}) = -0.0146$
6	$\xi_{3(6)} = 0.6$	$l_{(6)} = 0.80$	$\gamma_2(l_{(6)}) = 0.1094$	$\gamma_3(l_{(6)}) = -0.0128$
7	$\xi_{3(7)} = 0.6$	$l_{(7)} = 0.90$	$\gamma_2(l_{(7)}) = 0.1728$	$\gamma_3(l_{(7)}) = -0.0160$
8	$\xi_{3(8)} = 0.6$	$l_{(8)} = 0.95$	$\gamma_2(l_{(8)}) = 0.3102$	$\gamma_3(l_{(8)}) = -0.0258$

Table 6.2: Values of nonlinear parameters for the OFRF estimation.

7. In this example, the matrix $X_{\bar{M}}$ from Eq. (6.34) is

$$X_{\bar{M}} = \begin{bmatrix} 1 & 1 & \cdots & 1 \\ \gamma_{2(1)} & \gamma_{2(2)} & \cdots & \gamma_{2(8)} \\ \gamma_{2(1)}^2 & \gamma_{2(2)}^2 & \cdots & \gamma_{2(8)}^2 \\ \gamma_{3(1)} & \gamma_{3(2)} & \cdots & \gamma_{3(8)} \\ \gamma_{2(1)}\gamma_{3(1)} & \gamma_{2(2)}\gamma_{3(2)} & \cdots & \gamma_{2(8)}\gamma_{3(8)} \\ \gamma_{2(1)}^2\gamma_{3(1)} & \gamma_{2(2)}^2\gamma_{3(2)} & \cdots & \gamma_{2(8)}^2\gamma_{3(8)} \\ \xi_{3(1)} & \xi_{3(2)} & \cdots & \xi_{3(8)} \\ \gamma_{2(1)}\xi_{3(1)} & \gamma_{2(2)}\xi_{3(2)} & \cdots & \gamma_{2(8)}\xi_{3(8)} \\ \gamma_{2(1)}^2\xi_{3(1)} & \gamma_{2(2)}^2\xi_{3(2)} & \cdots & \gamma_{2(8)}^2\xi_{3(8)} \\ \gamma_{3(1)}\xi_{3(1)} & \gamma_{3(2)}\xi_{3(2)} & \cdots & \gamma_{3(8)}\xi_{3(8)} \\ \gamma_{2(1)}\gamma_{3(1)}\xi_{3(1)} & \gamma_{2(2)}\gamma_{3(2)}\xi_{3(2)} & \cdots & \gamma_{2(8)}\gamma_{3(8)}\xi_{3(8)} \\ \gamma_{2(1)}^2\gamma_{3(1)}\xi_{3(1)} & \gamma_{2(2)}^2\gamma_{3(2)}\xi_{3(2)} & \cdots & \gamma_{2(8)}^2\gamma_{3(8)}\xi_{3(8)} \end{bmatrix}^T . \quad (6.45)$$

Substituting Eq. (6.45) and the power transmissibility results from Step 5 into Eq. (6.33) gives the values of $\hat{Q}_{0,0,0}(\Omega), \cdots, \hat{Q}_{1,1,1}(\Omega)$.

8. Take $l = 0.75$ which is within the range of l in Table 6.2 and $\xi_3 = 0.6$ which is the maximum value of ξ_3 in the table. The corresponding γ_2 and γ_3 calculated from Eqs. (6.41) and (6.42) are 0.010 and -0.0001 respectively. Using these figures, the estimated power transmissibility evaluated from Eq. (6.35) gives $\hat{\Omega}_{max} = 0.54$ as shown in Fig. 6.10.

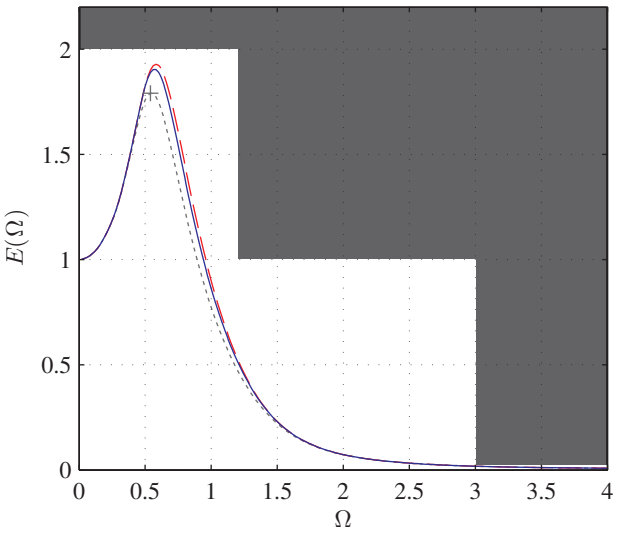

Figure 6.10: Design results. Dotted line: Estimated power transmissibility from Step 8 where $l = 0.75$ and $\xi_3 = 0.6$. The cross indicates the maximum power transmissibility at $\hat{\Omega}_{max} = 0.54$. Dashed line: Estimated power transmissibility from Step 9 with the designed parameters $l = 0.75$ and $\xi_3 = 0.49$. Solid line: power transmissibility curve of the simulated designed system.

9. Substituting $\gamma_2 = 0.010$, $\gamma_3 = -0.0001$ and $E_{Rmax} = 2$ in Eq. (6.44) gives

$$\begin{aligned}\hat{E}(\hat{\Omega}_{max}) = 0.95E_{Rmax} =& \hat{Q}_{0,0,0}(\hat{\Omega}_{max}) + \hat{Q}_{1,0,0}(\hat{\Omega}_{max})\gamma_2 \\ &+ \hat{Q}_{0,1,0}(\hat{\Omega}_{max})\gamma_3 + \hat{Q}_{1,1,0}(\hat{\Omega}_{max})\gamma_2\gamma_3 \\ &+ \Big[\hat{Q}_{0,0,1}(\hat{\Omega}_{max}) + \hat{Q}_{1,0,1}(\hat{\Omega}_{max})\gamma_2 \\ &+ \hat{Q}_{0,1,1}(\hat{\Omega}_{max})\gamma_3 + \hat{Q}_{1,1,1}(\hat{\Omega}_{max})\gamma_2\gamma_3\Big]\,\xi_3 \end{aligned} \quad (6.46)$$

   and the solution is $\xi_3 = 0.49$.

10. With $\gamma_1 = 0.72$ and $l = 0.75$, Eq. (6.40) gives $k = 0.42$. The complete design parameters are $k = 0.42$, $l = 0.75$, $\xi_1 = 0.28$ and $\xi_3 = 0.49$.

11. The power transmissibility curve generated using Eq. (6.35) where $\gamma_2 = 0.010$, $\gamma_3 = -0.0001$ and $\xi_3 = 0.49$ in given in Fig. 6.10. The maximum power transmissibility is 1.79 at $\Omega_{max} = 0.54$ which satisfies requirement (i) and shows that the estimation of Ω_{max} in Step 8 is sufficiently accurate.

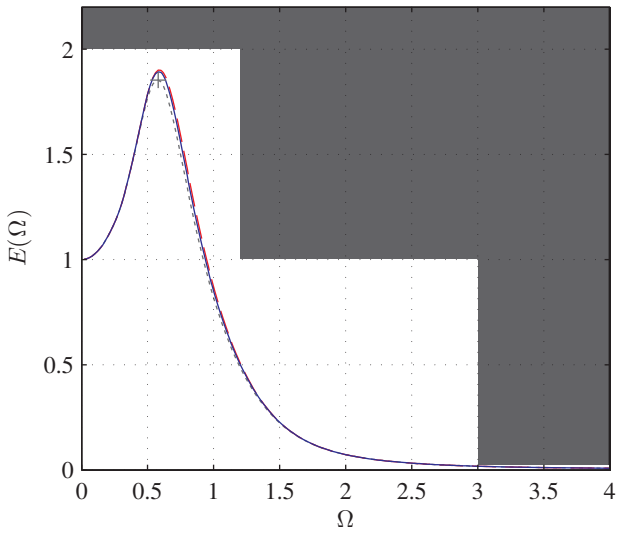

Figure 6.11: Alternative design results. Dotted line: Estimated power transmissibility from Step 8 where $l = 0.95$ and $\xi_3 = 0.56$. The cross indicates the maximum power transmissibility at $\hat{\Omega}_{max} = 0.58$. Dashed line: Estimated power transmissibility from Step 9 with the designed parameters $l = 0.95$ and $\xi_3 = 0.56$. Solid line: power transmissibility curve of the simulated designed system.

It can be also observed that $\hat{E}(\Omega) = 0.53$ at $\Omega = 1.2$ is less than the required $E_c = 1$. Requirement (ii) is therefore satisfied.

At $\Omega = \Omega_l = 3$, $\hat{E}(\Omega) = 0.018$ which is just less than the required E_R. Requirement (iii) is also satisfied.

Alternative solutions can be found by repeating Steps 8 to 11 by selecting different values of l. For example, when $l = 0.95$, k and ξ_3 are 2.66 and 0.56 respectively. The results of this design are presented in Fig.6.11.

These two different choices of l and the corresponding k demonstrate the phenomenon of the auxiliary springs explained in Section 6.5.1. Both designs satisfy all the transmissibility requirements. In the first case where $k = 0.42$ and $l = 0.75$, the stiffness of the auxiliary springs is softer than the primary spring but the 0.75 length ratio means that they are heavily compressed in the horizontal position, that is a strain of 25%. The second case where $k = 2.66$ and $l = 0.95$ provides an alternative solution. The auxiliary springs are only lightly compressed under a strain of 5% but their stiffness is now 2.66 times of the primary spring. In a prac-

tical application, there would be limits on the maximum strain experienced by the springs, which is restricted by their elastic range, as well as on the reaction force on the supporting structure. The choice of k and l would therefore be subjected to these constraints.

6.6.2 Design verification and discussions

Figs. 6.10 and 6.11 compare the results estimated using the OFRF approach in Section 6.6.1 with those obtained by simulation. All of these results satisfy the three design requirements and the discrepancies between the curves are small. This shows the effectiveness of the proposed design procedure in coping with a system with several nonlinear parameters. The numerical studies have demonstrated the following advantages of the OFRF based design.

(a) The power spectrum represented in the form of an OFRF provides a direct relationship between the nonlinear parameters and the power transmissibility at any frequency as given by Eq. (6.35). Therefore the effect of any of the nonlinear parameters on the power transmissibility $E(\Omega)$, which is specified by the design requirements, can be understood. This is hugely beneficial for the design of the nonlinear parameters in order to achieve an objective in the frequency domain.

(b) By measuring the performance of a vibration isolator with the power transmissibility, the OFRF based design method captures the effects of higher harmonics in the system output caused by the nonlinear terms. Fig. 6.12 shows three time domain responses of System (6.14) when excited by a sinusoidal input where Ω takes different values. It is clear that none of the outputs is a simple sinusoid. The higher order harmonics are significant when the excitation frequency is low and around the resonant region so must be considered when doing the system design.

The magnitude of each higher order harmonic can be calculated accurately using a higher order harmonic balance method. Nonetheless, it is unusual to include more than the first few harmonics as this will result in a large amount of simultaneous equations which are difficult and computationally demanding

to solve. The OFRF based design takes all higher harmonics into account by efficiently converting the input and output in the time domain into the power transmissibility in the frequency domain using Parseval's theorem in Eq. (6.21) without performing any Fourier transform. If needed, each individual harmonic can also be examined using this method.

(c) With all linear parameters held constant, the numerical example has shown that the nonlinear parameters k, l and ξ_3 can be deduced from only eight sets of simulation results. The estimation of the power transmissibility is generally very good except around the resonant regions. Obviously , this can be improved by raising the polynomial order M_2, M_3 and M_D in Eq. (6.35). But by keeping Eq. (6.35) as a first order multivariate polynomial, as in the above example, the problem is simplified and a solution can be found more quickly. Note that the estimation only needs to be good enough for the design to satisfy the requirements.

(d) Another key advantage of the OFRF approach is the use of simulation or experimental data. In the numerical example in Section 6.6.1, the simulation results were generated from a model of System (6.14) implemented in MATLAB where the actual nonlinear spring force given by Eq. (6.13), not the Taylor approximation, was used. In a practical situation, the eight sets of results would be real experimental data which may reflect some unmodelled behaviours. The OFRF approach provides a relationship between the nonlinear parameters and the real output power level including the unmodelled effects. The same design procedure can be applied to give a design based on a real physical system.

The above discussions have highlighted the advantages of the proposed nonlinear vibration isolation system design. Making use of the relationship between the nonlinear parameters and the power transmissibility provided by the OFRF approach, the nonlinear parameters can be designed using only a few sets of simulation or experimental results. This efficient way of determining nonlinear parameters according to requirements in the frequency domain can be easily adapted for other types of nonlinear systems.

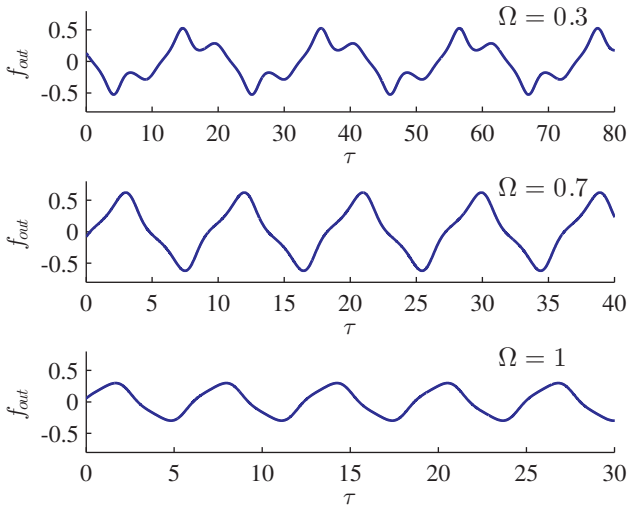

Figure 6.12: Time domain simulation results of System (6.14) where $\xi_1 = 0.1$, $\xi_3 = 0.3$, $k = 1$ and $l = 0.7$.

6.7 Conclusions

Conventional linear sdof vibration isolation systems have two main disadvantages. First, it is impossible to obtain a wider isolation range by reducing the cut-off frequency, which is fixed at $1/\sqrt{2}$ of the system resonant frequency. Second, there is a trade-off between the level of resonance suppression and the high frequency isolation capability. To address the first issue, springs with stiffness nonlinearity are widely used. As for the second problem, damping nonlinearity has been found to be beneficial across a wide frequency range.

The harmonic balance method is a well-established technique for the analysis of nonlinear vibration isolation systems. The concept is straightforward but heavy computation is required when higher order harmonics have to be considered. In addition, only an implicit relationship between the system parameters and output response can be produced by using the harmonic balance method. Recently, a new analysis method called the output frequency response function (OFRF) approach has been developed. The OFRF provides an explicit analytical description for the output frequency response of a wide class of nonlinear systems which can significantly facilitate the system analysis and design. In addition, when systems

are subject to harmonic excitations, the OFRF approach can readily take the effects of higher order harmonics into account without requiring heavy analytical computations.

In this chapter, a new vibration isolation system is proposed by exploiting the advantages of both nonlinear damping and stiffness in order to comprehensively overcome the weaknesses of conventional linear vibration isolators. A design technique for the vibration isolation system is developed which applies the OFRF approach to express the system power transmissibility in terms of the parameters that affects the system's nonlinearity. A detailed design procedure is provided, that, according to the design requirement specified by a transmissibility envelope, first determines the system linear parameters and then finds the nonlinear ones using the OFRF based representation for the power transmissibility. Simulation studies have been conducted to verify the effectiveness of the new design. The results show that the proposed vibration isolation system can achieve an ideal performance, namely, a large isolation range, a low resonant peak, and a low transmissibility over higher frequencies indicating the system has potential to be used for many engineering applications.

Chapter 7

Conclusions

The ever-growing demand for new technologies has led to the rapid development of vibration control. In many engineering applications, it is necessary to protect the plant from disturbances or to prevent the unwanted vibration travelling outward from the source. This is why vibration control has become an inherent part of many designs ranging from high-precision control for biochemical processes at the microscopic level to seismic protection of full-scale structures. The fundamental understanding of vibration control techniques and the design of practical vibration control systems are therefore having a growing significance.

Beginning with a general overview of the vibration problem regarding the shortfalls of linear vibration isolation, the weaknesses of common nonlinear analysis methods and some current realisation of nonlinearities, the thesis has covered some important aspects of vibration control focusing on passive vibration isolation. In the search for an ideal vibration isolator that has a low resonant peak, low high-frequency transmissibility and a large isolation range, the main objective of the thesis is to provide a comprehensive view of nonlinear vibration isolation systems from a solid theoretical foundation all the way through to their design and practical implementation. First, the theoretical studies of nonlinear vibration isolation systems have revealed their advantages over conventional linear vibration isolators over a wide excitation frequency range. Then, these vibration isolators with enhanced performance have been implemented experimentally using a semi-active device under feedback control. Finally, a systematic design method has been developed to select parameters for nonlinear systems according to some stringent

requirements in the frequency domain. A brief summary of each chapter containing original contributions is provided below.

Despite their reliability and intuitive appeal, linear vibration isolation systems are known for their performance deficiency. Their designs in a non-dimensional form are dominated by only one parameter, the damping ratio, which suppresses the resonance at the cost of the high frequency transmissibility. To tackle this inability to provide a satisfactory performance over the whole frequency range, spring and damping nonlinearities have been introduced to a force vibration isolation system in Chapter 3. Applying the output frequency response function (OFRF) approach, the force transmissibility of this nonlinear vibration isolator has been expressed as a polynomial in the nonlinear spring and the nonlinear damping coefficients, which enabled the theoretical analysis of their effects.

Although known for causing discontinuities, called jump-up or down, in the output spectra, nonlinear stiffness reduces the displacement output of a force vibration isolator. A cubic nonlinear damping characteristic has been shown to offer resonance suppression with minimal impacts on the non-resonant areas. The detailed examination of the system's output spectra has revealed the advantages of the combined use of these two types of nonlinearities, resulting in a force vibration isolator that has a low resonant peak, a low high-frequency transmissibility and a low level of output displacement. A table summarising the effects of the system parameters has been provided in Chapter 3.

Another type of vibration isolation system, a displacement vibration isolator, has been studied in Chapter 4. The effects of nonlinear viscous damping on a displacement vibration isolation system are very different from those on a system under force excitation. A comparison of the OFRF representations of the displacement transmissibility of systems with different nonlinear viscous damping characteristic over two frequency ranges has been conducted to show the importance of the damping exponents without the need of resorting to graphical examination. The theoretical analysis has concluded that for two vibration isolation systems with indifferent performance around the resonant region, the transmissibility of the system with a lower damping exponent is lower over the high frequency range and have lead to the conclusion that a nonlinear damping characteristic with a low damping exponent has an advantageous effect on a displacement vibration

isolation system.

Building upon the theoretical foundations in Chapters 3 and 4, the concept of nonlinear viscous damping has been implemented by an MR damper under feedback control in Chapter 5. Simulation studies together with experimental work have been presented to show the realisation of the theoretical viscous damping characteristic. The results collected from the experimental vibration isolation systems have validated the theoretical results shown in the previous two chapters. Another significant aspect of the experimental study is the unprecedented incorporation of an MR damper as a passive energy dissipating device into a physical vibration isolation system. Instead of placing the MR damper as an actuator in a vibration control system, the presented work has offered a more robust solution to vibration control problems.

The last main original contribution which is a novel and systematic way of designing nonlinear vibration isolation systems according to some transmissibility requirements has been presented in Chapter 6. Based on the OFRF estimation technique, the parameters of a force vibration isolation system with a nonlinear damping characteristic and a nonlinear stiffness provided by two auxiliary springs have been deduced. With a small set of simulation or experimental data, it is possible to calculate the values of the nonlinear parameters for specific frequency response requirements. The outcome of the design is a vibration isolator that has a low cut-off frequency, low resonant peak and low high-frequency transmissibility. This design approach is not only beneficial to vibration isolation systems, but also easily adaptable for the design of other types of nonlinear systems.

The major contributions presented in the thesis are highlighted below.

- The application of the OFRF approach to the analysis of nonlinear vibration isolation systems.

- The theoretical understanding of the strengths and weaknesses of nonlinear stiffness and nonlinear damping in a vibration isolation system excited by either force or displacement disturbance.

- The achievement of a vibration isolation with low transmissibility across the whole frequency.

- Experimental validation of the theoretical properties of nonlinear damping.
- The realisation of a nonlinear vibration isolation system with an ideal damping characteristic implemented by a feedback controlled MR damper.
- A systematic design process for nonlinear vibration isolation systems.

The three key elements of the thesis are the strong theoretical support in Chapters 3 and 4, the practical implementation of a desired damping force in Chapters 5, and the nonlinear vibration isolation system design method in Chapters 6. There are all very useful in many engineering applications for tackling the vibration problem. The theoretical analyses and the design method have been conducted in the non-dimensional form hence are applicable to systems of any order of magnitude, whereas the MR damper based implementation of the ideal nonlinear damping characteristic is only suitable where the required damping force is in the order of at least 200 N due to the properties of the currently commercially available MR dampers.

The results presented in this thesis have focused on the fundamental understanding, design and realisation of nonlinear vibration isolation systems. The conclusions based on a single-degree-of-freedom system have marked the beginning of the study of vibration control in the frequency domain and and have paved the way for many practical applications. To fully exploit the benefits of nonlinearities in vibration control, further investigation is required in the following areas.

- The analyses in the thesis has based the steady-state response a system under a single-tone sinusoidal input. In reality, the input vibration may have a rich frequency content. Therefore, the study of a nonlinear vibration isolation system under a multi-tone excitation would be beneficial.
- The study of the effects of nonlinear passive devices can be extended to systems with multi degrees of freedom, such as vibration absorbers and car suspension systems.
- The MR damper based implementation of nonlinear damping is only suitable for systems under vibration inputs with amplitudes within a certain range. A different realisation method is required for smaller scale systems.

- The practical application of the nonlinear vibration isolation system proposed in the thesis could be considered. Because of its robustness and reliability, the proposed system can be used in structural protection from seismic ground motion.

In this thesis, the rigorous theoretical approach supported by simulation and experimental validation has provided new valuable insights into the vibration control problem. Using a systematic design method, the beneficial effects of the damping and stiffness nonlinearities on vibration isolation systems have been exploited to create a robust vibration isolation system that provides a high level of vibration isolation over a wide frequency range. The results have great significance in both the theoretical understanding of nonlinear systems and the practical application of nonlinearities in vibration control problems. Further investigation in the nonlinear vibration control domain will extend the current studies and bring great advances in many engineering applications.

Appendix A - Proof of Proposition 3.2

According to [Lang & Billings, 1996], if System (3.2) is stable around zero equilibrium, the output spectra under the excitation of a sinusoidal input $u(\tau) = \sin(\Omega\tau)$ are given by

$$Y_J(j\omega) = \sum_{n=1}^{N} \frac{1}{2^n} \sum_{\omega_1+\cdots+\omega_n=\omega} H_n^{(J)}(j\omega_1, \ldots, j\omega_n)\bar{A}(\omega_1)\cdots\bar{A}(\omega_n) \tag{1}$$

where

$$\bar{A}(\omega_i) = \begin{cases} e^{j\angle A(\omega_i)} = e^{-j\pi/2} & \text{when } \omega_i = \Omega \\ e^{j\angle A(-\omega_i)} = e^{j\pi/2} & \text{when } \omega_i = -\Omega \\ 0 & \text{otherwise} \end{cases} \tag{2}$$

and

$$H_n^{(J)}(j\omega_1, \ldots, j\omega_n) = \int_{-\infty}^{\infty} \cdots \int_{-\infty}^{\infty} h_n^{(J)}(\tau_1, \ldots, \tau_n) e^{-j(\omega_1\tau_1+\cdots+\omega_n\tau_n)} d\tau_1 \cdots d\tau_n \tag{3}$$

is the nth order generalised frequency response functions (GFRF) [George, 1959] where $h_n^{(J)}(\tau_1, \cdots, \tau_n)$ is the nth order kernel in the Volterra series representation

of the system given by

$$y_J(\tau) = \sum_{n=1}^{N} \int_{-\infty}^{\infty} \cdots \int_{-\infty}^{\infty} h_n^{(J)}(\tau_1, \ldots, \tau_n) \prod_{i=1}^{n} u(t-\tau_i) d\tau_i. \tag{4}$$

The GFRFs of System (3.2) can be obtained by applying the results in [Swain & Billings, 2001] as follows:

$$H_1^{(1)}(j\omega_1) = -\frac{1}{(j\omega_1)^2 + \xi_1(j\omega_1) + 1} = -\frac{1}{L(j\omega_1)} \tag{5}$$

$$H_1^{(2)}(j\omega_1) = (1 + \xi_1(j\omega_1)) H_1^{(1)}(j\omega_1) \tag{6}$$

$$H_n^{(2)}(j\omega_1, \ldots, j\omega_n) = -(j\omega_1 + \cdots + j\omega_n)^2 H_n^{(1)}(j\omega_1, \ldots, j\omega_n), \qquad n = 2, \cdots, N \tag{7}$$

$$H_3^{(1)}(j\omega_1, j\omega_2, j\omega_3) = \gamma_2 \frac{\prod_{i=1}^{3} H_1^{(1)}(j\omega_i)}{L[j(\omega_1 + \omega_2 + \omega_3)]} + \xi_2 \frac{\prod_{i=1}^{3} j\omega_i H_1^{(1)}(j\omega_i)}{L[j(\omega_1 + \omega_2 + \omega_3)]} \tag{8}$$

$$H_{2\bar{n}+1}^{(1)}(j\omega_1, \ldots, j\omega_{2\bar{n}+1}) = \sum_{\bar{m}=0}^{\bar{n}} \gamma_2^{\bar{m}} \xi_2^{\bar{n}-\bar{m}} \frac{\prod_{i=1}^{2\bar{n}+1} H_1^{(1)}(j\omega_i)}{L[j(\omega_1 + \cdots + \omega_{2\bar{n}+1})]} \sum_{Z=1}^{N_{\bar{n}}} \frac{G_{\bar{m},\bar{n}-\bar{m}}\left(j\omega_{l_{i(1)}}^{Z}, \cdots, j\omega_{l_{i(j_i^{\bar{n}})}}^{Z}\right)}{\prod_{i=1}^{\bar{n}-1} L\left[j\omega_{l_{i(1)}}^{Z} + \cdots j\omega_{l_{i(j_i^{\bar{n}})}}^{Z}\right]} \tag{9}$$

where

$$L[j(\omega_1 + \cdots + \omega_n)] = -[(j\omega_1 + \cdots + j\omega_n)^2 + \xi_1(j\omega_1 + \cdots + j\omega_n) + 1] \tag{10}$$

$$j_i^{\bar{n}}, \quad i = 1, \ldots, \bar{n}-1 \quad \in \{3, 5, \ldots, 2\bar{n}-1\} \quad \text{for} \quad \bar{n} \geqslant 2 \tag{11}$$

$$\omega^Z_{l_{i(\bar{j})}}, \quad i = 1, \ldots, \bar{n}-1, \quad \bar{j} = 1, \ldots, j_i^{\bar{n}} \qquad \in \{\omega_1, \ldots, \omega_{2\bar{n}+1}\} \quad \text{for} \quad \bar{n} \geqslant 2, \tag{12}$$

$N_{\bar{n}}$ is an $\bar{n}$ dependent integer and $\lfloor (N-1)/2 \rfloor$ represents the largest integer less than or equal to $(N-1)/2$. $G_{\bar{m},\bar{n}-\bar{m}}\left(j\omega^Z_{l_{i(1)}}, \cdots, j\omega^Z_{l_{i(j_i^{\bar{n}})}}\right)$ is a multivariate polynomial in $j\omega^Z_{l_{i(1)}}, \cdots, j\omega^Z_{l_{i(j_i^{\bar{n}})}}$ given by

$$G_{\bar{m},\bar{n}-\bar{m}}\left(j\omega^Z_{l_{i(1)}}, \cdots, j\omega^Z_{l_{i(j_i^{\bar{n}})}}\right) = \sum_{k_1+\cdots+k_{(j_i^{\bar{n}})}=3(\bar{n}-\bar{m})} a_{\bar{m},\bar{n},k_1,\ldots,k_{(j_i^{\bar{n}})}} \left(j\omega^Z_{l_{i(1)}}\right)^{k_1} \cdots \left(j\omega^Z_{l_{i(j_i^{\bar{n}})}}\right)^{k_{(j_i^{\bar{n}})}} \tag{13}$$

and its coefficients are positive integers represented by $a_{\bar{m},\bar{n},k_1,\ldots,k_{(j_i^{\bar{n}})}}$ which depend on $\bar{m}, \bar{n}$ and $k_1, \ldots, k_{(j_i^{\bar{n}})}$. The sum of the power of all the variables in each polynomial term, i.e. $k_1 + \cdots + k_{(j_i^{\bar{n}})}$, equals to $\bar{n} - \bar{m}$, which is three times the power of ξ_2 in Eq. (3.18). Eq. (13) can be further simplified in two special cases: $\gamma_2 = 0$ and $\xi_2 = 0$. In the first case where $\gamma_2 = 0$, the system is equivalent to the system described in [Lang *et al.*, 2009] where a nonlinear damping is present without any nonlinear stiffness. The polynomial can be factorised to give

$$G_{0,\bar{n}}\left(j\omega^Z_{l_{i(1)}}, \cdots, j\omega^Z_{l_{i(j_i^{\bar{n}})}}\right) = \prod_{p=1}^{2\bar{n}+1} (j\omega_p) \prod_{i=1}^{\bar{n}-1} \left(j\omega^Z_{l_{i(1)}} + \cdots j\omega^Z_{l_{i(j_i^{\bar{n}})}}\right) \tag{14}$$

for $\bar{m} = 0$. Substituting Eq. (14) back into the general expression for $H^{(1)}_{2\bar{n}+1}(j\omega_1, \ldots, j\omega_{2\bar{n}+1})$ in Eq. (9) gives the same results as in [Lang *et al.*, 2009, Eq. (25)]. In the second case where $\xi_2 = 0$, Eq. (13) becomes

$$G_{\bar{n},0}\left(j\omega^Z_{l_{i(1)}}, \cdots, j\omega^Z_{l_{i(j_i^{\bar{n}})}}\right) = 1 \tag{15}$$

for $\bar{n} - \bar{m} = 0$.

Substituting Eq. (2)-(15) into Eq. (1) yields the spectrum of the first output of System (3.2) in the form of a polynomial in γ_2 and ξ_2 given by

$$Y_J(j\omega) = \sum_{\bar{n}=0}^{\lfloor (N-1)/2 \rfloor} \sum_{\bar{m}=0}^{\bar{n}} P^{(J)}_{\bar{m},\bar{n}-\bar{m}}(j\omega)\gamma_2^{\bar{m}}\xi_2^{\bar{n}-\bar{m}} \tag{16}$$

where

$$P^{(1)}_{0,0}(j\omega) = \frac{1}{2}H^{(1)}_1(j\omega)\bar{A}(\omega) = -\frac{1}{2}\cdot\frac{1}{L(j\omega)}\bar{A}(\omega) \tag{17}$$

$$P^{(2)}_{0,0}(j\omega) = \frac{1}{2}H^{(2)}_1(j\omega)\bar{A}(\omega) = \frac{1}{2}(1+\xi_1(j\omega))H^{(1)}_1(j\omega)\bar{A}(\omega) = (1+j\xi_1\omega)P^{(1)}_{0,0}(j\omega) \tag{18}$$

$$P^{(1)}_{\bar{m},\bar{n}-\bar{m}}(j\omega) = \frac{1}{2^{2\bar{n}+1}L(j\omega)} \sum_{\omega_1+\cdots+\omega_{2\bar{n}+1}=\omega} \prod_{i=1}^{2\bar{n}+1} H^{(1)}_1(j\omega_i)\bar{A}(\omega_i) \sum_{Z=1}^{N_{\bar{n}}} \frac{G_{\bar{m},\bar{n}-\bar{m}}\left(j\omega^Z_{l_{i(1)}},\cdots,j\omega^Z_{l_{i(j_i^{\bar{n}})}}\right)}{\prod_{i=1}^{\bar{n}-1} L\left[j\omega^Z_{l_{i(1)}}+\cdots j\omega^Z_{l_{i(j_i^{\bar{n}})}}\right]}$$
$$\bar{n} = 1,2,\cdots,\lfloor (N-1)/2 \rfloor \quad \bar{m} = 0,1,2\cdots,\bar{n} \tag{19}$$

$$P^{(2)}_{\bar{m},\bar{n}-\bar{m}}(j\omega) = -(j\omega)^2 P^{(1)}_{\bar{m},\bar{n}-\bar{m}}(j\omega) = \omega^2 P^{(1)}_{\bar{m},\bar{n}-\bar{m}}(j\omega)$$
$$\bar{n} = 1,2,\cdots,\lfloor (N-1)/2 \rfloor \quad \bar{m} = 0,1,2\cdots,\bar{n}. \tag{20}$$

and

$$\sum_{Z=1}^{N_{\bar{n}}} \frac{G_{\bar{m},\bar{n}-\bar{m}}\left(j\omega^Z_{l_{i(1)}},\cdots,j\omega^Z_{l_{i(j_i^{\bar{n}})}}\right)}{\prod_{i=1}^{\bar{n}-1} L\left[j\omega^Z_{l_{i(1)}}+\cdots j\omega^Z_{l_{i(j_i^{\bar{n}})}}\right]} = 1 \qquad \bar{n} = 1. \tag{21}$$

This completes the proof of Proposition 3.2.

Appendix B - Proof of Proposition 3.3

Squaring the magnitude of Eq. (3.19) gives

$$\begin{aligned}|Y_J(j\Omega)|^2 &= \left[\sum_{\bar{n}=0}^{\lfloor (N-1)/2 \rfloor} \sum_{\bar{m}=0}^{\bar{n}} P^{(J)}_{\bar{m},\bar{n}-\bar{m}}(j\Omega)\gamma_2^{\bar{m}}\xi_2^{\bar{n}-\bar{m}}\right]\left[\sum_{\bar{n}=0}^{\lfloor (N-1)/2 \rfloor} \sum_{\bar{m}=0}^{\bar{n}} P^{(J)}_{\bar{m},\bar{n}-\bar{m}}(-j\Omega)\gamma_2^{\bar{m}}\xi_2^{\bar{n}-\bar{m}}\right] \\ &= \sum_{\bar{n}=0}^{N-1}\sum_{\bar{m}=0}^{\bar{n}} \gamma_2^{\bar{m}}\xi_2^{\bar{n}-\bar{m}} \sum_{k=0}^{\bar{m}}\sum_{l=0}^{\bar{n}-\bar{m}} P^{(J)}_{k,l}(j\Omega)P^{(J)}_{\bar{m}-k,\bar{n}-\bar{m}-l}(-j\Omega). \end{aligned} \tag{22}$$

Evaluating the derivative with respect to γ_2 yields

$$\frac{\partial |Y_J(j\Omega)|^2}{\partial \gamma_2} = \mathrm{Re}\left[P^{(J)}_{0,0}(j\Omega)P^{(J)}_{1,0}(-j\Omega)\right] + \sum_{\bar{n}=2}^{N-1}\sum_{\bar{m}=1}^{\bar{n}} \bar{m}\gamma_2^{\bar{m}-1}\xi_2^{\bar{n}-\bar{m}} \sum_{k=0}^{\bar{m}}\sum_{l=0}^{\bar{n}-\bar{m}} P^{(J)}_{k,l}(j\Omega)P^{(J)}_{\bar{m}-k,\bar{n}-\bar{m}-l}(-j\Omega) \tag{23}$$

which is a polynomial in γ_2 and ξ_2 with a negative constant term

$$\mathrm{Re}\left[P^{(1)}_{0,0}(j\Omega)P^{(1)}_{1,0}(-j\Omega)\right] = \frac{-(1-\Omega^2)}{2^4\left[(1-\Omega^2)^2+(\xi_1\Omega)^2\right]^2\left|(1-\Omega^2)-j\xi_1\Omega\right|^2} < 0 \tag{24}$$

when $0 \leqslant \Omega < 1$. Eq. (23) therefore implies that there exists a $\bar{\gamma_2} > 0$ and a $\bar{\xi_2} \geqslant 0$ such that if $0 < \gamma_2 < \bar{\gamma_2}$ and $0 \leqslant \xi_2 < \bar{\xi_2}$

$$\left.\frac{\partial |Y_1(j\Omega)|^2}{\partial \gamma_2}\right|_{\Omega \ll 1} < 0 \tag{25}$$

which is result (i) of Proposition 3.3.

Taking the absolute value of Eq. (19) at $\omega = \Omega$ gives

$$\begin{aligned}
&\left|P^{(1)}_{\bar{m},\bar{n}-\bar{m}}(j\Omega)\right| \\
&= \frac{|j|}{2^{2\bar{n}+1}\left|\{L\left[j(\Omega)\right]\}^2\right| \left|L\left[j(\Omega)\right]\right|^{2\bar{n}}} \left| \sum_{\omega_1+\cdots+\omega_{2\bar{n}+1}=\Omega} \sum_{Z=1}^{N_{\bar{n}}} \frac{G_{\bar{m},\bar{n}-\bar{m}}\left(j\omega^Z_{l_{i(1)}}, \cdots, j\omega^Z_{l_{i(j_i^{\bar{n}})}}\right)}{\prod_{i=1}^{\bar{n}-1} L\left[j\omega^Z_{l_{i(1)}} + \cdots j\omega^Z_{l_{i(j_i^{\bar{n}})}}\right]} \right| \\
&\leq \frac{1}{2^{2\bar{n}+1}|L[j(\Omega)]|^{2\bar{n}+2}} \sum_{\omega_1+\cdots+\omega_{2\bar{n}+1}=\Omega} \sum_{Z=1}^{N_{\bar{n}}} \frac{\left|G_{\bar{m},\bar{n}-\bar{m}}\left(j\omega^Z_{l_{i(1)}}, \cdots, j\omega^Z_{l_{i(j_i^{\bar{n}})}}\right)\right|}{\left|\prod_{i=1}^{\bar{n}-1} L\left[j\omega^Z_{l_{i(1)}} + \cdots j\omega^Z_{l_{i(j_i^{\bar{n}})}}\right]\right|}.
\end{aligned} \tag{26}$$

Then, it can be obtained from Eq. (20) that

$$\left|P^{(2)}_{\bar{m},\bar{n}-\bar{m}}(j\Omega)\right| \leq \frac{\Omega^2}{2^{2\bar{n}+1}|L[j(\Omega)]|^{2\bar{n}+2}} \sum_{\omega_1+\cdots+\omega_{2\bar{n}+1}=\Omega} \sum_{Z=1}^{N_{\bar{n}}} \frac{\left|G_{\bar{m},\bar{n}-\bar{m}}\left(j\omega^Z_{l_{i(1)}}, \cdots, j\omega^Z_{l_{i(j_i^{\bar{n}})}}\right)\right|}{\left|\prod_{i=1}^{\bar{n}-1} L\left[j\omega^Z_{l_{i(1)}} + \cdots j\omega^Z_{l_{i(j_i^{\bar{n}})}}\right]\right|}. \tag{27}$$

When $\Omega \ll 1$, Eqs. (13) and Eq. (14) imply that the value of $\left|G_{\bar{m},\bar{n}-\bar{m}}\left(j\omega^Z_{l_{i(1)}}, \cdots, j\omega^Z_{l_{i(j_i^{\bar{n}})}}\right)\right|$ is bounded by $\left|G_{\bar{n},0}\left(j\omega^Z_{l_{i(1)}}, \cdots, j\omega^Z_{l_{i(j_i^{\bar{n}})}}\right)\right|$ which leads to

$$\left|G_{\bar{m},\bar{n}-\bar{m}}\left(j\omega^Z_{l_{i(1)}}, \cdots, j\omega^Z_{l_{i(j_i^{\bar{n}})}}\right)\right| < 1. \tag{28}$$

Substituting Eq. (10) and Eq. (28) into Eq. (26) gives

$$\left|P^{(2)}_{\bar{m},\bar{n}-\bar{m}}(j\Omega)\right| \leqslant \frac{\Omega^2}{2^{2\bar{n}+1}} \sum_{\omega_1+\cdots+\omega_{2\bar{n}+1}=\Omega} \sum_{Z=1}^{N_{\bar{n}}} \frac{1}{\prod_{i=1}^{\bar{n}-1} 1} = \frac{\Omega^2}{2^{2\bar{n}+1}} C_1(\bar{n}) \tag{29}$$

where

$$C_1(\bar{n}) = \sum_{\omega_1+\cdots+\omega_{2\bar{n}+1}=\Omega} \sum_{Z=1}^{N_{\bar{n}}} \frac{1}{\prod_{i=1}^{\bar{n}-1} 1} \tag{30}$$

is a bounded constant which is dependent on $\bar{n}$ but independent of Ω. Thus, when $\Omega \ll 1$

$$\left|P^{(2)}_{\bar{m},\bar{n}-\bar{m}}(j\Omega)\right| \leqslant \frac{\Omega^2}{2^{2\bar{n}+1}} C_1(\bar{n}) \approx 0 \tag{31}$$

for $\bar{n} = 1, 2, \ldots, \lfloor (N-1)/2 \rfloor$, $\bar{m} = 0, 1, 2 \ldots, \bar{n}$, hence the magnitude of $Y_2(j\Omega)$ in Eq. (3.19) can be written as

$$\left|Y_2(j\Omega)\big|_{\gamma_2,\xi_2 \geqslant 0}\right| = \left| P^{(2)}_{0,0}(j\Omega) + \underbrace{\sum_{\bar{n}=1}^{\lfloor (N-1)/2 \rfloor} \sum_{\bar{m}=0}^{\bar{n}} P^{(2)}_{\bar{m},\bar{n}-\bar{m}}(j\Omega)\gamma_2^{\bar{m}}\xi_2^{\bar{n}-\bar{m}}}_{\approx 0} \right| \approx \left|P^{(2)}_{0,0}(j\Omega)\right| = \left|Y_2(j\Omega)\big|_{\gamma_2,\xi_2=0}\right| \tag{32}$$

which is result (ii) of Proposition 3.3.

When $\Omega \approx 1$, it is known from Eq. (18) and Eq. (20) that

$$\mathrm{Re}\left[P^{(2)}_{0,0}(j\Omega)P^{(2)}_{1,0}(-j\Omega)\right] \approx \mathrm{Re}\left[\frac{-j(1+j\xi_1)}{2j\xi_1} \cdot \frac{-j}{2^2(-j\xi_1)^2|-j\xi_1|^2}\right] = \frac{1}{2^3\xi_1^4} > 0. \tag{33}$$

Substituting Eq. (33) into Eq. (23) gives

$$\frac{\partial|Y_2(j\Omega)|^2}{\partial\gamma_2} = \underbrace{\frac{3}{2^3\xi_1^4}}_{>0} + \sum_{\bar{n}=2}^{N-1}\sum_{\bar{m}=1}^{\bar{n}} \bar{m}\gamma_2^{\bar{m}-1}\xi_2^{\bar{n}-\bar{m}} \sum_{k=0}^{\bar{m}}\sum_{l=0}^{\bar{n}-\bar{m}} P_{k,l}^{(2)}(j\Omega)P_{\bar{m}-k,\bar{n}-\bar{m}-l}^{(2)}(-j\Omega). \tag{34}$$

which implies that when $\Omega \approx 1$, there exists a $\bar{\gamma_2} > 0$ and a $\bar{\xi_2} \geqslant 0$ such that if $0 < \gamma_2 < \bar{\gamma_2}$ and $0 \leqslant \xi_2 < \bar{\xi_2}$

$$\left.\frac{\partial|Y_2(j\Omega)|^2}{\partial\gamma_2}\right|_{\Omega\ll 1} > 0 \tag{35}$$

which is result (iii) of Proposition 3.3.

When $\Omega \gg 1$, from Eq. (13), it can be deduced that

$$\begin{aligned}\left|G_{\bar{m},\bar{n}-\bar{m}}\left(j\omega_{l_{i(1)}}^Z,\cdots,j\omega_{l_{i(j_i^{\bar{n}})}}^Z\right)\right| &= \left|\sum_{k_1+\cdots+k_{(j_i^{\bar{n}})}=3(\bar{n}-\bar{m})} a_{\bar{m},\bar{n},k_1,\ldots,k_{(j_i^{\bar{n}})}}\left(j\omega_{l_{i(1)}}^Z\right)^{k_1}\cdots\left(j\omega_{l_{i(j_i^{\bar{n}})}}^Z\right)^{k_{(j_i^{\bar{n}})}}\right| \\ &\leqslant \sum_{k_1+\cdots+k_{(j_i^{\bar{n}})}=3\bar{n}} a_{0,\bar{n},k_1,\ldots,k_{(j_i^{\bar{n}})}}\left|\left(j\omega_{l_{i(1)}}^Z\right)^{k_1}\right|\cdots\left|\left(j\omega_{l_{i(j_i^{\bar{n}})}}^Z\right)^{k_{(j_i^{\bar{n}})}}\right|\end{aligned} \tag{36}$$

hence

$$\left|P_{\bar{m},\bar{n}-\bar{m}}^{(1)}(j\Omega)\right| \leqslant \frac{\Omega^{3\bar{n}}}{2^{2\bar{n}+1}\left|L[j(\Omega)]\right|^{2\bar{n}+2}} \sum_{\omega_1+\cdots+\omega_{2\bar{n}+1}=\Omega}\sum_{Z=1}^{N_{\bar{n}}} \frac{A_{\bar{n}}}{\left|\prod_{i=1}^{\bar{n}-1} L\left[j\omega_{l_{i(1)}}^Z+\cdots j\omega_{l_{i(j_i^{\bar{n}})}}^Z\right]\right|} = \frac{C_2(\bar{n})}{2^{2\bar{n}+1}\Omega^{2\bar{n}+3}} \tag{37}$$

where $A_{\bar{n}}$ is a constant that is dependent on $\bar{n}$ and

$$C_2(\bar{n}) = \sum_{\omega_1+\cdots+\omega_{2\bar{n}+1}=\Omega} \sum_{Z=1}^{N_{\bar{n}}} A_{\bar{n}} \frac{\Omega}{\left| \prod_{i=1}^{\bar{n}-1} (j\omega^Z_{l_{i(1)}} + \cdots + j\omega^Z_{l_{i(j_i^{\bar{n}})}})^2 \right|} \tag{38}$$

is a bounded constant which is dependent on $\bar{n}$ but independent of Ω. Thus, when $\Omega \gg 1$

$$\left| P^{(1)}_{\bar{m},\bar{n}-\bar{m}}(j\Omega) \right| \leqslant \frac{C_2(\bar{n})}{2^{2\bar{n}+1}\Omega^{2\bar{n}+3}} \approx 0 \tag{39}$$

for $\bar{n} = 1, 2, \ldots, \lfloor (N-1)/2 \rfloor$, $\bar{m} = 0, 1, 2 \ldots, \bar{n}$. Substituting Eq. (39) into Eq. (20) gives

$$\left| P^{(2)}_{\bar{m},\bar{n}-\bar{m}}(j\Omega) \right| \leqslant \Omega^2 \frac{C_2(\bar{n})}{2^{2\bar{n}+1}\Omega^{2\bar{n}+3}} = \frac{C_2(\bar{n})}{2^{2\bar{n}+1}\Omega^{2\bar{n}+1}} \approx 0 \tag{40}$$

for $\bar{n} = 1, 2, \ldots, \lfloor (N-1)/2 \rfloor$, $\bar{m} = 0, 1, 2 \ldots, \bar{n}$. When $\Omega \gg 1$, the magnitudes of $Y_1(j\Omega)$ and $Y_2(j\Omega)$ in Eq. (3.19) can be written as

$$\left| Y_J(j\Omega)\big|_{\gamma_2,\xi_2 \geqslant 0} \right| = \left| P^{(J)}_{0,0}(j\Omega) + \underbrace{\sum_{\bar{n}=1}^{\lfloor (N-1)/2 \rfloor} \sum_{\bar{m}=0}^{\bar{n}} P^{(J)}_{\bar{m},\bar{n}-\bar{m}}(j\Omega) \gamma_2^{\bar{m}} \xi_2^{\bar{n}-\bar{m}}}_{\approx 0} \right| \approx \left| P^{(J)}_{0,0}(j\Omega) \right| = \left| Y_J(j\Omega)\big|_{\gamma_2,\xi_2=0} \right| \tag{41}$$

which is result (iv) of Proposition 3.3.

Appendix C - Proof of Proposition 3.4

Rewriting Eq. (22) as

$$|Y_J(j\Omega)|^2 = \sum_{\bar{n}=0}^{N-1} \sum_{\bar{m}=0}^{\bar{n}} \gamma_2^{\bar{n}-\bar{m}} \xi_2^{\bar{m}} \sum_{k=0}^{\bar{n}-\bar{m}} \sum_{l=0}^{\bar{m}} P_{k,l}^{(J)}(j\Omega) P_{\bar{n}-\bar{m}-k,\bar{m}-l}^{(J)}(-j\Omega) \tag{42}$$

gives its derivative with respect to ξ_2

$$\frac{\partial |Y_J(j\Omega)|^2}{\partial \xi_2} = \text{Re}\left[P_{0,0}^{(J)}(j\Omega) P_{0,1}^{(J)}(-j\Omega)\right] + \sum_{\bar{n}=2}^{N-1} \sum_{\bar{m}=1}^{\bar{n}} \bar{m} \gamma_2^{\bar{n}-\bar{m}} \xi_2^{\bar{m}-1} \sum_{k=0}^{\bar{n}-\bar{m}} \sum_{l=0}^{\bar{m}} P_{k,l}^{(J)}(j\Omega) P_{\bar{n}-\bar{m}-k,\bar{m}-l}^{(J)}(-j\Omega). \tag{43}$$

When $\Omega \approx 1$, it can be shown that

$$\text{Re}\left[P_{0,0}^{(J)}(j\Omega) P_{0,1}^{(J)}(-j\Omega)\right] < 0 \qquad J = 1, 2 \tag{44}$$

which implies that when $\Omega \approx 1$, there exists a $\bar{\gamma_2} \geqslant 0$ and a $\bar{\xi_2} > 0$ such that if $0 \leqslant \gamma_2 < \bar{\gamma_2}$ and $0 < \xi_2 < \bar{\xi_2}$

$$\left.\frac{\partial |Y_J(j\Omega)|^2}{\partial \xi_2}\right|_{\Omega \approx 1} < 0 \qquad J = 1, 2. \tag{45}$$

This is result (i) of Proposition 3.4.

The proof of Proposition 3.4(ii) is very similar to the proof of Proposition 3.3(ii). Separating out the variable ξ_2 in Eq. (22) gives

$$|Y_J(j\Omega)| = \left| P_{0,0}^{(J)}(j\Omega) + \sum_{\bar{n}=1}^{\lfloor (N-1)/2 \rfloor} P_{\bar{n},0}^{(J)}(j\Omega)\gamma_2^{\bar{n}} + \sum_{\bar{n}=1}^{\lfloor (N-1)/2 \rfloor} \sum_{\bar{m}=0}^{\bar{n}-1} P_{\bar{m},\bar{n}-\bar{m}}^{(J)}(j\Omega)\gamma_2^{\bar{m}}\xi_2^{\bar{n}-\bar{m}} \right| \tag{46}$$

When $\Omega \ll 1$, from Eq. (13), it can be shown that

$$\left| G_{\bar{m},\bar{n}-\bar{m}}\left(j\omega_{l_{i(1)}}^{Z}, \cdots, j\omega_{l_{i(j_i^{\bar{n}})}}^{Z} \right) \right| \leqslant \sum_{k_1+\cdots+k_{(j_i^{\bar{n}})}=3} a_{\bar{m},\bar{n},k_1,\ldots,k_{(j_i^{\bar{n}})}} \Omega^3$$

$$\bar{n} = 1, 2, \cdots, \lfloor (N-1)/2 \rfloor \quad \text{and} \quad \bar{m} = 0, 1, 2, \cdots, \bar{n}-1 \tag{47}$$

so

$$\left| P_{\bar{m},\bar{n}-\bar{m}}^{(1)}(j\Omega) \right| \leq \frac{\Omega^3}{2^{2\bar{n}+1}} \sum_{\omega_1+\cdots+\omega_{2\bar{n}+1}=\Omega} \sum_{Z=1}^{N_{\bar{n}}} \sum_{k_1+\cdots+k_{(j_i^{\bar{n}})}=3} a_{\bar{m},\bar{n},k_1,\ldots,k_{(j_i^{\bar{n}})}} = \frac{\Omega^3}{2^{2\bar{n}+1}} C_3(\bar{n})$$

and

$$\left| P_{\bar{m},\bar{n}-\bar{m}}^{(2)}(j\Omega) \right| = \frac{\Omega^5}{2^{2\bar{n}+1}} C_3(\bar{n}) \qquad \bar{n} = 1, 2, \cdots, \lfloor (N-1)/2 \rfloor \quad \text{and} \quad \bar{m} = 0, 1, 2, \cdots, \bar{n}-1 \tag{48}$$

where

$$C_3(\bar{n}) = \frac{1}{2^{2\bar{n}+1}} \sum_{\omega_1+\cdots+\omega_{2\bar{n}+1}=\Omega} \sum_{Z=1}^{N_{\bar{n}}} \sum_{k_1+\cdots+k_{(j_i^{\bar{n}})}=3} a_{\bar{m},\bar{n},k_1,\ldots,k_{(j_i^{\bar{n}})}} \tag{49}$$

is a bounded constant which is dependent on $\bar{n}$ but independent on Ω.

Both $\left| P_{\bar{m},\bar{n}-\bar{m}}^{(1)}(j\Omega) \right|$ and $\left| P_{\bar{m},\bar{n}-\bar{m}}^{(2)}(j\Omega) \right|$ are approximately zero for $\bar{n} = 1, 2, \cdots, \lfloor (N-1)/2 \rfloor$ and $\bar{m} = 0, 1, \cdots, \bar{n}-1$ when $\Omega \ll 1$. Thus, from Eq. (46), it can be shown

that

$$\left|Y_J(j\Omega)\Big|_{\gamma_2>0,\xi_2>0}\right| = \left|P_{0,0}^{(J)}(j\Omega) + \sum_{\bar{n}=1}^{\lfloor (N-1)/2\rfloor} P_{\bar{n},0}^{(J)}(j\Omega)\gamma_2^{\bar{n}} + \underbrace{\sum_{\bar{n}=1}^{\lfloor (N-1)/2\rfloor}\sum_{\bar{m}=0}^{\bar{n}-1} P_{\bar{m},\bar{n}-\bar{m}}^{(J)}(j\Omega)\gamma_2^{\bar{m}}\xi_2^{\bar{n}-\bar{m}}}_{\approx 0}\right|$$

$$\approx \left|P_{0,0}^{(J)}(j\Omega) + \sum_{\bar{n}=1}^{\lfloor (N-1)/2\rfloor} P_{\bar{n},0}^{(J)}(j\Omega)\gamma_2^{\bar{n}}\right| = \left|Y_J(j\Omega)\Big|_{\gamma_2>0,\xi_2=0}\right| \qquad J=1,2. \tag{50}$$

Eqs. (41) and (50) confirm that Eq. (3.30) holds and hence complete the proof of Proposition 3.4(ii).

Appendix D - Proof of Proposition 3.5

Differentiating $E_J(\Omega)$ with respect to ξ_2 gives

$$\frac{\partial E_J(\Omega)}{\partial \xi_2} = \sum_{p=1}^{\infty}\left\{\mathrm{Re}\left[P_{0,0}^{(J)}(jp\Omega)P_{0,1}^{(J)}(-jp\Omega)\right] + \sum_{\bar{n}=2}^{N-1}\sum_{\bar{m}=1}^{\bar{n}} \bar{m}\gamma_2^{\bar{n}-\bar{m}}\xi_2^{\bar{m}-1}\sum_{k=0}^{\bar{n}-\bar{m}}\sum_{l=0}^{\bar{m}} P_{k,l}^{(J)}(jp\Omega)P_{\bar{n}-\bar{m}-k,\bar{m}-l}^{(J)}(-jp\Omega)\right\}. \tag{51}$$

From Eq. (17),

$$P_{0,0}^{(J)}(jp\Omega) = 0 \qquad p = 3, 5, \cdots, \lfloor (N-1)/2 \rfloor, \quad J = 1, 2 \tag{52}$$

is true for all Ω so substituting Eq. (52) into Eq. (51) gives

$$\frac{\partial E_J(\Omega)}{\partial \xi_2} = \mathrm{Re}\left[P_{0,0}^{(J)}(j\Omega)P_{0,1}^{(J)}(-j\Omega)\right] + \sum_{p=1}^{\infty}\left\{\sum_{\bar{n}=2}^{N-1}\sum_{\bar{m}=1}^{\bar{n}} \bar{m}\gamma_2^{\bar{n}-\bar{m}}\xi_2^{\bar{m}-1}\sum_{k=0}^{\bar{n}-\bar{m}}\sum_{l=0}^{\bar{m}} P_{k,l}^{(J)}(jp\Omega)P_{\bar{n}-\bar{m}-k,\bar{m}-l}^{(J)}(-jp\Omega)\right\} \tag{53}$$

where $\mathrm{Re}\left[P_{0,0}^{(J)}(j\Omega)P_{0,1}^{(J)}(-j\Omega)\right]$ is a negative constant independent of γ_2 and ξ_2 when $\Omega \approx 1$. Therefore Eq. (53) implies that there exists a $\bar{\gamma_2} > 0$ and a $\bar{\xi_2} > 0$ such that if $0 < \gamma_2 < \bar{\gamma_2}$ and $0 < \xi_2 < \bar{\xi_2}$

$$\left.\frac{\partial E_J(\Omega)}{\partial \xi_2}\right|_{\Omega\approx 1} < 0, \qquad J = 1, 2 \tag{54}$$

which is result (i) of Proposition 3.5.

Substituting $\omega = p\Omega$ into Eqs. (17), (18), (19) and (20) gives the expression of $P^{(J)}_{\bar{m},\bar{n}-\bar{m}}(jp\Omega)$ and following the same procedure in 7, it can be shown that when $\Omega \ll 1$ and $\Omega \gg 1$

$$\left|P^{(J)}_{\bar{m},\bar{n}-\bar{m}}(jp\Omega)\right| \approx 0 \qquad \bar{n} = 1, 2, \cdots, \lfloor (N-1)/2 \rfloor, \quad \bar{m} = 1, 2 \ldots, \bar{n}, \quad J = 1, 2. \tag{55}$$

From Eqs. (3.20), (52) and (55) it can be deduced that

$$\begin{aligned} E_J(\Omega)\Big|_{\xi_2>0} &= \sum_{p=0}^{\infty} \left| P^{(J)}_{0,0}(jp\Omega) + \sum_{\bar{n}=1}^{\lfloor (N-1)/2 \rfloor} P^{(J)}_{\bar{n},0}(jp\Omega)\gamma_2^{\bar{n}} + \underbrace{\sum_{\bar{n}=1}^{\lfloor (N-1)/2 \rfloor} \sum_{\bar{m}=0}^{\bar{n}-1} P^{(J)}_{\bar{m},\bar{n}-\bar{m}}(jp\Omega)\gamma_2^{\bar{m}}\xi_2^{\bar{n}-\bar{m}}}_{\approx 0} \right|^2 \\ &\approx \sum_{p=0}^{\infty} \left| P^{(J)}_{0,0}(jp\Omega) + \sum_{\bar{n}=1}^{\lfloor (N-1)/2 \rfloor} P^{(J)}_{\bar{n},0}(jp\Omega)\gamma_2^{\bar{n}} \right|^2 = E_J(\Omega)\Big|_{\xi_2=0} \quad J = 1, 2 \end{aligned} \tag{56}$$

This is result (ii) of Proposition 3.5.

References

(1969). *SV. Sound and Vibration.* No. v. 3 in SV. Sound and vibration, Acoustical Publications, Incorporated.

Alabuzhev, P., Alabuzhev, P.M. & Rivin, E.I. (1989). *Vibration protecting and measuring systems with quasi-zero stiffness*. Taylor & Francis.

Allen, D.E. (1990). Building vibrations from human activities. *Concrete International*, **12**, 66–73.

Anderson, B., Jackson, J. & Sitharam, M. (1998). Descartes' rule of signs revisited. *The American mathematical monthly*, **105**, 447–451.

Apostol, T.M. (1970). Resultants of cyclotomic polynomials. In *Proc. Amer. Math. Soc*, vol. 24, 457–462.

Bachmann, H. (1995). *Vibration problems in structures: Practical guidelines*. Springer.

Baltanas, J.P., Trueba, J.L. & Sanjuan, M.A.F. (2001). Energy dissipation in a nonlinearly damped Duffing oscillator. *Physica D: Nonlinear Phenomena*, **159**, 22–34.

Batterbee, D.C. & Sims, N.D. (2005). Vibration isolation with smart fluid dampers: a benchmarking study. *Smart Structures and Systems*, **1**, 235–256.

Bishop, R. (1979). *Vibration*. Cambridge University Press, Cambridge New York.

Bogoliubov, N.N. (1961). *Asymptotic methods in the theory of non-linear oscillations*, vol. 10. Routledge.

Bossis, G., Volkova, O., Lacis, S. & Meunier, A. (2003). Magnetorheology: Fluids, structures and rheology. *Ferrofluids*, 202–230.

Boyd, S. & Chua, L. (1985). Fading memory and the problem of approximating nonlinear operators with Volterra series. *Circuits and Systems, IEEE Transactions on*, **32**, 1150–1161.

Brennan, M.J., Kovacic, I., Carrella, A. & Waters, T.P. (2008). On the jump-up and jump-down frequencies of the Duffing oscillator. *Journal of Sound and Vibration*, **318**, 1250–1261.

Bush, A.W. (1992). *Perturbation methods for engineers and scientists*. CRC.

Carrella, A., Brennan, M.J., Kovacic, I. & Waters, T.P. (2009). On the force transmissibility of a vibration isolator with quasi-zero-stiffness. *Journal of Sound and Vibration*, **322**, 707–717.

Carrella, A., Brennan, M.J., Waters, T.P. & Lopes Jr, V. (2012). Force and displacement transmissibility of a nonlinear isolator with high-static-low-dynamic-stiffness. *International Journal of Mechanical Sciences*, **55**, 22–29.

Chandra Shekhar, N., Hatwal, H. & Mallik, A.K. (1998). Response of non-linear dissipative shock isolators. *Journal of Sound and Vibration*, **214**, 589–603.

Chandra Shekhar, N., Hatwal, H. & Mallik, A.K. (1999). Performance of non-linear isolators and absorbers to shock excitations. *Journal of Sound and Vibration*, **227**, 293–307.

Chen, Y.M. & Liu, J.K. (2007). A new method based on the harmonic balance method for nonlinear oscillators. *Physics Letters A*, **368**, 371–378.

Chen, Z.Q., Wang, X.Y., Ko, J.M., Ni, Y.Q., Spencer, B.F. & Yang, G. (2003). MR damping system on Dongting Lake cable-stayed bridge. *Proc. SPIE*, **5057**, 229.

Cho, S.W., Jung, H.J. & Lee, I.W. (2005). Smart passive system based on magnetorheological damper. *Smart Materials and Structures*, **14**, 707.

Crede, C.E. (1951). *Vibration and shock isolation*. Wiley, New York.

Cveticanin, L. (2009). Oscillator with fraction order restoring force. *Journal of Sound and Vibration*, **320**, 1064–1077.

Dallard, P., Fitzpatrick, A.J., Flint, A., Le Bourva, S., Low, A., Ridsdill Smith, R.M. & Willford, M. (2001). The London millennium footbridge. *Structural Engineer*, **79**, 17–21.

Du, H., Yim Sze, K. & Lam, J. (2005). Semi-active h∞ control of vehicle suspension with magneto-rheological dampers. *Journal of Sound and Vibration*, **283**, 981–996.

Duan, Y.F., Ni, Y.Q. & Ko, J.M. (2006). Cable vibration control using magnetorheological dampers. *Journal of intelligent material systems and structures*, **17**, 321–325.

Duffing, G. (1918). *Erzwungene Schwingungen bei veränderlicher Eigenfrequenz und ihre technische Bedeutung*. 41-42, F. Vieweg & sohn.

Dyke, S.J., Spencer Jr, B.F., Sain, M.K. & Carlson, J.D. (1996). Modeling and control of magnetorheological dampers for seismic response reduction. *Smart Materials and Structures*, **5**, 565.

Fuller, C.C., Elliott, S. & Nelson, P.A. (1996). *Active control of vibration*. Academic Press, London.

Genesio, R. & Tesi, A. (1992). Harmonic balance methods for the analysis of chaotic dynamics in nonlinear systems. *Automatica*, **28**, 531–548.

George, D.A. (1959). *Continuous nonlinear systems*. Research Laboratory of Electronics, Massachusetts Institute of Technology.

Ginder, J.M., Davis, L.C. & Elie, L.D. (1996). Rheology of magnetorheological fluids: Models and measurements. *International Journal of Modern Physics B*, **10**, 3293–3303.

Gordaninejad, F., Saiidi, M., Hansen, B.C., Ericksen, E.O. & Chang, F.K. (2002). Magneto-rheological fluid dampers for control of bridges. *Journal of intelligent material systems and structures*, **13**, 167–180.

Guo, D.L., Hu, H.Y. & Yi, J.Q. (2004). Neural network control for a semi-active vehicle suspension with a magnetorheological damper. *Journal of Vibration and Control*, **10**, 461–471.

Guo, P.F., Lang, Z.Q. & Peng, Z.K. (2012). Analysis and design of the force and displacement transmissibility of nonlinear viscous damper based vibration isolation systems. *Nonlinear Dynamics*, **67**, 2671–2687.

Hall, K.C., Thomas, J.P. & Clark, W.S. (2002). Computation of unsteady nonlinear flows in cascades using a harmonic balance technique. *AIAA journal*, **40**, 879–886.

Hayashi, C., Shepard, S., Winkler, I., Glenn, S., Harris, E., Quaid, D., Hershey, B., Kaufman, P., Chartoff, R. & Wolfe, T. (1964). *Nonlinear oscillations in physical systems*, vol. 33. McGraw-Hill, New York.

He, J.H. (2002). Homotopy perturbation method for bifurcation of nonlinear problems. *Journal of Non-Linear Mechanics*, **37**, 309–314.

He, J.H. (2006). Some asymptotic methods for strongly nonlinear equations. *International Journal of Modern Physics B*, **20**, 1141–1199.

Housner, G.W., Bergman, L..A., Caughey, T.K., Chassiakos, A.G., Claus, R.O., Masri, S.F., Skelton, R.E., Soong, T.T., Spencer, B.F. & Yao, J.T. (1997). Structural control: past, present, and future. *Journal of engineering mechanics*, **123**, 897–971.

Hu, H. & Tang, J.H. (2006). Solution of a Duffing-harmonic oscillator by the method of harmonic balance. *Journal of Sound and Vibration*, **294**, 637–639.

Hundal, M.S. (1981). Response of shock isolators with linear and quadratic damping. *Journal of Sound and Vibration*, **76**, 273–281.

Ibrahim, R.A. (2008). Recent advances in nonlinear passive vibration isolators. *Journal of Sound and Vibration*, **314**, 371–452.

Jansen, L.M. & Dyke, S.J. (2000). Semiactive control strategies for MR dampers: comparative study. *Journal of Engineering Mechanics*, **126**, 795–803.

Jeary, A.P. (1996). The description and measurement of nonlinear damping in structures. *Journal of wind engineering and industrial aerodynamics*, **59**, 103–114.

Ju, L. & Blair, D.G. (1994). Low resonant frequency cantilever spring vibration isolator for gravitational wave detectors. *Review of scientific instruments*, **65**, 3482–3488.

Kim, Y., Langari, R. & Hurlebaus, S. (2009). Semiactive nonlinear control of a building with a magnetorheological damper system. *Mechanical Systems and Signal Processing*, **23**, 300–315.

Kolovsky, M.Z., Babitsky, V.I. & Wittenburg, J. (1999). *Nonlinear dynamics of active and passive systems of vibration protection*. Springer.

Kovacic, I. & Brennan, M.J. (2011). *The Duffing equation: Nonlinear oscillators and their behaviour*. Wiley.

Kovacic, I., Brennan, M.J. & Lineton, B. (2008). On the resonance response of an asymmetric Duffing oscillator. *International Journal of Non-Linear Mechanics*, **43**, 858–867.

Krylov, N.N. & Bogoliubov, N.N. (1947). Introduction to nonlinear mechanics. Acad. Sci. Ukr. SSR. *English translation, Princeton University Press, Princeton*.

Laalej, H. & Lang, Z.Q. (2010). Numerical investigation of the effects of MR damper characteristic parameters on vibration isolation of sdof systems under harmonic excitations. *Journal of Intelligent Material Systems and Structures*, **21**, 483.

Laalej, H., Lang, Z.Q., Sapinski, B. & Martynowicz, P. (2012). MR damper based implementation of nonlinear damping for a pitch plane suspension system. *Smart Materials and Structures*, **21**, 045006.

Lai, C.Y. & Liao, W.H. (2002). Vibration control of a suspension system via a magnetorheological fluid damper. *Journal of Vibration and Control*, **8**, 527–547.

Lam, K.H., Chen, Z.H., Ni, Y.Q. & Chan, H.L.W. (2010). A magnetorheological damper capable of force and displacement sensing. *Sensors and Actuators A: Physical*, **158**, 51–59.

Lang, Z., Jing, X., Billings, S., Tomlinson, G. & Peng, Z. (2009). Theoretical study of the effects of nonlinear viscous damping on vibration isolation of sdof systems. *Journal of Sound and Vibration*, **323**, 352–365.

Lang, Z.Q. & Billings, S.A. (1996). Output frequency characteristics of nonlinear systems. *International Journal of Control*, **64**, 1049–1067.

Lang, Z.Q. & Billings, S.A. (1997). Output frequencies of nonlinear systems. *International Journal of Control*, **67**, 713–730.

Lang, Z.Q., Billings, S.A., Yue, R. & Li, J. (2007). Output frequency response function of nonlinear Volterra systems. *Automatica*, **43**, 805–816.

Lee, H.S. & Choi, S.B. (2000). Control and response characteristics of a magneto-rheological fluid damper for passenger vehicles. *Journal of Intelligent Material Systems and Structures*, **11**, 80–87.

Lim, C.W. & Wu, B.S. (2002). A modified Mickens procedure for certain nonlinear oscillators. *Journal of Sound and Vibration*, **257**, 202–206.

Lim, C.W. & Wu, B.S. (2003). A new analytical approach to the Duffing-harmonic oscillator. *Physics Letters A*, **311**, 365–373.

Lim, C.W., Wu, B.S. & Sun, W.P. (2006). Higher accuracy analytical approximations to the Duffing-harmonic oscillator. *Journal of Sound and Vibration*, **296**, 1039–1045.

Liu, L., Thomas, J.P., Dowell, E.H., Attar, P. & Hall, K.C. (2006). A comparison of classical and high dimensional harmonic balance approaches for a Duffing oscillator. *Journal of Computational Physics*, **215**, 298–320.

Lueg, P. (1936). Process of silencing sound. US Patent 2,043,416.

MacDonald, N. (1993). Choices in the harmonic balance technique. *Journal of Physics A: Mathematical and General*, **26**, 6367.

Maia, N.M.M., e Silva, J.M.M. & (Portugal), I.S.T. (1997). *Theoretical and experimental modal analysis*. Research Studies Press Hertfordshire, UK.

Malatkar, P. & Nayfeh, A.H. (2002). Calculation of the jump frequencies in the response of sdof non-linear systems. *Journal of Sound and Vibration*, **254**, 1005–1011.

McClamroch, N.H. & Gavin, H.P. (1995). Closed loop structural control using electrorheological dampers. In *American Control Conference, 1995. Proceedings of the*, vol. 6, 4173–4177.

Mead, D.J. (1999). *Passive vibration control*. John Wiley & Sons Inc.

Mickens, R.E. (1984). Comments on the method of harmonic balance. *Journal of Sound and Vibration*, **94**, 456–460.

Mickens, R.E. (1986). A generalization of the method of harmonic balance. *Journal of Sound and Vibration*, **111**, 515–518.

Mickens, R.E. (1987). Iteration procedure for determining approximate solutions to non-linear oscillator equations. *Journal of Sound and Vibration*, **116**, 185–187.

Mickens, R.E. (1999). Generalization of the senator-bapat method to systems having limit cycles. *Journal of Sound and Vibration*, **224**, 167–171.

Mickens, R.E. (2005). A generalized iteration procedure for calculating approximations to periodic solutions of "truly nonlinear oscillators". *Journal of Sound and Vibration*, **287**, 1045–1051.

Mickens, R.E. (2010). *Truly nonlinear oscillations: harmonic balance, parameter expansions, iteration, and averaging methods*. World Scientific Pub Co Inc.

Milovanovic, Z., Kovacic, I. & Brennan, M.J. (2009). On the displacement transmissibility of a base excited viscously damped nonlinear vibration isolator. *Journal of Vibration and Acoustics*, **131**, 054502.

Napier, A., Gayadeen, S. & Duncan, S.R. (2011). Fast orbit beam stabilisation for a synchrotron. In *Control Applications (CCA), 2011 IEEE International Conference on*, 1094–1099.

Nayfeh, A.H. & Corporation, E. (1973). *Perturbation methods*, vol. 6. Wiley Online Library.

Nayfeh, A.H. & Mook, D.T. (1995). *Nonlinear Oscillations*. Wiley-VCH.

Peleg, K. (1979). Frequency response of non-linear single degree-of-freedom systems. *International Journal of Mechanical Sciences*, **21**, 75–84.

Peng, Z.K., Lang, Z.Q., Billings, S.A. & Tomlinson, G.R. (2008). Comparisons between harmonic balance and nonlinear output frequency response function in nonlinear system analysis. *Journal of Sound and Vibration*, **311**, 56–73.

Peng, Z.K., Lang, Z.Q., Zhao, L., Billings, S.A., Tomlinson, G.R. & Guo, P.F. (2011). The force transmissibility of mdof structures with a nonlinear viscous damping device. *International Journal of Non-Linear Mechanics*, **46**, 1305–1314.

Potts, R.B. (1981). Exact solution of a difference approximation to Duffing's equation. *The Journal of the Australian Mathematical Society. Series B. Applied Mathematics*, **23**, 64–77.

Potts, R.B. (1982). Best difference equation approximation to Duffing's equation. *The Journal of the Australian Mathematical Society. Series B. Applied Mathematics*, **23**, 349–356.

Preumont, A. (1999). Vibration control of active structures: an introduction. *Meccanica*, **34**, 139–139.

Ravindra, B. & Mallik, A.K. (1993). Hard duffing-type vibration isolator with combined Coulomb and viscous damping. *International Journal of non-linear mechanics*, **28**, 427–440.

Ravindra, B. & Mallik, A.K. (1994a). Performance of nonlinear vibration isolators under harmonic excitation. *Journal of Sound and Vibration*, **170**, 325–337.

Ravindra, B. & Mallik, A.K. (1994b). Role of nonlinear dissipation in soft Duffing oscillators. *Physical Review E*, **49**, 4950.

Ravindra, B. & Mallik, A.K. (1994c). Stability analysis of a non-linearly damped Duffing oscillator. *Journal of Sound and Vibration*, **171**, 708–716.

Ravindra, B. & Mallik, A.K. (1995). Chaotic response of a harmonically excited mass on an isolator with non-linear stiffness and damping characteristics. *Journal of Sound and Vibration*, **182**, 345–353.

Rijlaarsdam, D., Nuij, P., Schoukens, J. & Steinbuch, M. (2012). Frequency domain based nonlinear feed forward control design for friction compensation. *Mechanical Systems and Signal Processing*, **27**, 551–562.

Rijlaarsdam, D.J., Setiadi, A.C., Nuij, P.W.J.M., Schoukens, J. & Steinbuch, M. (2013). Frequency domain-based nonlinearity detection and compensation in Lur'e systems. *International Journal of Robust and Nonlinear Control*.

Rivin, E.I. (2003). *Passive vibration isolation*. Asme Press, New York.

Rugh, W.J. (1981). *Nonlinear System Theory: The Volterra/Wiener Approach.*. Johns Hopkins University Press, Baltimore.

Ruzicka, J.E. & Derby, T.F. (1971). *Influence of damping in vibration isolation*. The Shock and Vibration Information Center, Washington, D.C.

Sapiński, B., Martynowicz, P. & Jastrzębski, Ł. (2010). Symulacja układu redukcji drgań z tłumikiem magnetoreologicznym i elektromagnetycznym przetwornikiem energii (Simulation of vibration reduction system with an MR damper and an electromagnetic transducer). *Modelowanie Inżynierskie*, **8**, 177–184.

Schetzen, M. (1980). *The Volterra and Wiener theories of nonlinear systems*. John Wiley & Sons Inc, New York.

Schmidt, G. & Tondl, A. (1986). *Non-linear vibrations*, vol. 66. Cambridge Univ Pr.

Senator, M. & Bapat, C.N. (1993). A perturbation technique that works even when the non-linearity is not small. *Journal of Sound and Vibration*, **164**, 1–27.

Sims, N.D., Stanway, R., Peel, D.J., Bullough, W.A. & Johnson, A.R. (1999). Controllable viscous damping: an experimental study of an electrorheological long-stroke damper under proportional feedback control. *Smart Materials and Structures*, **8**, 601.

Sims, N.D., Stanway, R., Johnson, A.R., Peel, D.J. & Bullough, W.A. (2000). Smart fluid damping: shaping the force/velocity response through feedback control. *Journal of Intelligent Material Systems and Structures*, **11**, 945–958.

Snowdon, J.C. (1968). *Vibration and shock in damped mechanical systems*. J. Wiley.

Snowdon, J.C. (1979). Vibration isolation: use and characterization. *The Journal of the Acoustical Society of America*, **66**, 1245.

Society of Automotive Engineers. Committee G-5: Aerospace Shock and Vibration (1962). *Design of vibration isolation systems*, vol. 3. Society of Automotive Engineers.

Soong, T. (1990). *Active structural control: theory and practice*. Longman structural engineering & structural mechanics series, Addison-Wesley, London.

Soong, T.T. & Costantinou, M.C. (1994). *Passive and active structural vibration control in civil engineering*. Springer-Verlag, New York.

Soong, T.T. & Spencer Jr, B.F. (2002). Supplemental energy dissipation: state-of-the-art and state-of-the-practice. *Engineering Structures*, **24**, 243–259.

Spencer, B.F.J. & Nagarajaiah, S. (2003). State of the art of structural control. *Journal of structural engineering*, **129**, 845–856.

Spencer, B.F.J., Dyke, S.J., Sain, M.K. & Carlson, J.D. (1997). Phenomenological model for magnetorheological dampers. *Journal of Engineering Mechanics*, **123**, 230–238.

Spencer Jr, B.F. & Sain, M.K. (1997). Controlling buildings: a new frontier in feedback. *Control Systems, IEEE*, **17**, 19–35.

Stanway, R. (2004). Smart fluids: current and future developments. *Materials Science and Technology*, **20**, 931–939.

Struik, D.J. (1969). *A source book in mathematics: 1200-1800*. Harvard University Press.

Swain, A.K. & Billings, S.A. (2001). Generalized frequency response function matrix for MIMO non-linear systems. *International Journal of Control*, **74**, 829–844.

Takewaki, I. (2011). *Building control with passive dampers: optimal performance-based design for earthquakes*. John Wiley & Sons.

Thomas, J.P., Dowell, E.H. & Hall, K.C. (2002). Nonlinear inviscid aerodynamic effects on transonic divergence, flutter, and limit-cycle oscillations. *AIAA journal*, **40**, 638–646.

Thureau, P., Lecler, D. & Grosjean, J. (1981). *An introduction to the principles of vibrations of linear systems*. Thornes.

Tokhi, M.O. & Veres, S.M. (2002). *Active sound and vibration control: theory and applications*, vol. 62. IET, London.

Trueba, J.L., Rams, J. & Sanjuan, M.A.F. (2000). Analytical estimates of the effect of nonlinear damping in some nonlinear oscillators. *International Journal of Bifurcation and Chaos in Applied Sciences and Engineering*, **10**, 2257–2268.

Vernon, J.B. (1967). *Linear vibration theory*. Wiley.

Virgin, L.N., Santillan, S.T. & Plaut, R.H. (2008). Vibration isolation using extreme geometric nonlinearity. *Journal of Sound and Vibration*, **315**, 721–731.

Weiss, K.D., Carlson, J.D. & Nixon, D.A. (1994). Viscoelastic properties of magneto-and electro-rheological fluids. *Journal of Intelligent Material Systems and Structures*, **5**, 772–775.

Wen, Y.K. (1976). Method for random vibration of hysteretic systems. *Journal of the Engineering Mechanics Division*, **102**, 249–263.

Wu, B.S., Lim, C.W. & Ma, Y.F. (2003). Analytical approximation to large-amplitude oscillation of a non-linear conservative system. *International Journal of non-linear mechanics*, **38**, 1037–1043.

Xu, Z.D., Shen, Y.P. & Guo, Y.Q. (2003). Semi-active control of structures incorporated with magnetorheological dampers using neural networks. *Smart Materials and Structures*, **12**, 80.

Yao, G.Z., Yap, F.F., Chen, G., Li, W.H. & Yeo, S.H. (2002). MR damper and its application for semi-active control of vehicle suspension system. *Mechatronics*, **12**, 963–973.

Yi, F., Dyke, S.J., Caicedo, J.M. & Carlson, J.D. (2001). Experimental verification of multiinput seismic control strategies for smart dampers. *Journal of Engineering Mechanics*, **127**, 1152–1164.

Yu, P. & Leung, A.Y.T. (2003). A perturbation method for computing the simplest normal forms of dynamical systems. *Journal of Sound and Vibration*, **261**, 123–151.

Zhou, L., Chang, C.C. & Wang, L.X. (2003). Adaptive fuzzy control for nonlinear building-magnetorheological damper system. *Journal of Structural Engineering*, **129**, 905–913.